Free Abrasive Finishing with Dynamic Shear Jamming Fluid

FREE ABRASIVE FINISHING WITH DYNAMIC SHEAR JAMMING FLUID

BY

JOSEPH HENRY SPAN, B.ENG.

A THESIS

SUBMITTED TO THE DEPARTMENT OF MECHANICAL ENGINEERING

AND THE SCHOOL OF GRADUATE STUDIES

OF MCMASTER UNIVERSITY

IN PARTIAL FULFILMENT OF THE REQUIREMENTS

FOR THE DEGREE OF

MASTER OF APPLIED SCIENCE

Master of Applied Science (2016) McMaster University

(Mechanical Engineering) Hamilton, Ontario, Canada

TITLE:	Free Abrasive Finishing with Dynamic Shear Jamming Fluid
AUTHOR:	Joseph Henry Span B.ENG. (Mechanical Engineering) McMaster University, Hamilton, Canada
SUPERVISOR:	Dr. Philip Koshy
NUMBER OF PAGES:	xii, 109

To My Loving Supportive Parents

Abstract

Abrasive finishing is a machining process which alters the surface of a workpiece to achieve a specific property. Typical abrasive finishing processes focus on geometric tolerances and surface topography. Abrasive finishing is primarily dependent on finishing forces, relative velocities, and abrasive size. The material removal rate in finishing is inversely related to the surface finish. Magnetic and electric fields have been used to control the force applied to abrasives which finish the workpiece. These processes show an increase in performance when the field is used to control the process. Field assisted finishing processes can be energy intensive and expensive. A novel finishing media is proposed which does not require a field to achieve a similar force response. This media has inherent thickening mechanisms driven by shear jamming. This shear jamming mechanism can deliver forces an order of magnitude higher than shear thickening mechanisms. This novel slurry is demonstrated as a viable finishing media with performance similar to magnetic abrasive finishing.

Acknowledgements

I would like to acknowledge a number of people who helped make this work possible.

First and foremost I would like to thank my supervisor Dr. Philip Koshy. Your tireless patience and thirst for knowledge inspired me. This would not be achievable without your guidance. Your high standards helped me grow my passions and myself. I could not ask for a better supervisor.

I would like to thank all my peers and mentors in the MSL. Terry Wagg and Brady Semple for your helpful influence and constant support. Salomon Gabriel for your valuable constructive input and motivation. Mostafa Yakout for the many hours spent talking through obstacles and for all the joy you bring to the lab. You all make the MSL a great working environment and stimulate growth in others.

I would also like to thank the members of the Mechanical Engineering Machine Shop, Ron Lodewyks, Michael Lee, Dan Wright, Mark MacKenzie, and John Colenbrander. Your ideas and influence helped simplify and solve what seemed to be insurmountable problems.

Finally I would like to thank my friends and family. Tim and Jackie for your constant support and encouragement. Nicole Fakhri for your love and reassurance. You inspire me and push me to be a better person every day.

Contents

List of Tables

List of Figures

Chapter 1

Introduction

When manufacturing precision parts, finishing is often necessary after material - conversion processes such as casting, forging, milling, turning, 3d printing, or other similar processes. Finishing is used to ensure that specifications on geometry, dimensional accuracy, and surface topography are met. Typical material conversion processes focus on geometry and shape whereas finishing focuses on the surface of the workpiece. The focus of material conversion processes lie primarily in the macro scale whereas finishing lies in the micro scale. This chapter explains the motivations behind these operations, influencing process parameters, and a novel fluid proposed as the finishing medium.

1.1 Finishing Processes

Abrasive finishing refers to a process where microscopic amounts of material are either removed or altered to enhance a specific quality of the workpiece surface. Generally finishing refers to processes after material conversion processes. Finishing is usually

required when the tolerances specified for a manufacturing process are physically unachievable using a single step in a cost effective manner. An example of this is through abrasive flow machining of complex internal passages in aircraft valve bodies [1]. When manufacturing aircraft valve bodies, the presence of burrs or coarse surface roughness is not acceptable. Finishing these passages by hand is costly, and so abrasive flow machining is used. Some other typical applications of abrasive finishing are shown in Figure 1.1.

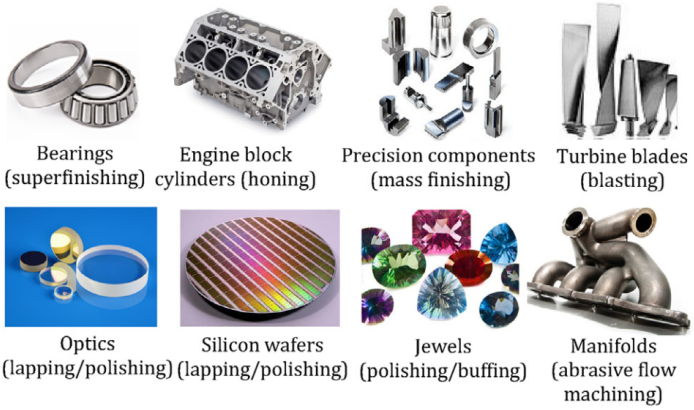

Figure 1.1: Critical Components Finished by Abrasive Finishing [2].

Abrasive finishing can be classified into two different processes. The first is defined as a motion copying process. A motion copying process controls the motion of the abrasives which in turn controls the depth of cut. An example of a motion copying process is grinding. Typically motion copying processes focus on the form and dimension of a workpiece. Pressure copying processes focus on the finish of the workpiece. Typically pressure copying processes follow grinding processes when further finishing is required [2]. Figure 1.2 shows some of the common pressure copying processes and further classifies them as using either bonded abrasives or unbonded abrasives.

Although some processes, such as magnetic abrasive finishing, can also use bonded

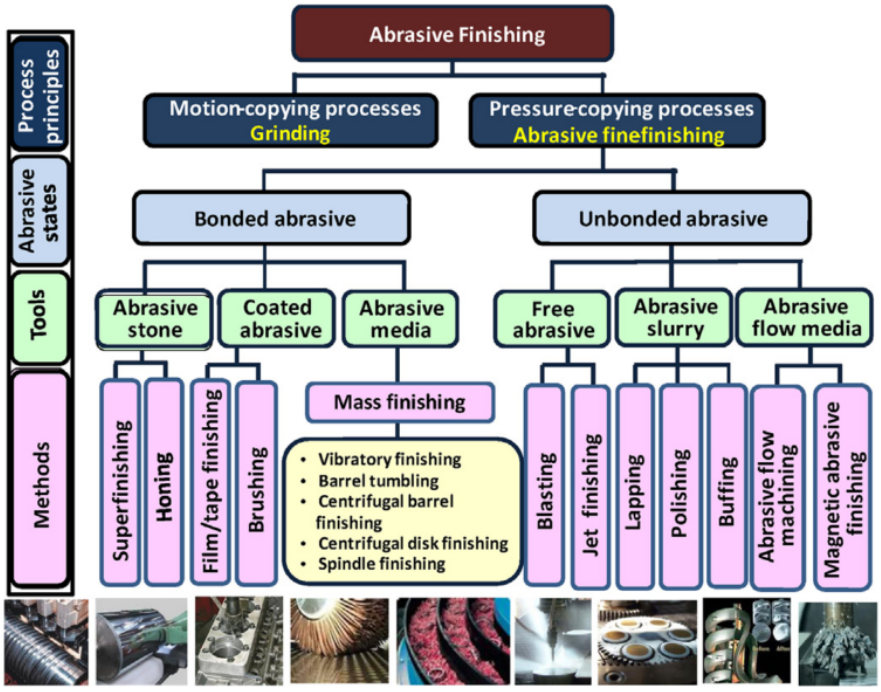

Figure 1.2: Classifications of Typical Abrasive Finishing Processes [2].

abrasives it is typical for these processes to use unbonded ones [3]. This work focuses on free abrasive finishing so emphasis is put on unbonded abrasive processes. Although bonded abrasive media is not a focus in this work, it is worth mentioning for further exploration. Some conventional shapes of bonded media are shown in Figure 1.3.

One of the best known applications of bonded abrasives is that of mass finishing. There are five main groups of mass finishing processes: barrel, vibratory, centrifugal barrel, centrifugal disk, and spin/spindle finishing. These types of finishing are typically used due to their low cost when compared to that of a manual surface refinement [4]. Vibratory finishing is currently the most employed form of mass finishing due to its efficiency, consistency, and versatility [4], [5], [6]. Although vibratory finishing

is considered efficient in contrast to other mass finishing processes, it is heavily energy intensive. It has a specific energy range between 200-1200 J/mm^3 where only 1-5 percent of the total energy supplied is actually used for material removal. When compared to the 20-70 percent of specific energy used for material removal in grinding it is fairly inefficient. It is estimated that the primary specific energy waste is due to ploughing and sliding of the media on the workpiece surfaces as well as part on part interaction [2].

Figure 1.3: Types of Ceramic Media Used in Mass Finishing [7].

Spin/spindle finishing is a process where a workpiece is affixed to a spindle and placed into a rotating tub of finishing media. The workpiece and spindle rotate while the tub of finishing media is also rotating. This is similar to drag finishing, which, uses a stationary tub while a rotating spindle follows a planetary orbit. Both of these processes drag a workpiece through a tub of abrasive media. Figure 1.4 shows a drag

finishing machine. Drag finishing is used for finishing cutting tools. It has been shown that after drag finishing the tool life increases [8]. This is because finishing smooths and rounds the edge which reduces the chance of chipping during cutting.

Figure 1.4: Drag Finishing Machine [8].

1.2 Influencing Parameters in Finishing

The material removal mechanisms in finishing can be quite complex due to the variety of mechanisms such as fatigue, cutting, and rolling. Fatigue is typically found in forms of finishing where abrasives are bombarded on the surface of a workpiece causing micro-cracks to form. The constant bombardment eventually creates sufficient

damage to remove a volume of material [2]. Cutting, or two bodied abrasion, refers to the form of cutting when the abrasive slides across the workpiece, scratching the surface, removing material. Rolling, or three-bodied abrasion, refers to a material removal mechanism where the abrasive is free to roll across the workpiece and does not necessarily scratch the surface. Although these terms seem quite well defined, still multiple interpretations of two body and three body abrasion exist [9]. For the purpose of this thesis, two body abrasion refers to a circumstance where the abrasive does not have the ability to roll, and three body is where the abrasive is free to roll.

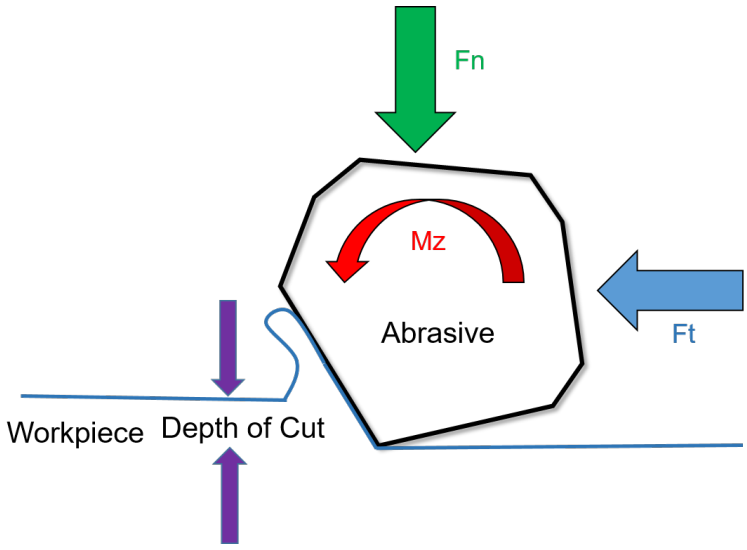

Figure 1.5: Basic Abrasive Finishing Parameters.

Some of the influential parameters for abrasive finishing are shown in Figure 1.5. Here we can see an abrasive grain cutting a workpiece. The tangential force (Ft) causes a relative velocity between the abrasive and the workpiece. The normal force (Fn) pushes the abrasive into the workpiece. The interaction of these two cause a specific depth of cut. The force generated by cutting the workpiece and the tangential force cause a moment. If this moment is sufficient to rotate the abrasive, the wear

can be considered three body, if not, the abrasion can be considered two body. The primary outcome of two versus three body abrasion is the wear rate. In two body abrasion, the typical rate is one to three orders of magnitude higher than three body abrasion [9].

There are two primary forms of cutting which can occur in abrasive finishing. The first is brittle cutting. This is where the workpiece shears removing material but typically causes radial and lateral cracks. The second form of cutting is ductile cutting. This is where the workpiece endures plastic deformation, and sliding or ploughing occurs. In brittle materials the form of cutting depends on the critical depth of cut. The smaller the depth of cut, the tendency for plastic deformation to occur is higher. The critical depth of cut can be calculated by the Bifano equation which is a function of the elastic modulus, fracture toughness, and Vickers hardness [10].

Two additional parameters which are very influential in finishing are the abrasive size and relative hardness of the workpiece. The relative hardness between the abrasive and the workpiece has been found to directly influence the material removal rate [11]. The abrasive grain size has also been directly correlated with the material removal rate and subsequent scratch depth of cut. Figure 1.6 shows the relationship found when lapping glass specimens with alumina. As the grain size decreases, the average peak to valley height decreases [12]. Unfortunately the smaller grain size also increases the required finishing time, making surface finish and required finishing time to be correlated. Finer finishes require more time.

Finishing fields that are fairly well researched are lapping, polishing and buffing [2]. All three of these processes contain a workpiece, granule, carrier fluid, and some

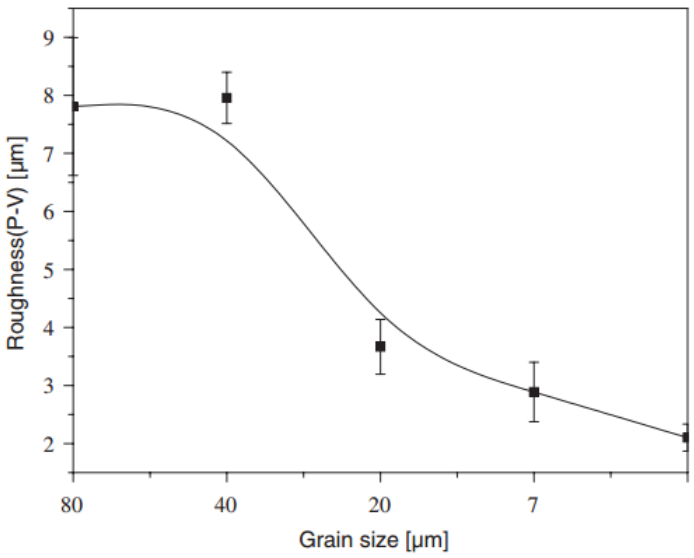

Figure 1.6: Abrasive Grain Size Effect on Surface Roughness [12].

sort of a lap or a platen to cause relative velocity. To model the abrasive wear in glass polishing machines, Preston developed the following equation [2]:

$$MRR = \frac{\Delta h}{\Delta t} = \frac{\Delta V}{\Delta t} = Cpv_s \tag{1.1}$$

MRR = Material Removal Rate

h = Height of Sample

t = Time

V = Volume

C = Material Combination Constant

p = Pressure

v_s = Relative Velocity

This equation states a linear relationship between the applied contact pressure (p), linear velocity (v_s), and material removal rate (MRR). It has been stated that

this model does not work in all ranges of lapping [13]. Due to this, many additional models have been constructed to expand Preston's equation to account for additional effects at various speeds and pressures. Despite these limited parameter ranges, the model captures the correlation between velocity and pressure on the material removal rate.

When engineering finishing media, it is important to consider which form of abrasion is desired. Bonded abrasives are used to enhance finishing speed by restricting abrasive rotation. When the abrasive is unable to rotate, two body abrasion occurs which has a high material removal rate. When bonded abrasives are used, complex geometries can be difficult to finish. Sharp or small corners constrain the size and shape of bonded abrasives that can be used. Research has been done to use free, or unbonded, abrasives which are more conformal to complex geometries. The material removal rate in free abrasive finishing is relatively slow. The abrasives are free to rotate which often leads to three body abrasion. To enhance this process magnetic or electric fields can be used to control the forces between the abrasive and workpiece by manipulating the medium [3], [14]. The present work focuses on suspensions that can be manipulated through process kinematics instead of electric or magnetic fields. Dense suspensions of cornstarch in water change physical properties depending on how they are deformed. The following chapter introduces a few of these properties and their potential application to finishing.

1.3 Dynamics of Cornstarch Suspensions

Cornstarch suspensions have rather fascinating properties. They are a fluid at rest, but when agitated the fluid solidifies into an amorphous solid. After the agitation

stops, the fluid "melts" back into its original state. Figure 1.7 shows two amazing phenomena native to cornstarch suspensions. In Figure 1.7 (a) an adult is running on a cornstarch suspension. If it were most other fluids, the adult should sink. In Figure 1.7 (b) strange "monster" like creatures creep from a vibrating speaker. Although patterns typically arise when specific frequencies excite a fluid or group of particles, such as in the case of Chladni Plates [15], the forms made by densely packed particle suspensions, such as cornstarch dispersed in Newtonian fluids are unique.

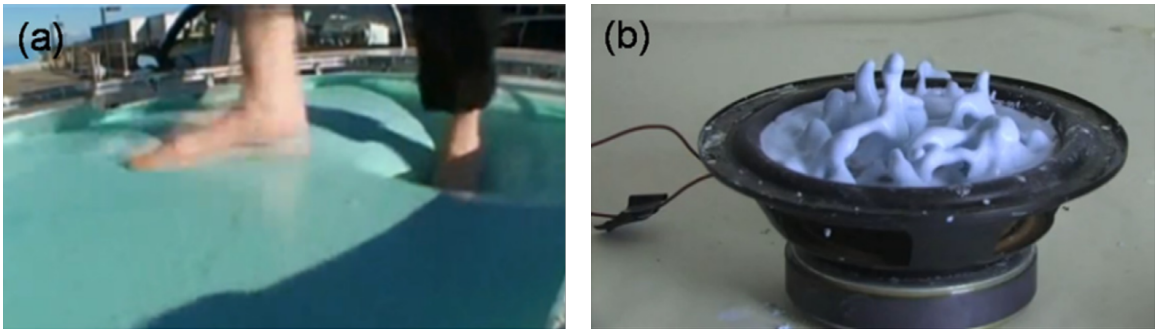

Figure 1.7: Cornstarch Suspensions (a) Supporting a Person's Weight (b) Forming "Monsters" Through Vibration [16]

These phenomenon are typically assumed to be due to the non-Newtonian characteristics of cornstarch suspensions. The fluid develops a normal force when subject to transient loading. Currently Non-Newtonian fluids are used in applications such as damping devices, body armour, and smart structures [17]. Further applications for these fluids are still being discovered.

The force response in non-Newtonian fluids is desirable for finishing applications. Cornstarch suspensions are conformal which is necessary when finishing complex geometries. They can also develop strong normal forces to the workpiece. Normal force, or pressure, has been shown to be correlated to the material removal rate in finishing.

This work focuses on utilizing cornstarch suspensions and free abrasives as a novel finishing media. This medium utilizes the conformal nature of cornstarch suspensions and the dynamic force response to enhance a drag finishing process.

1.4 Scope of Thesis

To study the performance of the novel finishing media, first preliminary finishing experiments were performed. Coupons were fabricated and finished in a drag finishing setup. The coupons were first finished in a stand still location while varying the spindle RPM. The coupons were then finished with both a spindle rotation and an orbital rotation while measuring the resulting forces. Further kinematic studies were performed without abrasives present to study the response characteristics of the fluid. The cornstarch concentration was varied to study the effect of different mass fractions on force. Various boundary conditions, orbital paths, spindle speeds, and spindle/orbit rotational directions were varied to establish relationships between input parameters and force. Abrasives were then added to the slurry. The abrasive concentration and grit size was varied while measuring the forces to study their effect on the slurry. From the kinematic and abrasive tests, parameters were chosen to finish coupons and edge hone cutting tools, demonstrating the finishing capabilities of the novel media.

Chapter 2

Literature Review

Abrasive finishing has been used as early as the Neolithic Period (15,000-5000 BC)[2]. It has been developed over many years. Many attempts have been made to improve the finishing process and new technologies are still being researched and invented.

This chapter gives an overview of some of the abrasive finishing processes and their influencing parameters. From these finishing processes, important qualities of abrasive media are outlined. The dynamics of cornstarch suspensions are then related to existing abrasive media. These two subjects are presented to provide a background to the present work.

2.1 Finishing Processes

2.1.1 Magnetic Abrasive Finishing

Magnetic abrasive finishing (MAF) is a process where a magnetic field is used to control the pressure that abrasives, suspended in a ferrous media, exert on a workpiece. Typical abrasives used are diamond, aluminium oxide, and silicon carbide [2]. These abrasives are non-ferrous so they are either cast into bonded abrasives or are coated on iron spheres. This is advantageous as the interaction between the abrasive and the magnetic field is a function of the particle volume. Typical abrasives do not have sufficient volume to interact with the magnetic field and generate forces strong enough for magnetic abrasive finishing [3]. When the abrasive media is influenced by a magnetic field, the ferrous material agglomerates and brushes are formed [18]. These brushes can apply finishing pressures between 5 and 400 kPa [2].

Figure 2.1 shows a cylindrical MAF process where a permanent magnet is used to apply a magnetic field which interacts with the workpiece [3]. The magnetic field can be produced by permanent magnets or through an induction coil [19].

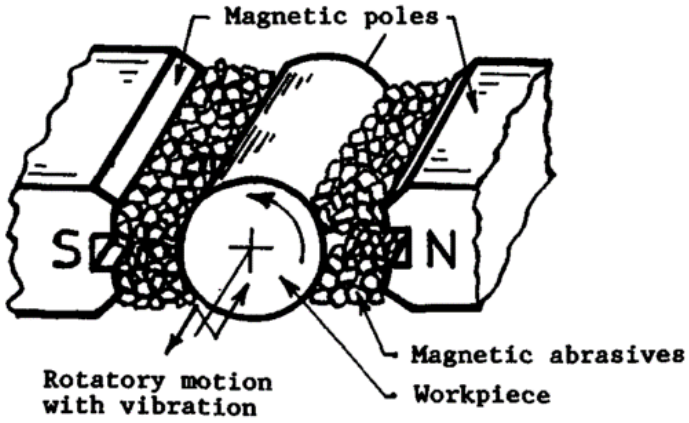

Figure 2.1: Cylindrical Magnetic Abrasive Finishing Setup [3].

MAF has many applications due to the compliant brushes. Complex geometries can be finished such as curvilinear surfaces where other finishing technologies are limited. It has also shown potential for deburring, machining cast parts, internal machining, and tool edge honing [2], [3], [18], [20], [21]. Finishing times for MAF greatly depend on the surface characteristics and tolerances desired. The range can be within seconds to hours depending on the process parameters. Figure 2.2 shows a trend for finishing ceramic bars with a diamond coated iron based abrasive. Here a significant reduction in surface roughness was achieved in 30 minutes [3].

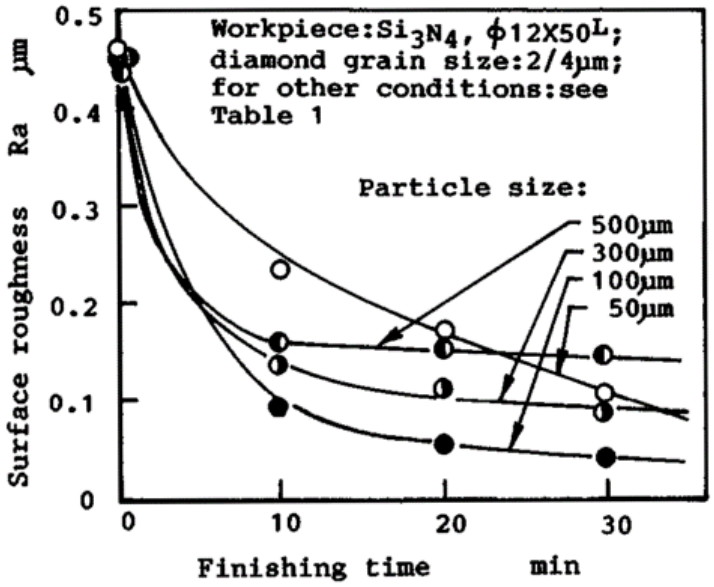

Figure 2.2: Typical Change of Surface Roughness Vs. Time in a MAF Process [3].

2.1.2 Magnetorheological Finishing

Magnetorheological finishing (MRF) has many similarities to MAF. The primary difference between the two is the way the abrasive is transported. In MRF, the abrasive particles are carried by a fluid containing carbonyl iron particles and a carrier media [22]. The fluid is usually a blend between various liquids to achieve specific qualities [23]. Figure 2.3 shows a typical MRF setup for finishing optical lenses. Here a wheel transports the media supplied by a nozzle across an electromagnet which in turn finishes a lens. The fluid is collected and conditioned thereafter. This conditioning is used to prevent agglomerations of particles. The primary driving factor is the applied electromagnetic field. The higher the field intensity, the stiffer the fluid becomes [23].

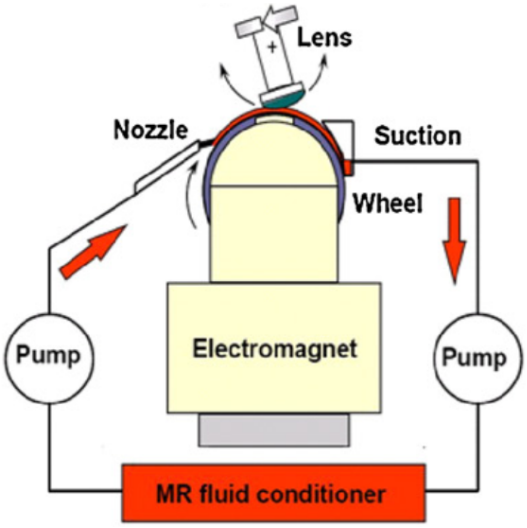

Figure 2.3: Magnetorheological Finishing Setup For Optics [24].

The magnetic particles in the slurry are attracted towards the electromagnet which causes the abrasive particles to levitate to the surface between the wheel and the lens. This partial separation between abrasive and carrier fluid separates this process from MAF. Studies have shown that adding glycerol to deionized water with cerium oxide as an abrasive is effective for finishing optical components. Because cerium oxide is chemically reactive to certain types of glass, the finishing performance is greatly dependent on the applied force. Typical forces in this process are between 1-30 N [25]. These forces are applied to a small area making typical stresses between 0.08-0.20 MPa [26]. Great care is taken to control the fluid viscosity which in turn controls the finishing forces [23]. MRF has been shown to be an effective finishing method for planarization, optical lens fabrication, deburring, spot finishing, and other applications requiring minimal surface/subsurface damage and little residual stress [27].

2.1.3 Electro Rheological Finishing

Electro rheological Finishing (ERF) is a process similar to MRF where an electrical field is used to modify the fluids viscosity to enhance a finishing process. Super fine abrasives are dispersed in a dielectric fluid mixed with electro rheological particles and used as the finishing media. Electro rheological fluids can either be made of particles or a liquid crystal polymer [14]. Figure 2.4 shows a typical setup for finishing a conductive workpiece [28]. An electric field is formed between the tool electrode and the workpiece. This field forms brushes out of the conductive abrasives similarly to the brushes formed in MAF. This brush is formed by polarizing the electro rheological particles and abrasives which create chain like structures [28]. Typical forces in ERF between 0.5-1 μN with an applied voltage between 800 and 2000 V [14]. A typical surface finish achieved through ERF is in the low nm Ra values [29]. Although the setup described in Figure 2.4 is for a conductive workpiece, finishing non conductive materials such as glass is also possible [29].

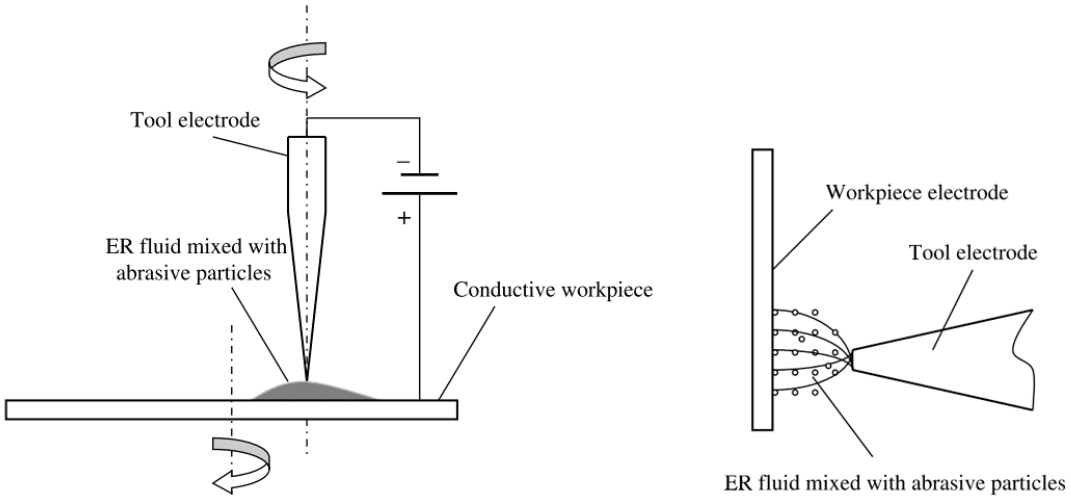

Figure 2.4: Electro Rheological Finishing Setup [28].

2.1.4 Elastic Emission Machining

Elastic emission machining (EEM) is one of the only finishing technologies able to produce tolerances on the atomic level. EEM employs a non traditional aproach to finishing as the material removal method is not on the micro scale but on the atomic scale. Figure 2.5 shows a schematic of a numerically controlled EEM process. Here a polyurethane sphere is held above, but not in contact with, the surface of a workpiece. The sphere is rotated and microscopic abrasives are accelerated in the gap. The working area of EEM is in the order of 10 nm^2 [30]. Surface atoms on the workpiece interact with the abrasives removing themselves from the workpiece and coating the abrasive [31]. Due to the atomic material removal method, EEM is one of the only finishing methods which does not induce plastic deformation and effectively finishes to atomic dimensions (2-4 angstroms)[24].

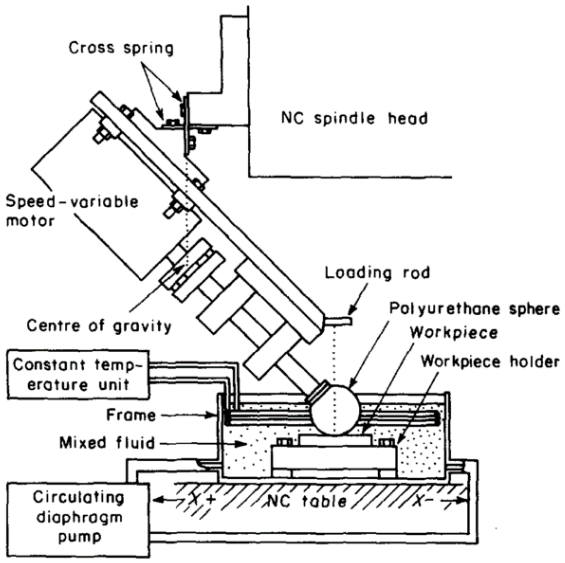

Figure 2.5: Numerically Controlled Elastic Emission Machining [30].

2.1.5 Abrasive Flow Machining

Abrasive flow machining (AFM) is a process where a transport media is extruded through or around a workpiece. Typical AFM uses a viscoelastic polymer which carries abrasive particles such as silicon carbide, boron carbide, aluminium oxide, or diamond. AFM is primarily used for internal finishing due to its ability to edge hone and deburr internal features but can be also used in certain applications for external finishing [2]. Figure 2.6 shows the basic setup of an AFM process. Here two cylinders drive the abrasive media through a workpiece finishing its internal features.

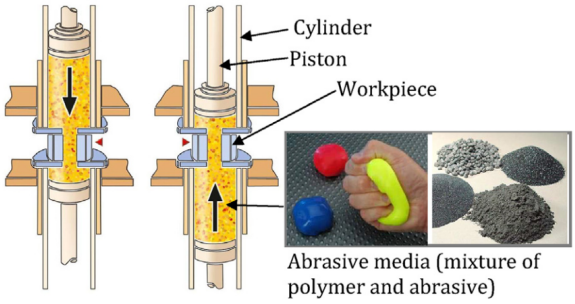

Figure 2.6: Abrasive Flow Machining Setup [2].

Fixtures are necessary to direct the media to the desired finishing locations when the media is not otherwise constrained. Some of the input variables in AFM are the initial surface condition, media viscosity, abrasive and abrasive size, and extrusion pressure. Typical abrasive concentrations can be as high as 80 percent by weight and have been seen as the dominant input variable [32]. This has been attributed to the low quantity of abrasives which act on the surface compared to that which pass through the part without any interaction. A study was performed which utilized an electromagnet to attract abrasives to the workpiece surface. This caused an increase in material removal rate and a decrease in surface roughness [33]. It has been shown that specific pre-machined surfaces, such as surfaces manufactured through wire electrical discharge machining (WEDM), show promising results from AFM [34]. This could be due to the positively skewed texture found on typical parts produced in WEDM.

2.1.6 Abrasive Fluid Jet Finishing

Abrasive fluid jet polishing, or abrasive fluid jet finishing (AFJ) was originally invented to finish aspherical optical components [35]. AFJ comprises a pressurized stream of abrasive slurry which impinges on a workpiece. Figure 2.7 shows a fluid jet

impinging on a rotating workpiece. Fluid pressure, fluid properties, flow rate, abrasive properties, stand off distance, and impingement angle are the primary control parameters for AFJ [2]. Typical ranges for abrasive grit size range from 0.1-50 μm and pressures between 4 and 20 bar [36]. Depending on the parameters specified, the material removal mechanism can change from ductile cutting to erosion and fatigue.

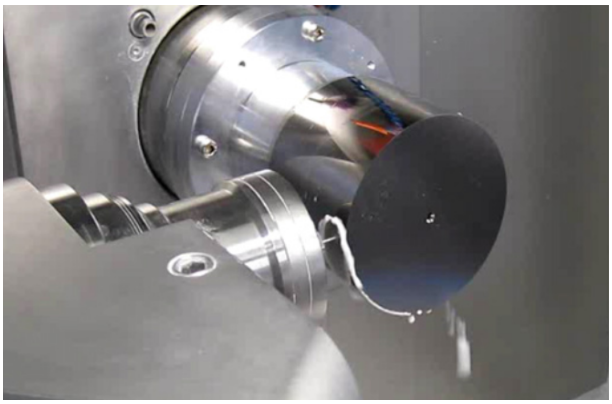

Figure 2.7: Fluid Jet Polishing Setup [36].

Stand off distance is a critical parameter primarily because of the formation of turbulence. This limits the geometries which can be produced. Research has been done on jet stabilization through the magnetorheological effect. This employs an axial magnetic field which suppresses initial disturbances thus enabling a coherent jet [37].

2.1.7 Shear-Thickening Polishing Method

Shear thickening polishing (STP) is a new finishing method where a Non-Newtonian power law fluid is used to enhance finishing performance. Fluids that shear thicken increase viscosity when sheared. Currently, a multi-hydroxyl polymer and a dispersant combined with aluminium oxide has been studied [38]. Results have shown that

shear thickening polishing has a high material removal rate and is capable of achieving fine surface finishes. The material removal mechanism is shown in Figure 2.8. Here an abrasive is shown interacting with a workpiece. Without shear thickening, (a), the abrasive is free to roll over the roughness peak without removing material. With shear thickening, it is shown that particle clusters restrict abrasive rotation which enhances material removal (c). The particle clusters interact with the abrasive which creates a normal force (F_D) which is met by an opposing material removal force (F_R). A model was developed and then later improved [39]. The model showed significant correlation to the observed polishing performance.

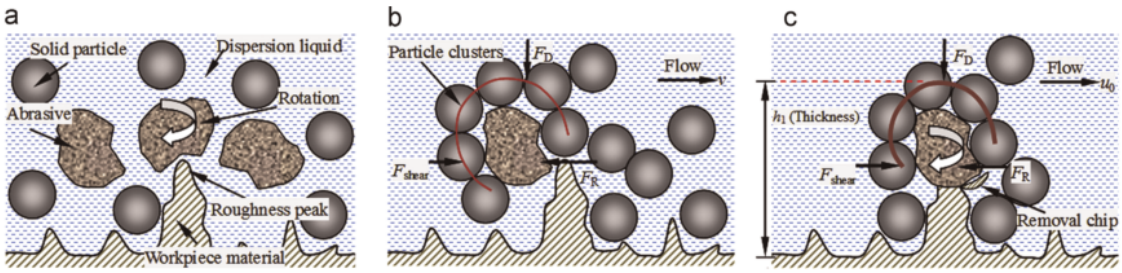

Figure 2.8: Material Removal (a) Without Shear Thickening, (b) With Shear Thickening, (c) With Shear Thickening Removing a Chip [38].

One of the oldest known applications of non-Newtonian polishing was suggested in 1976 [40]. It was found that titanium dioxide suspended in water provided an improvement to surface finish and polishing time. The exact details of the polishing method, nor the particle size or concentrations were listed. The author did not mention the rheological properties of the slurry but focused on finishing optical components. Titanium dioxide has been studied since then and has been known to show both shear thinning and shear thickening trends dependent on shear strain rate and

particle size, particle size distribution, and concentration [41]. As shear thickening has been shown to be beneficial to material removal mechanisms in finishing processes, the basics of non-Newtonain fluids are presented in the following section.

2.2 Fundamentals of Non-Newtonian Fluids

To understand the capabilities of a non-Newtonain fluid, the basic physics of rheology must be first described. The term rheology was invented by Professor Eugene Bingham. The term rheology was formed from the greek word "rhein" which means flow, thus rheology is "the theory of deformation and flow of matter" [42]. To study the flow of matter, a few fundamentals must be established.

The first fundamental is the concept of viscosity. Viscosity can be described as a fluid's resistance to shear. Often resistance is considered a steady state variable, but in terms of viscosity it can be transient and rate dependent. Figure 2.9 shows the primary fundamentals of shearing a fluid. Here the top moving wall moves with a speed dV_x which is sustained by a force F_x and resisted by a shear force Fs_x. The two walls are separated by a distance d_y and each have a surface area of A.

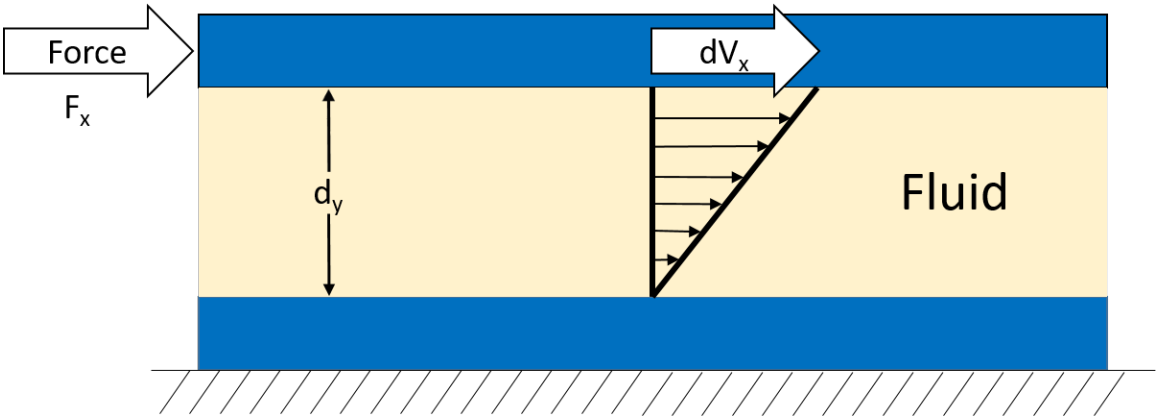

Figure 2.9: Shear Stress Vs. Shear Rate

Using the terms described above, the driving force F_x can be described by the following equation:

$$Fx = \eta A \frac{dVx}{dy} \tag{2.1}$$

where the rate that the fluid is sheared $\dot{\gamma}$ and the shear stress τ are defined by:

$$\dot{\gamma} = \frac{dVx}{dy} \qquad \tau = \frac{F}{A} \tag{2.2}$$

And in the same manner, the viscosity of the fluid can be described by the following (assuming the fluid is incompressible):

$$\eta = \frac{\tau}{\dot{\gamma}} \tag{2.3}$$

Using this relationship we can see that for fluid which has a constant viscosity, the relationship between shear stress and shear rate is a positively correlated linear function as seen in Figure 2.10. These types of fluids are called Newtonian fluids.

There, however, exists fluids which exhibit properties which are not linear. Two types of these fluids are dilatant and pseudo-plastic fluids. Pseudo-plastic fluids are fluids which display "thinning" under certain shear rates. These types of fluids can be found in many applications such as paint systems and printing inks [43]. The opposite of these fluids are dilatant fluids. Dilatant fluids exhibit a "thickening" behaviour as shear rate increases. Typically when referring to these two classifications of fluids, the terms shear-thickening and shear-thinning are used. This is primarily important for dilatant fluids as dilatation indicates an increase in volume where not all shear thickening fluids are necessarily dilatants. Classification of fluids into these types of categories must be done so with care as it typically results in a gross oversimplification [44]. It is possible for fluids to exhibit both shear thickening and shear thinning at different shear rates. For the purpose of this thesis, the classifications will be used to describe the trends examined but not as a label associated with any fluid.

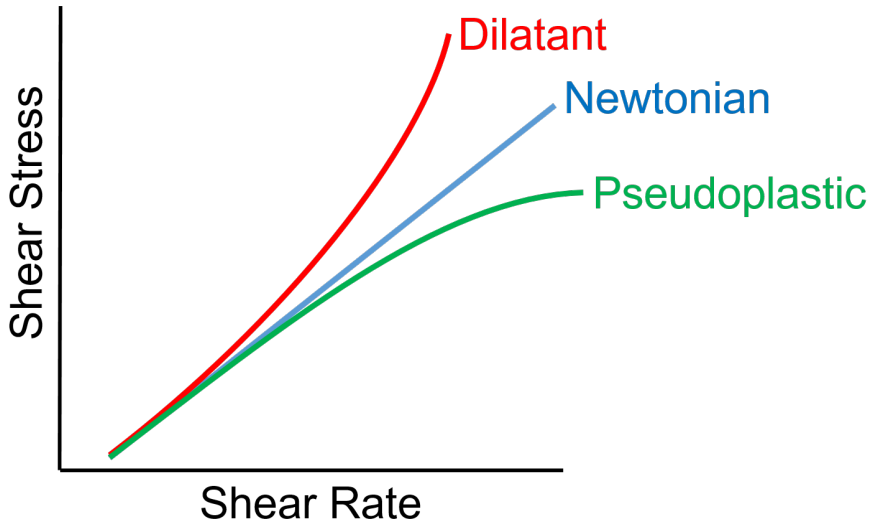

Figure 2.10: Shear Stress Vs. Shear Rate for Various Fluids.

Two additional traits, which fluids may exhibit, are rheoplexy and thixotropy. Both rheoplexy and thixotropy refer to transient viscosities. A rheopectic fluid is one which shows an increase in viscosity over time during steady state shear. On the other hand a thixotropic fluid shows a decrease in viscosity over time during steady state shear. [42]. The effect of both rheoplexy and thixotropy can be reversible which can lead to hysteresis as shown in Figure 2.11.

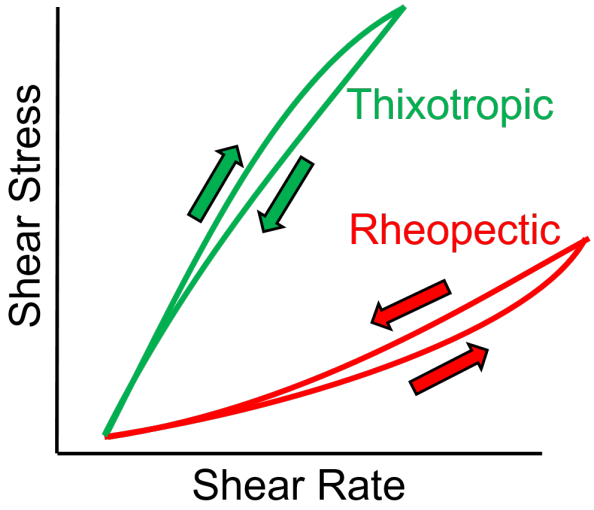

Figure 2.11: Shear Rate Hysteresis.

This is typical during rheological studies where the shear rate is ramped up and then ramped down while torque measurements are taken. This type of ramp is called a loop test. Another method to further understand thixotropic and rheopectic features is through a step test. This is where a shear rate is applied and sustained for a specific duration while the shear stress is measured. This type of test is typically more time intensive than loop tests but can be advantageous to characterise the transient response of the fluid as well as determine if an equilibrium state exists [45]. This also shows the difference between viscoelasticity and thixotropy. Viscoelastic

systems show a time dependent response to a flow stress because the microstructures cannot respond quickly. In this regard, they show both viscous effects and elastic effects.

Figure 2.12 shows the basic setup of a cylindrical viscometer used for rheological studies. The outer wall of the cylinder, typically called the cup, stays stationary during the experiments while the inner cylinder, called the bob, rotates. During rotation, the required driving torque, Mz, is measured and the viscosity is then calculated from the rotational speed, required torque, and geometries of the setup. One common challenge in viscometers is wall depletion or slip. It has been shown that studies examining the viscosity characteristic of the bulk fluid can be improved by surface texturing of the cup and bob through roughing or profiling. As an extreme instance of profiling, a vane geometry can be used [46]. However, studies which induce slip may be beneficial to specific industries as slip effects can be seen in flow through smooth pipes, conduits, and in manufacturing processes such as screw extrusion.

2.2.1 Dynamic Shear Jamming Fluid

The phenomenon of shear thickening is native to many different liquids. Detergents, specific polymers, inks, paints, and various coatings are some examples [45]. To limit the scope of this literature review to material relevant to dynamic shear jamming fluids only shear thickening behaviours of particle suspensions will be covered. H.A. Barnes came to the conclusion that "We shall find that so many kinds of suspensions show shear-thickening that one is soon forced to the conclusion that given the right circumstances, all suspensions of solid particles will show the phenomenon" [47]. The "right circumstances" are dependent on many factors and will be examined in the

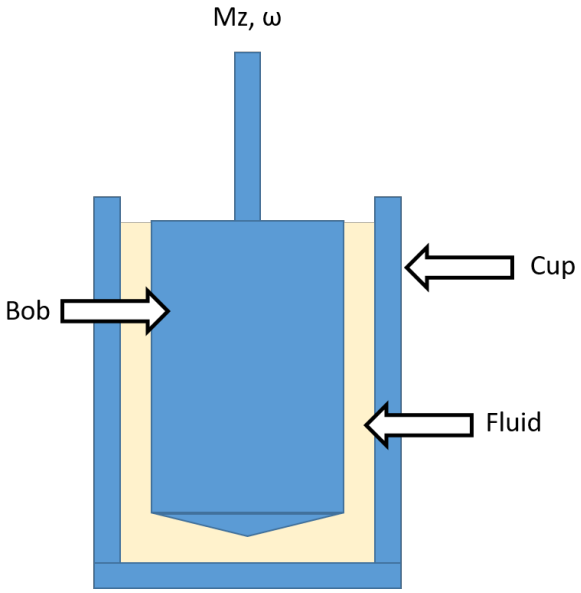

Figure 2.12: Cylinder Viscometer.

foregoing.

2.2.2 Important Parameters for Shear Thickening

The first important parameter to thickening in suspensions is the volume fraction ϕ_v or mass fraction ϕ_m. Both the mass and volume fraction refer to the amount of solid particles suspended in a liquid. The volume fraction is also referred to as the packing fraction. The challenge is that these parameters are calculated assuming that the solid particles do not contain any moisture before dispersion. If the moisture content is known and the moisture in the solid particles is the same as the suspension liquid, a more accurate calculation of the volume fraction can be calculated with the following formula. This is assuming that the particles are suspended in water and the moisture content is pure water [48]:

$$\phi_v = \frac{(1-\beta)\frac{m_{ps}}{\rho_{ps}}}{(1-\beta)\frac{m_{ps}}{\rho_{ps}} + \frac{m_w}{\rho_w} + \beta\frac{m_{ps}}{\rho_w}} \tag{2.4}$$

β = Mass Fraction of Moisture

m_{ps} = Mass of Particles

ρ_{ps} = Density of Particles

m_w = Mass of Water

ρ_w = Density of Water

In order to achieve thickening, an adequate packing fraction ϕ_v and an adequate shear rate $\dot{\gamma}$ must be reached. The relationship between shear rate required to initiate thickening and the volume packing fraction can be seen in Figure 2.13.

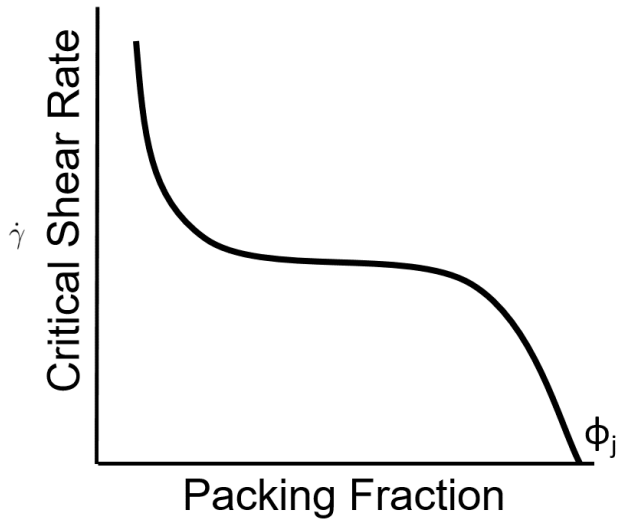

Figure 2.13: Critical Shear Rate for Shear Thickening [47].

The range in which typical suspensions will exhibit shear thickening is between a lower threshold to an upper limit defined as ϕ_j. For cornstarch suspensions, which is the primary medium used in this thesis, the upper and lower limits of ϕ_v for thickening to exist are between 30 and 60 percent [47]. Figure 2.14 shows the effect

of changing the mass fraction between 45 to 55 percent for cornstarch suspensions. It was noted that the volume fraction had significant errors due to water absorbed by the atmosphere but was estimated that 52.5 percent mass fraction correlated to a volume fraction $\phi_v = 0.42$ [16].

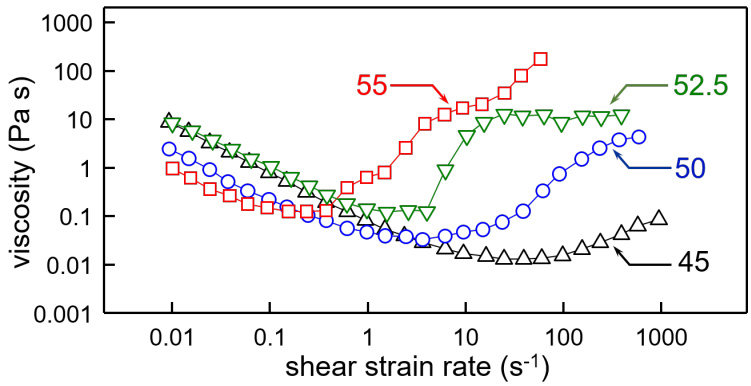

Figure 2.14: Viscosity Vs. Shear Strain Rate for Cornstarch Suspensions [16].

The second important parameter is the particle size and size distribution of dispersed particles. It has been shown that shear thickening exists over a wide range of particle sizes between 0.01 to 100 microns. The general trend is that the smaller particles require a higher critical shear rate $\dot{\gamma}_c$ to thicken [47]. One important aspect to consider is that the particle size not only influences the critical shear rate but also influences how the system responds. It has been shown in studies where various sized silicon carbide particles were suspended in a mixture of fumed silica and polyethylene glycol that there is a negative correlation between particle size and the thickening effect [17]. The particle size distribution also plays a role in the thickening nature of a dispersion. Widening a particle size distribution increases the maximum packing fraction ϕ_m and subsequently increases the critical shear rate $\dot{\gamma}_c$. This phenomenon

was examined extensively in a study where acrylic particles of various sizes were dispersed into hydrocarbons with high boiling points. It was found that when a small single mono disperse particle size was used a maximum packing fraction $\phi_m = 45$ percent could be obtained. When multiple particle sizes are introduced, level of shear thickening decreases. This effect is amplified when lattice size ratios of 4/1 or greater were mixed at equal volume fractions reducing the slurry's ability to shear thicken [49]. This was also observed when the volume fraction of small particles is increased [50].

The third important parameter is the particle shape and interaction. It has been shown that more anisotropic particles tend to shear thicken easier than isotropic particles [47]. This could be due to the frictional contact between particles.

2.2.3 Cornstarch Suspensions

Among the various types of colloidal suspensions which show shear thickening behaviour, a mixture of cornstarch and water remains one of the best known and most widely available mixtures [51]. The mixture of cornstarch and water has many distinct interesting properties from forming "monsters" while excited by vibration, ability to support a fast moving human, to showing cracking while impacted with sufficient velocity [51],[16],[52]. There has been much debate on the mechanisms that excite the extreme changes in the slurry. The different regimes can be classified as shear thinning, continuous shear thickening (CST), discontinuous shear thickening (DST), shear jamming, and jamming regions. These regions can be seen in Figure 2.15 as a function of volume fraction [53].

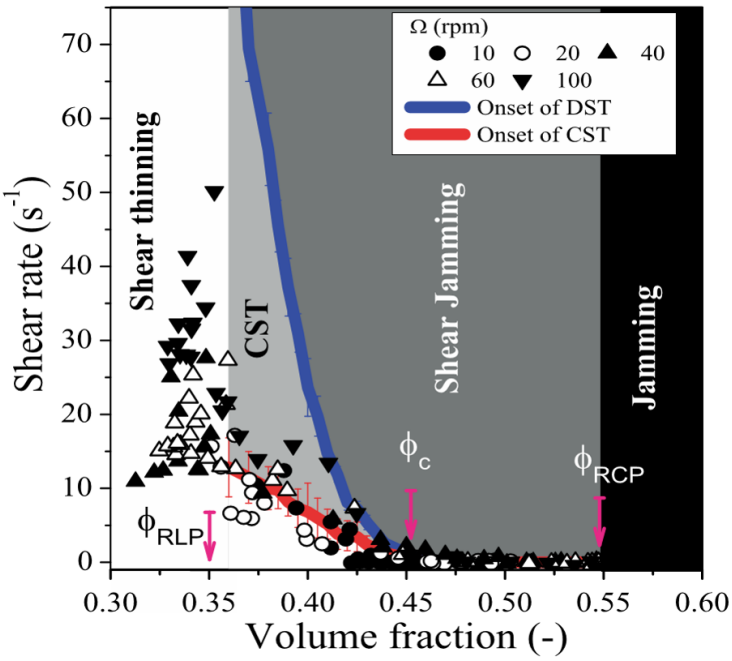

Figure 2.15: Phase diagram of Cornstarch Suspensions at Various Volume Fractions [53].

Shear thinning is a phenomenon known to various particle suspensions including clay suspensions, cornstarch suspensions, polyvinylchloride in dioc-tylphthalate dispersions, and titanium dioxide at low shear rates and volume fractions [54]. The shear thinning regime is typically at very low shear strain rates with a transition to shear thickening falling between 1 and 10 s^{-1}. This transition has been stated as the critical shear rate [55]. Once sufficient shear strain is present to cause thickening, cornstarch suspensions can show either continuous shear thickening or discontinuous shear thickening as shown in Figure 2.16. Discontinuous shear thickening is a phenomenon where there is a sudden jump in stress when the strain rate crosses a specific value depending on the mass fraction [53]. Discontinuous shear thickening has been observed, but is not as common as continuous shear thickening. It has been

shown that refined cornstarch suspensions have a higher tendency to show discontinuous shear thickening than bulk cornstarch [16]. Some factors which are thought to influence discontinuous shear thickening are surface chemistry, degree of cross-linking within the particles, particle anisotropy, and particle size distribution [16],[47],[56]. Both refined cornstarch and bulk cornstarch showed the same average particle size 15.0±4.2μm, 15.8±4.8μm respectively, but the distribution of bulk cornstarch was larger than that of refined. An increase of particle distribution has been shown to decrease the effect of thickening in other suspensions and thus was attributed as the driving cause of diverging from discontinuous to continuous shear thickening [16], [47].

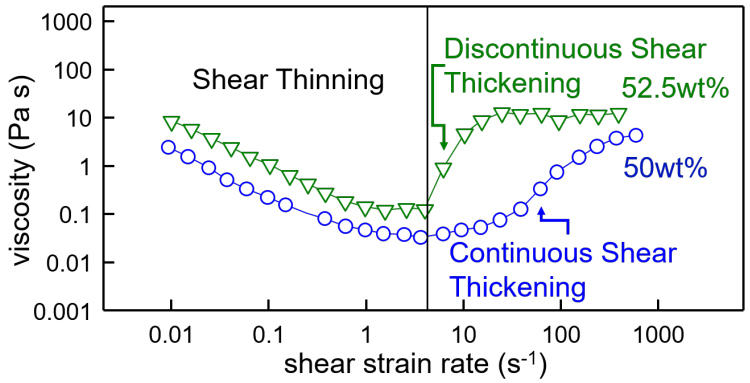

Figure 2.16: Viscosity Vs. Shear Strain Rate Showing Discontinuous and Continuous Shear Thickening [16].

Shear jamming and jamming are phenomenon common to cornstarch suspensions and are still being studied. Jamming can be split into two categories, shear jamming and jamming. Jamming typically is considered to only occur when the volume fraction of the dispersed particles exceeds ϕ_{RCP} as seen in Figure 2.15. This is also shown in Figure 2.13 as ϕ_m where the critical shear rate for thickening approaches zero. This region is where shear thickening breaks down and no flow exists [47]. The volume

fraction for cornstarch to become jammed has been found to be between 55 to 60 percent [47],[53].

Shear jamming is the mechanism where particle suspensions show remarkable resistance to impact or steady state force. A well known example of this is when the suspension supports a running adult. It has been estimated that to support a grown adult running across the suspension, a normal stress of 40 kPa must be sustained [51]. It has been shown in dense suspensions of hard particles that shear stress and normal stress are proportional to one another. Figure 2.17 shows various tests performed on silica particles dispersed in water.

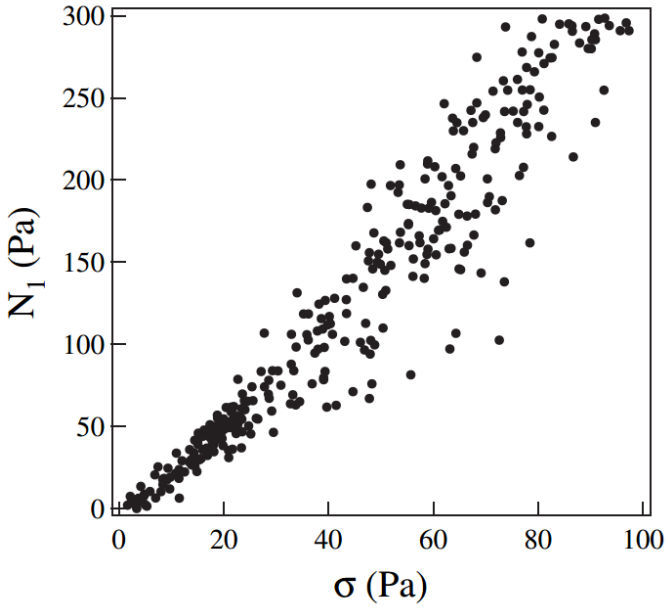

Figure 2.17: Coupling Between Normal Stress and Shear Stress [57].

Since the normal stress is correlated to the shear stress, the two can be directly compared. 40 kPa is an order of magnitude higher then the stress level τ_{max} for shear thickening [51]. This remarkable feature has been attributed to the rearrangement of

particles being inhibited and termed dynamic shear jamming.

To test how dense suspensions shear jam, studies have been performed where objects are driven through suspensions and forces are measured. One study was performed by driving various sized plastic spheres into a cornstarch suspension with a linear motor [58]. Moulding clay was placed on the bottom boundary to measure the force transmission through the suspension. The sphere was stopped 1 mm above the clay so that the sphere and clay never touched. Figure 2.18 shows the basic setup.

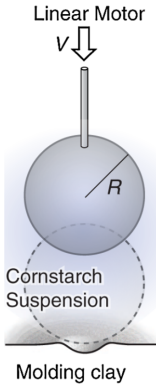

Figure 2.18: Sphere Moving Through Cornstarch Suspension Towards Moulding Clay [58].

It was found that the force transmitted through dense packed suspension was quite focused. When the sphere was halted just before the bottom it imparted a hemisphere into the clay with a radius smaller than the radius of the sphere. Newtonian fluids, despite their viscosity, did not reproduce this result. Dry granular material also did not produce this result but rather dissipated the force over a broader area. This test was also performed with a cylindrical geometry instead of the sphere. The results of this test are shown in Figure 2.19. Here the geometry imparted into the clay is shown to be related to the velocity of the cylinder. The higher the velocity, the deeper the

depression. It was noted that the force required to drive the cylinder increased once the cylinder approached the clay. The force required to drive the cylinder close to the clay was on the order of 1000 times that when the cylinder was before the onset distance.

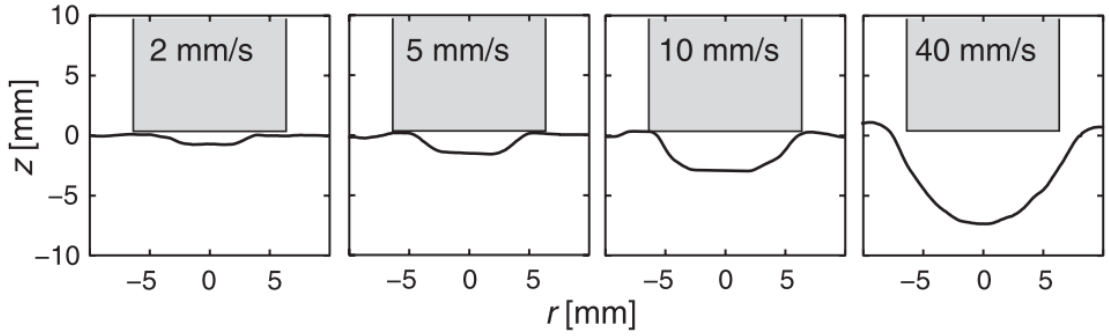

Figure 2.19: Cylinder Approaching a Clay Substrate at Various Speeds [58].

Spheres have also been observed to have velocity oscillations while settling in dense suspensions [59]. Spheres settling in Newtonian fluids accelerate to a terminal velocity and maintain this velocity until they reach a boundary. For dense suspensions, this is not the case. In Figure 2.20 (a) velocity oscillations can be seen as a sphere translates through a suspension of cornstarch and water. The suspension thickens as the sphere accelerates causing rapid deceleration until the sphere stops. The suspension then relaxes and the sphere accelerates again repeating the process until the sphere reaches the lower boundary. The container size also changes the dynamic. Small containers showed higher initial decelerations than larger containers but suppressed the number of oscillations. This experiment was also performed with different particle suspensions. Figure 2.20 (b) shows the results of using quartz flour, glass beads, polystyrene beads, and cornstarch. It was shown that the velocity oscillations are not

present in these other suspensions. The reason for this is not well understood but may be attributed to particle size and distribution [59].

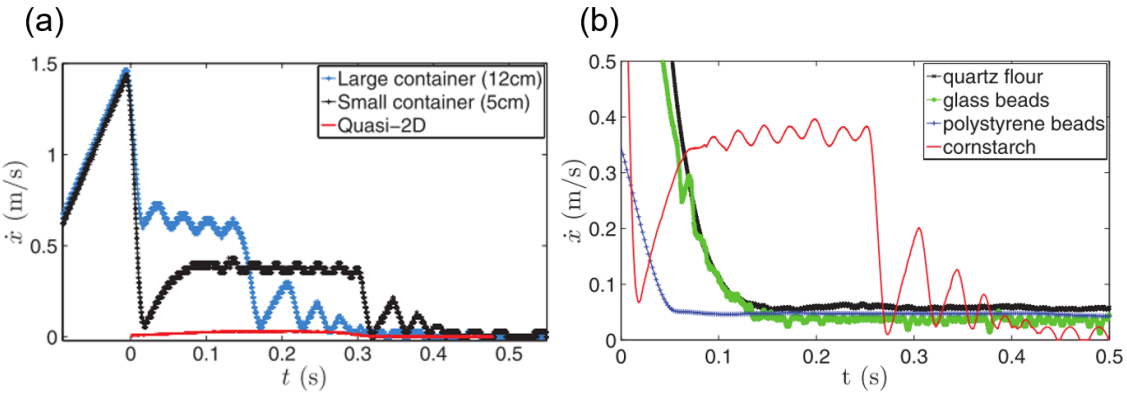

Figure 2.20: Sphere Settling in (a) Various Container Sizes (b) Various Suspensions [59].

One influential study performed at the University of Chicago by Scott R Waitukaitis studied the Impact-Activated Solidification of Cornstarch and Water Suspensions [60]. It defined the shear jammed state as "one in which a granular material with $\phi < \phi_j$ develops solid like properties, such as bulk and shear modulus, as a result of the application of a finite amount of shear" [52]. One test performed studied the surface of an impacted cornstarch slurry as well as accelerations of the impactor. The step for this experiment is described in Figure 2.21 (a). Here we see an impactor with an attached accelerator placed in a slingshot above a cornstarch suspension on top of a force sensor. In Figure 2.21 (b) we see the resulting displacement field after impact.

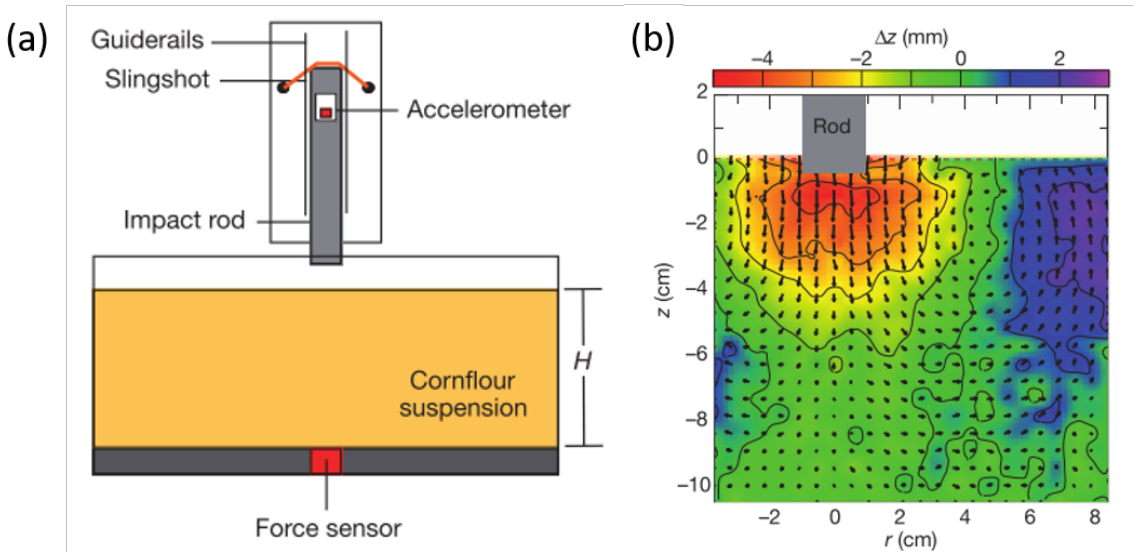

Figure 2.21: Impact Setup and Resulting PIV Velocity Field [60].

This test showed that the suspension under the impact rod developed a focused solidified region. This observation was also observed while studying spheres and cylinders driven to a boundary [58]. The focused solidified region had a propagation speed v_s. This propagation speed was measured by comparing the force at the bottom of the container and the acceleration of the impact rod. The following model was presented to predict the velocity of the front [60], [61].

$$v_f = \frac{\phi_j}{\phi_j - \phi_o} v_p \tag{2.5}$$

v_f = Front Propagation Speed

v_p = Impactor Speed

ϕ_j = Jammed Volume Fraction

ϕ_o = Current Volume Fraction

Here the front propagation speed was shown to be a function of the impactor

speed and volume packing fractions. An interesting phenomenon observed is that the fluid height directly relates to the time required for the second acceleration spike as seen in Figure 2.22. The volumetric packing fraction had an influence on the severity of the acceleration. This agrees with equation 2.5 as the time necessary for the front to propagate to a boundary is dependent on the distance to that boundary. As the distance increases, the time required for the front to reach the boundary also increases. This test also confirmed that there was a deficiency on how the transient response of particle suspensions is measured. This work showed that the response of the system depended on both the shear strain rate and the applied strain indicating that the response cannot be fully captured in traditional steady state rheology [52],[60].

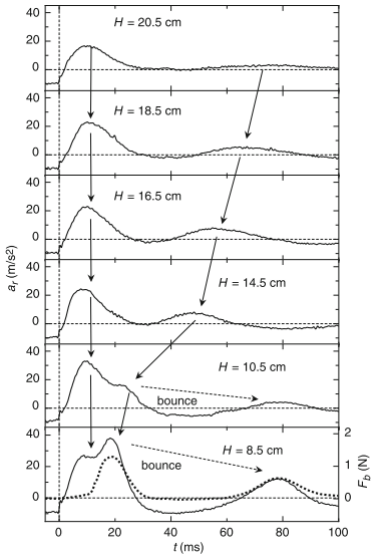

Figure 2.22: Bounce Effect Dependency on Fluid Depth [52].

These tests lead to a theory on how dense suspensions thicken. It was suggested that compression along the packing density axis changed the density of the suspension directly below the impactor. This was assumed to be because the dispersed particles

become jammed while the dispersant fluid flows between the particles. This changes the local density, under the impactor, from the initial packing fraction ϕ_o to a jammed packing fraction ϕ_j [60], [61].

$$\Delta\phi = \phi_j - \phi \tag{2.6}$$

Although an interesting and innovative idea, further studies disprove the notion that the density is transient in the system by measuring the speed of sound through both a resting and jammed slurry. In dense suspensions, the speed of sound increased linearly as the volume packing fraction ϕ_o was increased. This made local density measurements possible. The speed of sound was measured in both a resting and impacted suspension. It was found that the increase in density was only 0.006 percent. This increase was not sufficient to change density of $\phi_o \rightarrow \phi_j$ and thus disproving the theory and equation 2.6. This study also showed that the jamming fronts created by impact was in the same location as the maximum local shear rate. This indicates that the driving mechanism for thickening is dynamic shear jamming and not densification [48].

An interesting study focusing on dynamic shear jamming was conducted through extension tests. Here a rheometer was fitted with a circular plate, placed on the surface of the suspension, then pulled upwards with a constant velocity. The force trend as a function of time was recorded for various speeds. The setup described can be seen in Figure 2.23.

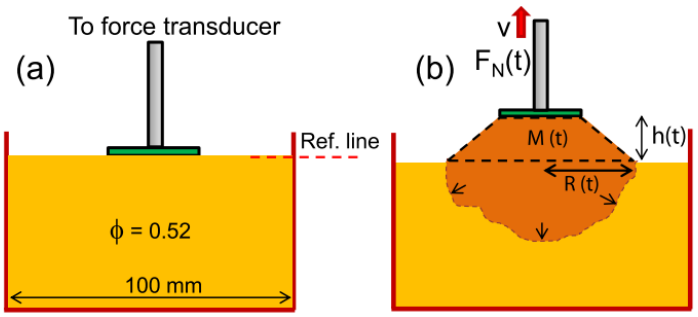

Figure 2.23: Dynamic Shear Jamming Under Extension Setup [62].

As velocity is increased, a sudden increase in normal force is observed. This only happened at speeds exceeding 8 mm/s. Further tests with ultrasound imaging show that a jamming front propagates to the container boundaries. When that front interacts with the boundaries, the force increases. This shows significant proof that the jamming observed is through shear as the tests described are all in tension [62].

The primary driving factor for the resulting normal forces observed in the dynamic shear jamming regions described above is a breakdown of hydrodynamic lubrication resulting in frictional contacts [62],[63]. Although this has not been directly proven through observation because of the opaque nature of cornstarch dispersions, sufficient supporting documentation exists to make such a claim.

2.3 Concluding Remarks

In manufacturing critical components, finishing remains as the final step to achieving quality parts. Various finishing methods have been described and primary input parameters specified. Technologies such as MAF, and MRF use external fields to control forces in the process. This has been shown to be effective at increasing the finishing

performance. AFJ utilizes fluid velocity to control the impact force of the abrasive on a workpiece. AFM and STP use shear thickening properties in the abrasive media to control force. Since force is critical to finishing performance, a novel finishing media was introduced. The media shows potential to deliver stresses which are an order of magnitude higher than shear thickening fluids. The various mechanisms for thickening were discussed. Volume fraction, impact/translational velocity, boundary conditions, and physical particle properties were the primary influencing parameters to generate shear jamming. This literature survey reveals an opportunity to utilise shear jamming fluids for finishing and study their characteristics.

Chapter 3

Experimental

Finishing experiments were performed on a computer numerically controlled milling machine (CNC Milling Machine) to explore the finishing potential of the novel finishing media. The objectives of these experiments were to provide a proof of concept for the novel finishing media, determine the kinematic response of the finishing media, and to utilize the response to enhance a spindle finishing process. Experiments were run to test the influence of several process parameters including various geometrical boundary conditions, translational velocity, rotational velocity, workpiece translational path, abrasive media concentrations, and slurry compositions on finishing performance and process force. This chapter will detail the set-ups, machines, and steps taken to study these parameters.

3.1 Machine Setup

The experiments were performed with the resources in the Machining Systems Laboratory (MSL) at McMaster University.

The CNC Mill was a Matsuura FX-5G shown in Figure 3.1. This 3 axis vertical milling machine has a maximum rapid feed of 25 m/min, 27 horsepower spindle power, 27,000 RPM maximum spindle speed, and is controlled with a FANUC 15iM Control. This machine has high precision and high rigidity which allows for repeatable testing conditions.

Figure 3.1: Matsuura FX-5G CNC Milling Machine.

3.2 Experimental Apparatus Setup

A Kistler Type 9272 4-Component Dynamometer with a Bison 4 jaw independent Chuck was affixed to the bed of the CNC Mill, shown in Figure 3.2. The dynamometer was connected to 4 Kistler type 5010 dual mode charge amplifiers. The 4 amplifiers were independently amplifying the X, Y, Z, and Mz channels converting the charge signal produced by the dynamometer to voltages. The amplifiers were connected to a National Instruments Hi-Speed USB Carrier (NI USB-9162) which fed the voltage signals to LabVIEW. The dynamometer was tested to ensure it was properly calibrated in all channels.

A setup was created with a removable boundary in the center which could be held by the dynamometer. It had a 135 mm internal diameter and a 75 mm height. The removable center was bolted to a silicone seal that enabled the container to be water tight. The removable center allowed for various geometrical constraints to be tested. It also provided one of the mating surfaces for the dynamometer to be mounted to. As seen in Figure 3.2 the jaws of the dynamometer rested on the centrepiece while they opened catching the internal diameter of the baseplate. This allowed for a rigid setup to endure the forces applied to the fluid. The dynamometer and setup were centred using a dial indicator rotated about the spindle. The dynamometer was centred using a Mitutoyo dial indicator with a resolution of 2.54 μm. The container was then centred using the independent 4 jaw chuck of the dynamometer with a Mitutoyo dial indicator with a resolution of 25.4 μm. This produced a positioning accuracy which was over an order of magnitude larger than the smallest gap size measured. The base plate and side walls of the container were made out of aluminium while the center plate and center block were formed from acrylic. These materials were chosen because of their

relatively high strengths, corrosion resistance, and were readily available. The bed of the CNC mill was covered by a plastic drop sheet to protect it from any spillover which could occur.

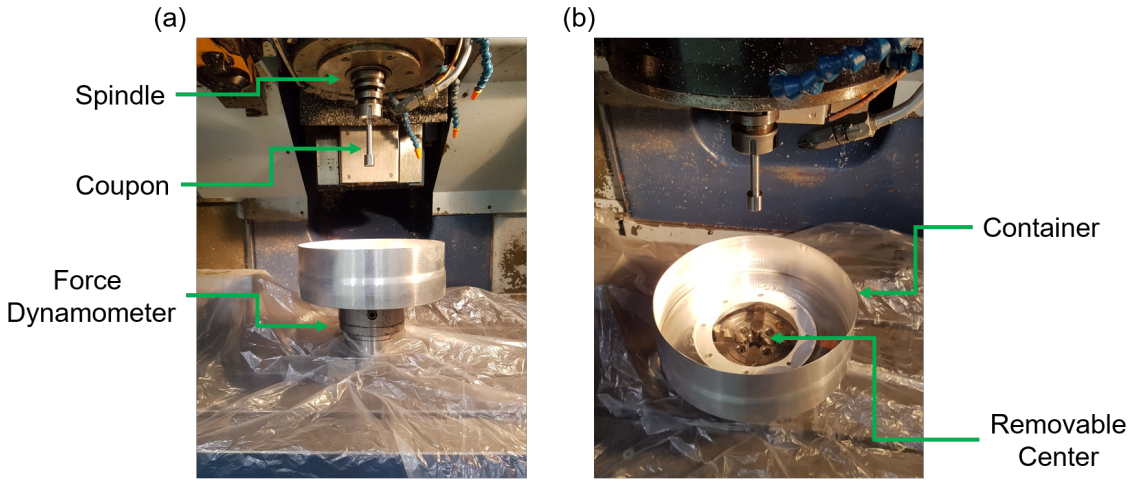

Figure 3.2: Dynamometer and Container Setup.

Ground mild steel rods were cut to 127 mm and turned down by an Okuma Crown-s, BB CNC Lathe. The coupons were turned down to reduce the chance of abrasive slurry spillover. Each coupon was measured to ensure that it was produced within a tolerance of 0.01 mm. Each coupon was 19.05 mm in outer diameter with a finishing surface of 20.00 mm. The raw stock material and finished sample are shown in Figure 3.3 The initial surface roughness of the samples were measured and only coupons with an initial Ra within 25 nm of the target 500 nm were used.

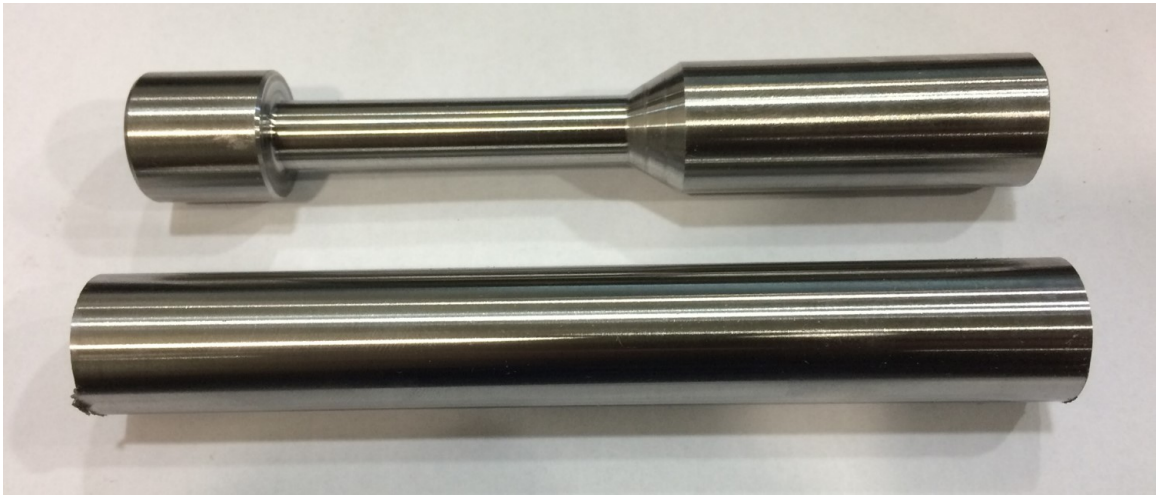

Figure 3.3: Undercut and Straight Coupon.

The coupons were made from mild steel which had the following material properties as specified by the manufacturer.

AISI 1045 Medium Carbon Steel Properties		
Hardness	21	Rockwell HRC
Hardness	229	Brinell HB
Carbon	0.420-0.50	Percent
Iron	98.51-98.98	Percent
Condition	Hot Rolled Cylindrical Ground	

Table 3.1: Coupon Properties.

To determine the surface roughness of the coupons before and after finishing a Mitutoyo SJ 201 Surface Roughness Tester was used. The coupon was marked on the opposite side of the finished section as shown in Figure 3.4. This marking was aligned with an indent in the sample holder to ensure the same surface was measured throughout the experiments. The hand held unit was placed on a holder which lined up both the center of the coupon with the stylus and referenced the middle of the

coupon. These components were placed on a ground flat surface to ensure the coupon and the stylus axis were aligned.

There are many ways to classify surfaces. The arithmetic mean of the magnitude of the deviation of the profile from the mean line (Ra) is the most used and universally recognized parameter [64]. Because it is the most widely used and applicable to ground surfaces Ra was chosen as the primary roughness measurement unit for this work. This method finds the mean line of the profile and averages the distance from the mean line to the absolute value of measured points on the surface. As specified in ISO 4278-1996, Ra can be calculated by the following formula:

$$Ra = \frac{1}{l_r} \int_0^{l_r} \mid z(x) \mid dx \tag{3.1}$$

l_r = Measured Distance

z(x) = Height of Profile

The resolution of the hand held surface roughness tester was 10 nm and was tested for repeatability and accuracy against a supplied Mitutoyo standard.

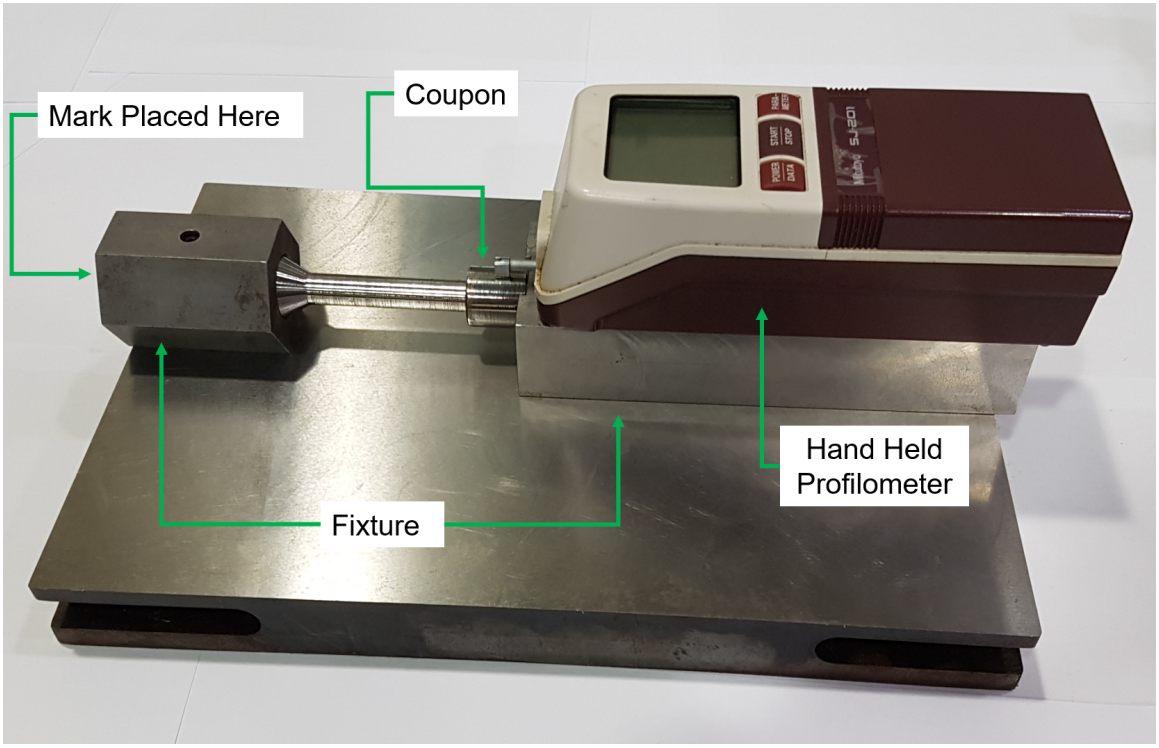

Figure 3.4: Surface Roughness Measurement Fixture.

The hand held unit was also tested against a calibrated surface roughness standards set produced by Flexbar Set No. 16008. These samples were produced from solid electro formed nickel to ANSI-B-46.1-1985 specifications. This standard allows for a maximum deviation from the nominal value specified of 6 percent. Four measurements per standard surface were taken and averaged. The results shown in Figure 3.5 show that the surface roughness tester provided accurate readings within 10 percent of the calibration samples roughness which was assumed to be adequate for this work.

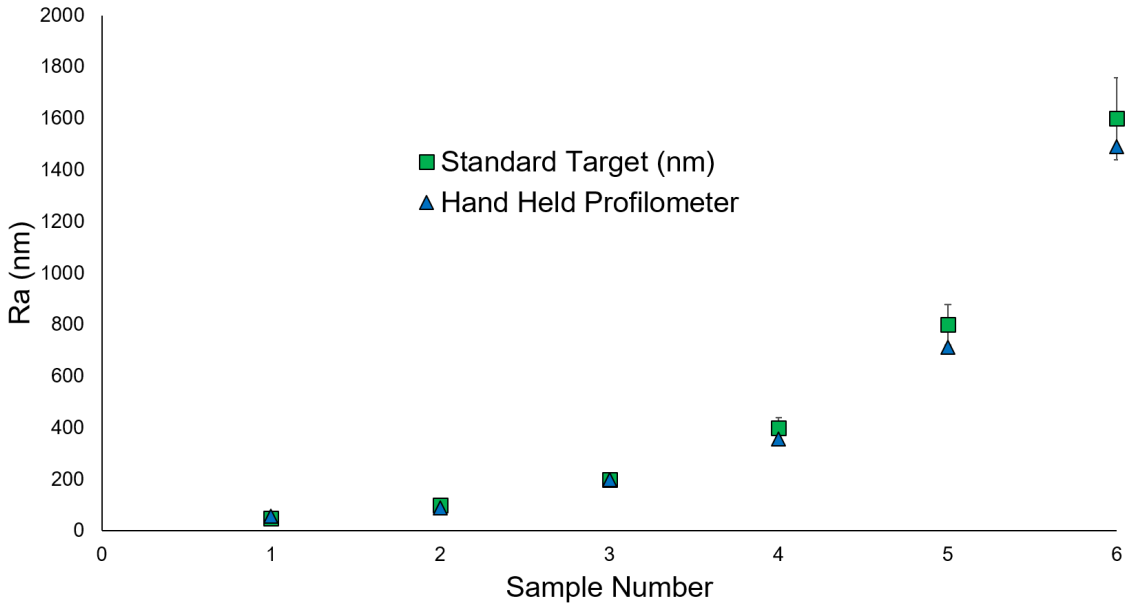

Figure 3.5: Mitutoyo SJ 201 Calibration Test.

To study the effects of various boundary conditions, three boundary set-ups were used. The first shown in Figure 3.2 was a single boundary container. The second, shown in Figure 3.6, was a double boundary setup. The double boundary setup had a gap of 32 mm. This allowed the coupon to have a 6.5 mm gap on either side while orbiting unless otherwise stated. The third boundary set-up, shown in Figure 3.6, was formed by using the double boundary setup and adding a blockade. The blockade was clamped securely and provided a 1 mm gap between the coupon and the aluminium block when the coupon was translated to the end of its path. The sides of the blockade were sealed with foam adhesive weather stripping.

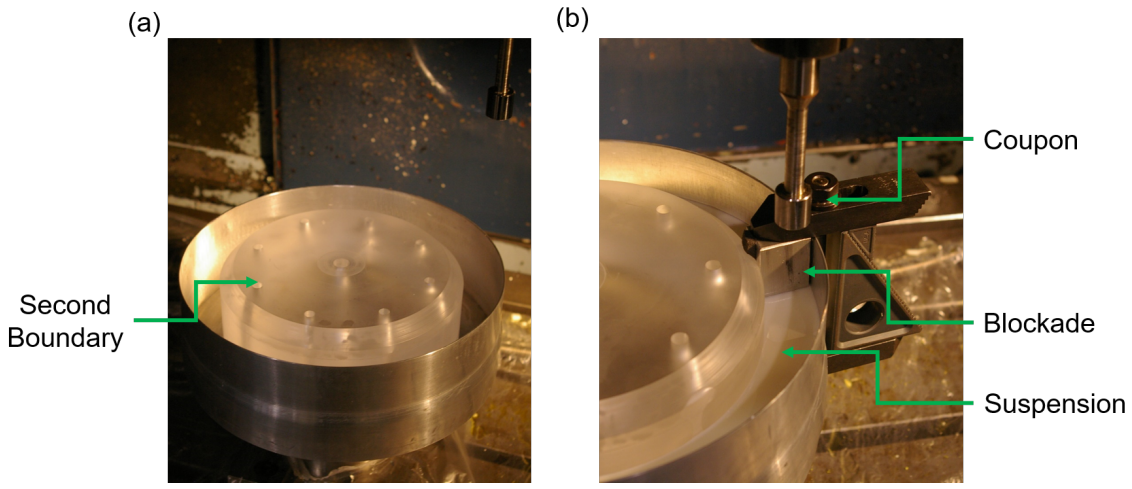

Figure 3.6: Various Geometric Boundary Conditions.

Typical force signals for an orbital motion in the setup described in Figure 3.6 are sinusoidal waves in the X and Y channel. This is because the force is normal to the coupon's path. A typical force signal can be seen in Figure 3.7.

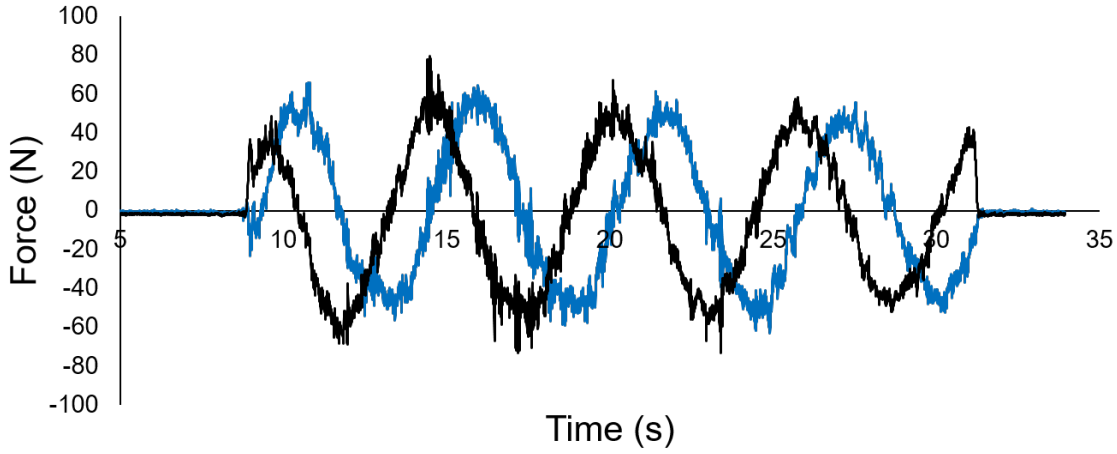

Figure 3.7: Typical Force Signal Vs. Time

A useful tool to compare sinusoidal curves is to calculate the RMS (root mean

square) value of the voltage. This allows direct comparison of multiple signals and simplifies the complexity of data analysis. The RMS value is calculated by the following formulae:

$$V_{rms} = \sqrt{\frac{\sum_{i=1}^{n} v_i^2}{n}} \tag{3.2}$$

$$n = \frac{F_h z}{T_c} \tag{3.3}$$

v_i = Raw Voltage

n = Number of Samples

$F_h z$ = Sampling Frequency

T_c = Time Constant or Window Size

In order to calculate RMS values from raw force signals an appropriate time constant must be determined. A segment of force signal was taken while the coupon was orbiting at 8 m/min and rotating at 1500 RPM in a 52.5 weight percent cornstarch slurry. The force signal, shown in Figure 3.7, was used for this test. Five RMS values were calculated using equation 3.2 while varying the time constant. The start times for each segment were started 10 percent of the window size after one another. This was done so that there would be no overlap between each window. The five samples were then averaged and the variance between the five was calculated. The results of this can be seen in Figure 3.8. It can be seen that the variance significantly decreases when a 2 second window size is used. This window size was adopted and kept constant for all force measurements for the entirety of this work.

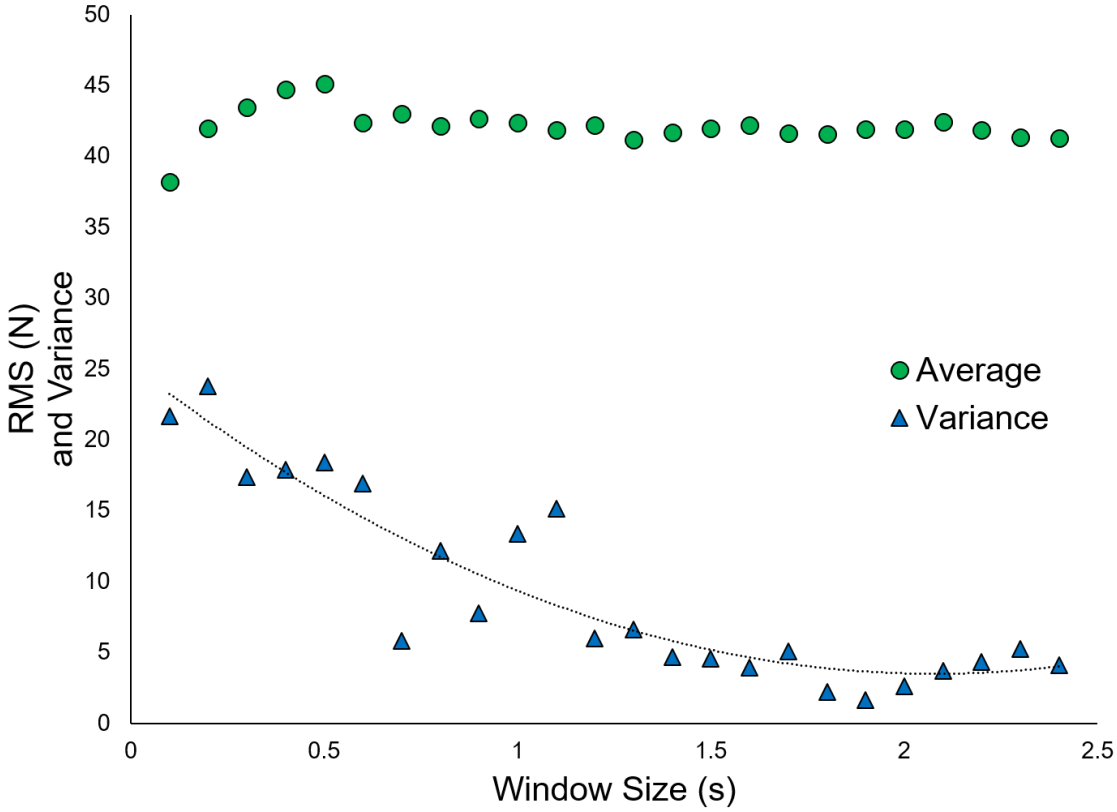

Figure 3.8: Window Size Vs. Variance for 5 Samples.

To ensure that the fluids were properly mixed a tumbler was used. The tumbler, shown in Figure 3.9, had a maximum capacity of 3.5 litres or 8 kilograms and a maximum tumbling speed of 100 RPM. The tumbler had a variable direction mode which changed tumbling directions in intervals specified by the user. When mixing the slurries, it was observed in preliminary equipment tests that the slurry would not mix at a high RPM. The slurry would be held to the drum via centrifugal force and failed to tumble. It was found that 42 RPM allowed proper tumbling and adequately mixed the fluid. All fluids were mixed at this speed.

Figure 3.9: Hexagonal Drum Brass Tumbler.

3.3 Preliminary Finishing Experiments Setup

The initial finishing experiments were all performed with a single boundary condition. The samples were first cleaned with acetone and an initial surface roughness reading was taken. The samples then were marked and placed in the coupon holding fixture, shown in Figure 3.5, to ensure that the same general location was measured each time. After measurement, the coupon was held by a 19.05 mm ER-32 collet and placed in the spindle of the CNC milling machine.

The fluid was mixed with a 50 percent cornstarch to distilled water ratio measured by weight. The cornstarch used in all experiments was Fleischmann's Canada Corn

Starch. Abrasives were added to the mixture at 15 percent of the total cornstarch water mass by weight. To calculate the mass percentages the following formula can be used

$$CS_{\%} = \frac{CS_m}{CS_m + W_m} * 100\% \quad A_{\%} = \frac{A_m}{CS_m + W_m} * 100\% \tag{3.4}$$

$CS_{\%}$ = Cornstarch Percent

CS_m = Cornstarch Mass

W_m = Water Mass

$A_{\%}$ = Abrasive Percent

A_m = Abrasive Mass

400 grit white aluminium oxide abrasives supplied by White Abrasives had an average particle size between 16.3-18.3 microns and a Moh hardness of 9. Tables 3.2, 3.3 show the physical and chemical properties of the aluminium oxide used. This information was provided by the supplier.

Grit Size	50 % Value		Type
	Min (micron)	Max (micron)	
100	106	150	Brown
220	45	75	Brown
400	16.3	18.3	White
600	8.3	10.3	White
1200	2.5	3.5	Brown
Determined According To DIN 69 101			

Table 3.2: Abrasive Particle Size.

Chemical Composition	Brown Aluminum	White Aluminum
Colour	Dark Brown	White
Hardness (Moh)	9	9
Bulk Density (Kg/m^3)	2400	2400
Particle S.G	3.92	3.92
AL2O3	95.00%	99.30%
Fe2O3	1.00%	0.04%
TiO2	3.00%	0.07%
Si02	0.72%	0.07%
CaO	0.30%	0.04%
Na2O	0.00%	0.48%

Table 3.3: Abrasive Chemical Composition.

The fluid was mixed for a minimum of 30 minutes in a tumbler shown in Figure 3.9. The tumbler was set to 42 RPM and changed tumbling directions every minute as described in 3.2. The fluid was then checked for consistency and, if necessary, the tumbling process was repeated. When the fluid was properly mixed, it was placed into the single boundary container. The container was centred on the torque dynomometer as specified in section 3.2. The fluid was poured to a 40 mm height so that the coupon head was fully submerged.

Coupons were then finished first in a stand still location 6.5 mm from the boundary wall at various speeds for intervals of 2 minutes as shown in Figure 3.10 (a). After 2 minutes the sample was removed from the collet and the surface roughness (Ra) was measured. Before measuring the coupon, it was first placed in an ultrasonic cleaner for 20 seconds. The ultrasonic cleaner proved to be effective for removing the abrasives from the coupon which would otherwise damage the surface during measurement. The coupon was then rinsed with acetone to remove any remaining debris or residues and dried with a lint free wipe. The coupon was measured 6 times in the area marked on the back of the coupon described in section 3.2. The coupon was then placed back in the collet and finished for another 2 minutes. This process was repeated for three

RPM's for a total finishing time of 10 minutes per sample.

Coupons were also finished in an orbiting motion, shown in Figure 3.10 (b), with the same procedure as before while keeping the spindle speed constant at 1500 RPM. The orbit speed was varied from 4-10 m/min while keeping the polishing interval within 2.5 percent of the stand still experiment. The polishing interval was controlled through the number of orbit cycles.

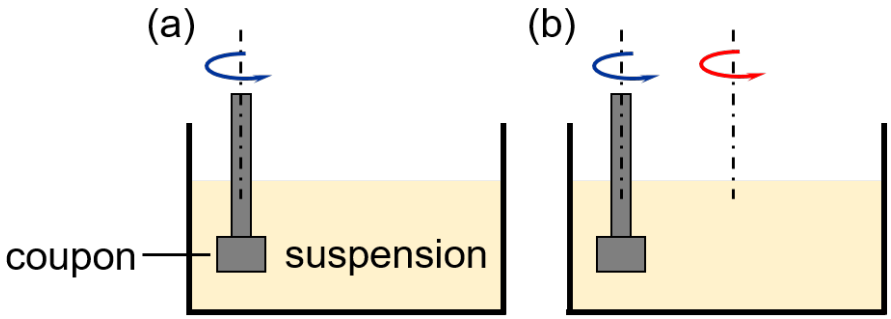

Figure 3.10: Stand Still Vs. Orbiting Motions.

Then, coupons were finished in an orbiting motion varied from 2-10 meters per minutes in a total interval of 10 minutes. The coupons were cleaned and surface roughness was measured before and after finishing in the same manner as stated before. The forces were measured during these experiments by the dynamometer.

3.4 Dynamic and Abrasive Experiments Setup

The effect of various dynamic aspects of the fluid was studied. For these experiments a mixture of 52.5 percent cornstarch was used in both double or single boundary conditions. Each experiment kept the fluid height at 40 mm as before to remain consistent. When studying the effect of multiple parameters, the tests were performed

in a random order. First the effect of gap size and boundary condition were studied. Figure 3.11 shows the general idea of a double boundary where Figure 3.6 (a) shows the exact double boundary used.

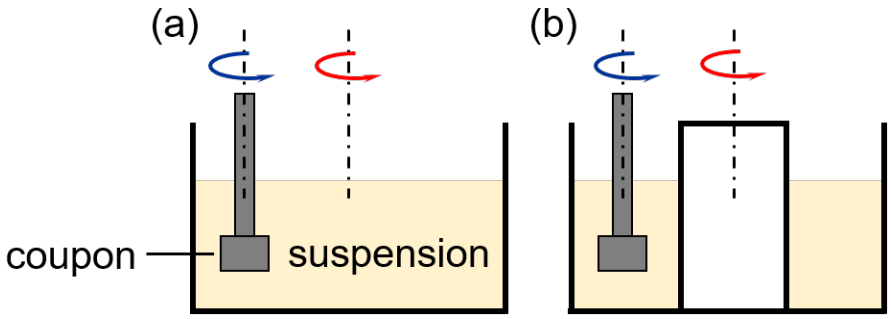

Figure 3.11: Single Vs. Double Boundary Conditions.

Other boundary conditions and variables were also considered and tested. The primary input factors tested were effects of the gap between the coupon and container, RPM, orbit speed, spindle and orbit rotational orientations, cornstarch concentration, coupon translational path, abrasive concentration, and abrasive grit size.

3.5 Finishing Experiments Setup

To test the finishing capabilities of the novel slurry, various input parameters were selected to be tested. The first was the abrasive grit size, second was boundary and path dependency, and third was orbit speed and mid process parameters. The experimental process was kept constant with that described in Section 3.3 except that the finishing time was varied.

An additional setup was used to test the effect of a linear channel. The goal of this setup was to reduce and eliminate slurry spillover. This setup was created from 6061

aluminium and was bolted to the inside of the original single boundary container. The channel cut into the aluminium had a length of 150 mm and a width of 32 mm. The corners had a radius of 9.5 mm to match the coupon radius. The setup can be seen in Figure 3.12.

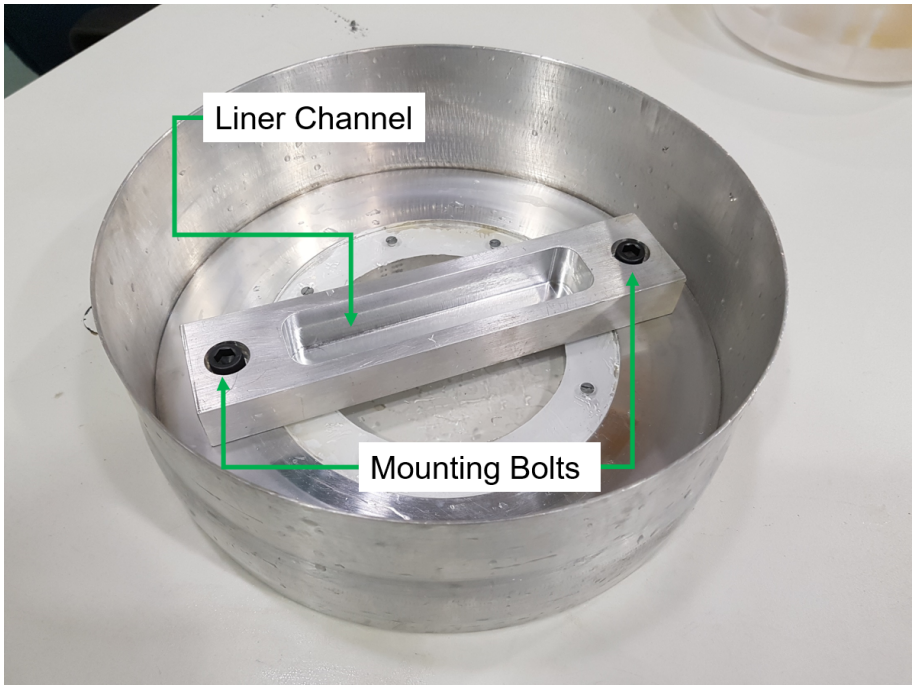

Figure 3.12: Linear Channel Setup.

These experiments were used to provide a proof of concept for free abrasive dynamic shear jamming finishing and show potential for use spindle finishing.

Chapter 4

Results and Discussion

4.1 Preliminary Finishing Experiments

The first step to exploring the potential of this novel finishing media was through preliminary finishing experiments. The goal of these experiments was to provide a proof of concept and to test the experimental setup. The experimental conditions were chosen to activate the shear thickening mechanisms of the fluid. Because the coupon and container are different than the geometry of a rheometer, the coupon was not placed in the center of the container. The apparent shear rate, in this case, is not easily calculated. The coupon and the external wall were assumed to be infinite flat parallel plates as depicted in Figure 4.1 (b).

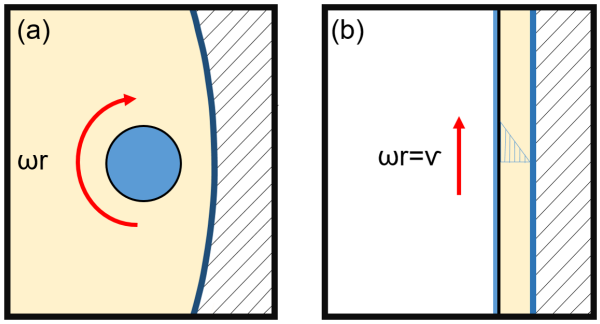

Figure 4.1: Shear Rate Assumption

This basic assumption was that the shear rate can be defined by the maximum tangential surface velocity of the coupon and the minimum gap between the container and coupon. Using this assumption the shear rate can be calculated with the following formula:

$$\dot{\gamma} = \frac{v}{h} \tag{4.1}$$

where the velocity v is the tangential velocity of the coupon and the distance h is the gap size. In this case, the velocity was varied from $0.050, 0.50, 1.5$ m/s with a gap size of 6.5 mm resulting in shear rates of $7.7, 77, 231\ s^{-}1$. These shear rates, according to Figure 2.14, correspond to the regimes before, during, and after shear thickening.

Results from the first test, in Figure 4.2 (a), show that while the coupon was rotating in place, the RPM did not significantly change the surface condition of the workpiece. There was a variation in the surface roughness as the initial sample was not fully uniform and the location repeatability of these tests was on the order of 1 mm. This variation was common in the coupons before finishing. The trend does not show much, if any, reduction in roughness in this time frame. This was not expected

as an increase in RPM would increase the shear rate which should thicken the slurry. Because RPM alone did not show a change in Ra, another motion was introduced.

In Figure 4.2 (b) the finishing performance seems to have a significant increase as the coupon is translated through the media. Furthermore, the increase seems to be positively correlated with the rate at which the coupon translates.

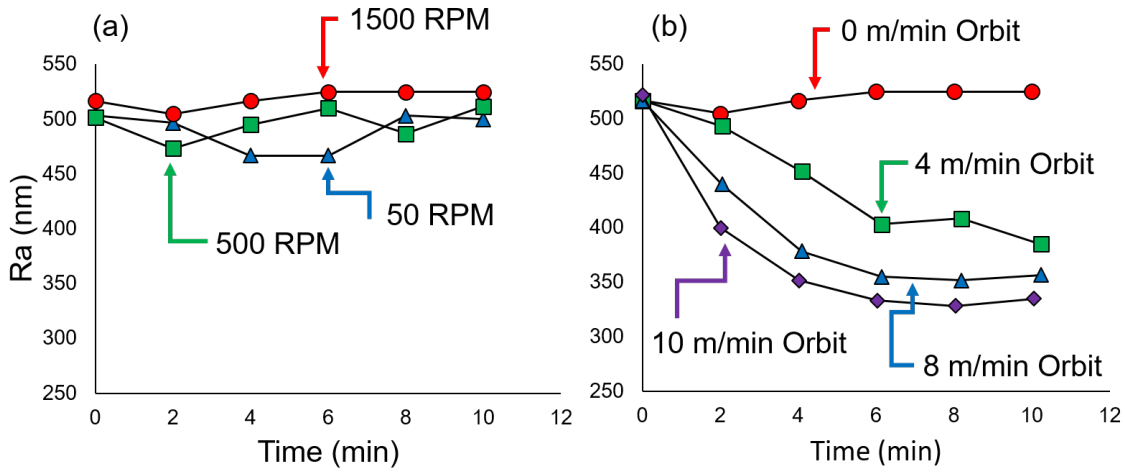

Figure 4.2: Ra Vs. Time for (a) Coupon Rotating in Place (b) Coupon Rotating and Orbiting

Further investigation into the relationship between the orbiting velocity and the finishing performance was performed through measuring the resultant forces. This was achieved through calculating the RMS force normal to the orbiting direction as described in section 3.2. Here the finishing performance is captured by measuring the change in Ra after 10 minutes of finishing. The starting roughness was kept constant at 500 nm. Only samples with this starting Ra were chosen. The results, shown in Figure 4.3 (a), shows a positive linear correlation between finishing performance and normal RMS force. This agrees with Preston's equation described in section 1.2.

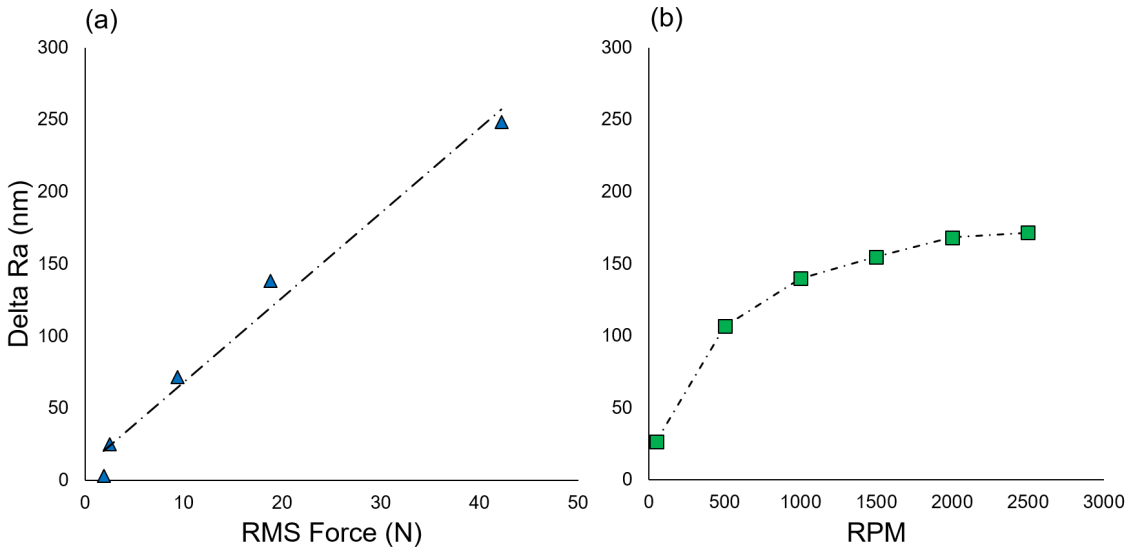

Figure 4.3: Change in Surface Roughness after 10 minutes for (a) Increasing RMS Normal Force (b) Increasing RPM

To determine the pressure applied to the coupon, the projected area of the coupon must be determined. Figure 4.4 shows the dimensions of the coupon. The total area which moves through the fluid is a combination of the coupon finishing surface and the coupon stem. The area of the finishing surface is 381 mm^2 and the stem 180 mm^2. The total combined area is 561 mm^2. The highest force observed in Figure 4.3 was 42 N which makes the maximum stress 75 kPa. This is higher than the stress required to support a human being [51]. This implies that the mechanism for thickening is beyond the shear thickening regime and likely in the shear jamming regime.

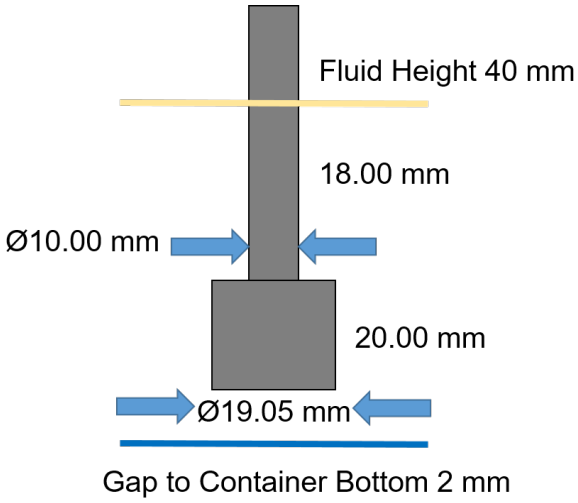

Figure 4.4: Coupon Dimensions

In Preston's equation, described in section 1.2, a linear response to normal force is expected. Preston's equation also specifies that the relative velocity between abrasive and workpiece should yield a linear relationship. In these experiments, the coupon RPM is responsible for the relative velocity between coupon and abrasive. To explore this further an experiment was performed varying the coupon RPM while orbiting. This is different from Figure 4.2 (a), as RPM was varied but did not have sufficient normal force for finishing. The results are shown in Figure 4.3 (b). Here it can be seen that the finishing performance is positively correlated to RPM but is not linear. This indicates that the RPM is important when an orbit is present but not significant without an orbit. This is important for further experiments as both the coupon RPM and linear velocity must be sufficient for finishing to occur. In rheological studies, it has been shown that high rotational velocities induce wall depletion which causes slip to occur [46]. This slip causes a relative velocity between the abrasive media and the workpiece surface. The relative velocity is required for finishing to occur. The steep

increase in finishing performance at low rotational speeds could indicate the point at which slip occurs. Another important discovery is that there is almost no discernible increase in performance after 2000 RPM. It has been stated that Preston's equation is not valid for all velocities [2]. It could be that 2000 RPM is too high for the model to relate. Studies in chemical-mechanical finishing have also found this trend at high velocities [65]. This could be due to a variety of causes including the formation of hydrodynamic lubrication between abrasive and workpiece or local shear thinning of the carrier fluid.

From these two experiments, the finishing performance is clearly related to the normal force exerted on the coupon and the velocity of the coupon translating through the media. To study the kinematics of shear jamming fluid, studies without abrasives were performed initially. This was done to first study how the fluid responds to the drag finishing setup and relate the trends to that found in literature. The effect of adding abrasives was then studied and compared with the performance of just the fluid.

4.2 Dynamic Experiments

From tests driving various objects such as spheres and cylinders through dense particle suspensions, one important interaction is that between fluid and boundary [60], [58]. Typically forces observed are higher when the suspension is confined. To study the effect of various boundary conditions an experiment was run to compare a single boundary verses a double boundary condition. The single and double boundary set-ups are shown in section 3.2. This was done by testing the same fluid composition in both a single boundary and double boundary condition varying the gap between the

coupon and the outer wall. The gap is dictated as the distance between the surface of the coupon and the outer wall of the container as per Figure 4.5.

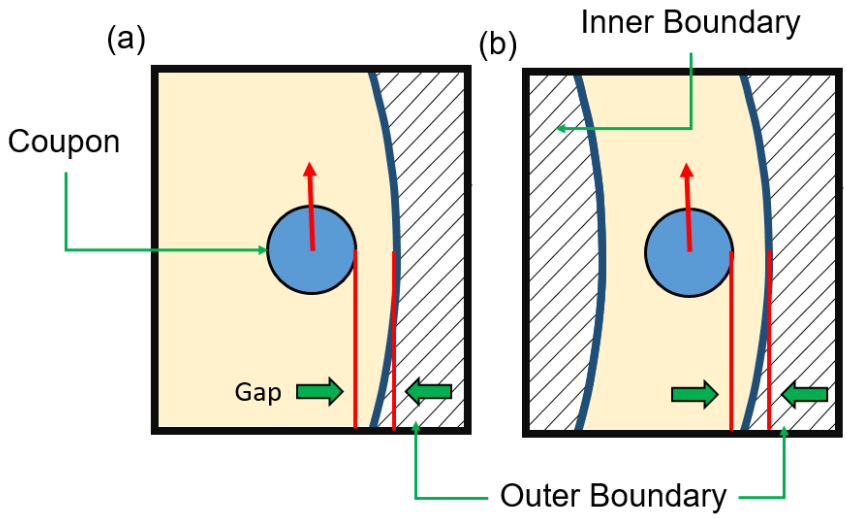

Figure 4.5: Single Vs. Double Boundary Gap Diagram (Top View)

Figure 4.6 shows that the RMS normal force has a negative slope as gap size increases for both single and double boundary conditions. The double boundary condition, however, provides a higher RMS force for all gap sizes studied. This indicates that the fluid is more sensitive to the presence of a second boundary than to the proximity to a single boundary. The gap size and the rotational velocity dictate the shear rate as per equation 4.1. In this experiment, the rotational velocity was kept constant at 2000 RPM and the orbit velocity was 8 m/min. An interesting phenomenon is that the double boundary sustained higher RMS normal force for all gap sizes. This indicates that shear thickening could not be the dominant mechanism driving the normal force. This experiment also shows an additional parameter to control during the finishing process. It is possible to either insert a second boundary during the rough finishing stage and then remove it to control the normal force or to

alter the gap to vary the normal force.

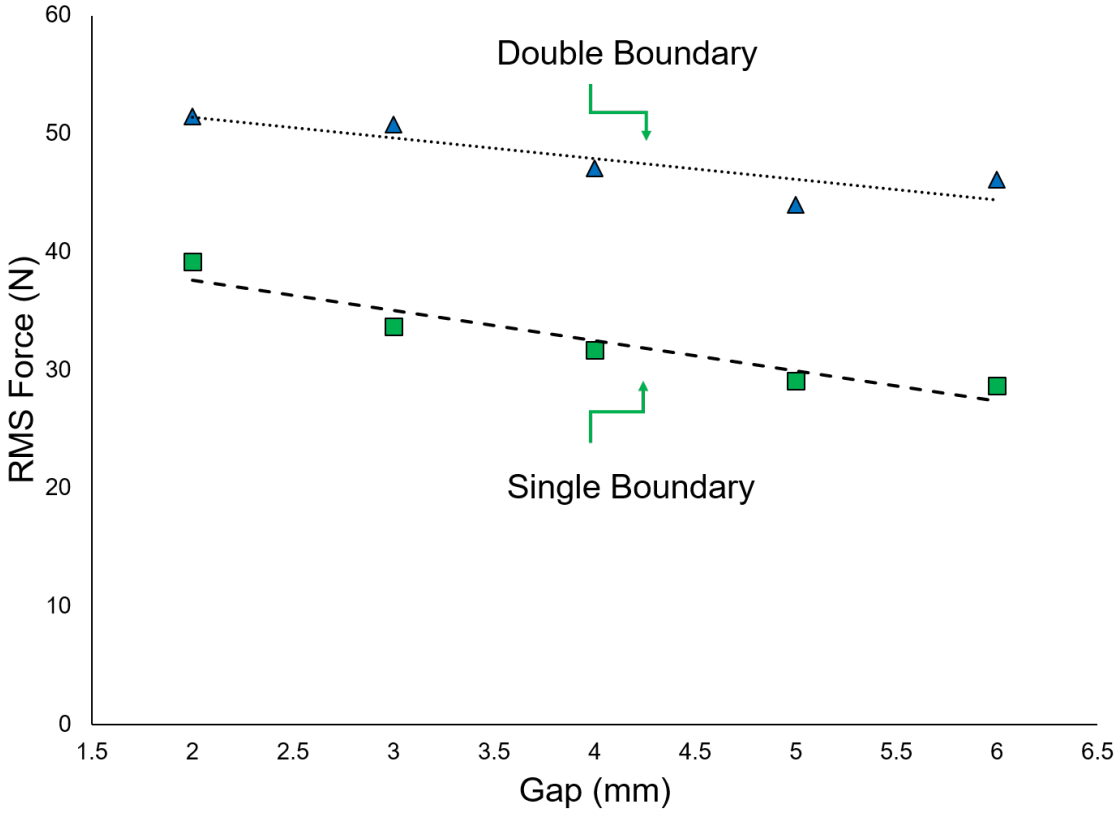

Figure 4.6: Effect of Gap Size Relative to Boundary Condition

To further study the interaction between various kinematic parameters on the normal force an experiment was run which compared two orbital speeds at various rotational speeds. The results can be seen in Figure 4.7. There is a slight negative correlation between rotational speed and normal force while there is a large difference between the normal force for the two orbiting velocities. This indicates that the RPM has only a slight effect on the normal force. This is interesting as the RPM also has a direct relationship to the shear rate yet does not seem to have a significant influence on the normal force. Both the gap and RPM do not seem to be as significant as orbit

speed and boundary condition.

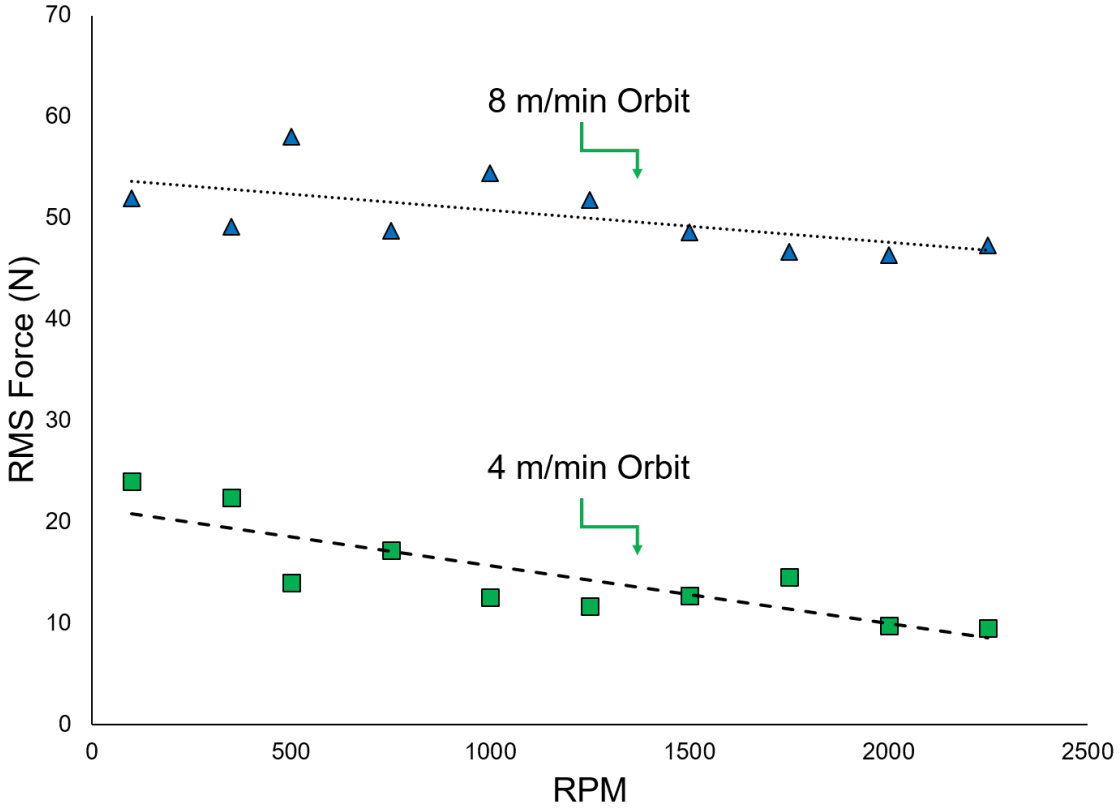

Figure 4.7: Effect of RPM Relative to Orbit on RMS Force

Since gap and RPM do not seem to be as significant as orbit speed or boundary condition, the mechanism for thickening could be shear jamming. Shear jamming requires an interaction between a driving force and a boundary. This was shown in a variety of studies including extensional rheology [62] and impact activated solidification [52]. An experiment was performed to test the interaction between the coupon's rotational direction and orbiting direction. This test was done to further confirm that the mechanism observed was jamming and not shear thickening. The spindle was first rotated clockwise with a counter clockwise orbit. The spindle direction was

then reversed as seen in Figure 4.8 (a)-(b). The experiment was then repeated in a clockwise orbit, as shown in Figure 4.8 (c)-(d), to confirm that the phenomenon was not influenced by other parameters and purely a function of direction.

When the spindle and orbit are in the same direction, the media directly in front of the coupon is jammed against the container boundary. This can be seen in Figure 4.8 (a) and (c). When the orbit or spindle are not in the same direction, the media is not jammed in front of the boundary, but rather the two motions increase the relative velocity between the coupon surface and boundary. This study was performed to test if the force response of the fluid was due to shear thickening or shear jamming. Figure 4.9 shows that the force while in a jammed state is significantly higher than the force in the sheared state. This also was very repeatable as reversing the orbit directly inverted the measured normal force. This trend is useful as it adds another method to control the force in finishing while using a single boundary. It is possible to rough finish in a jammed state then reduce the force by inverting the spindle rotation while keeping the orbit velocity constant. This added method to control force further simplifies industrial applications for this media. To change the finishing forces, the spindle rotation direction can be changed as well as changing the speed.

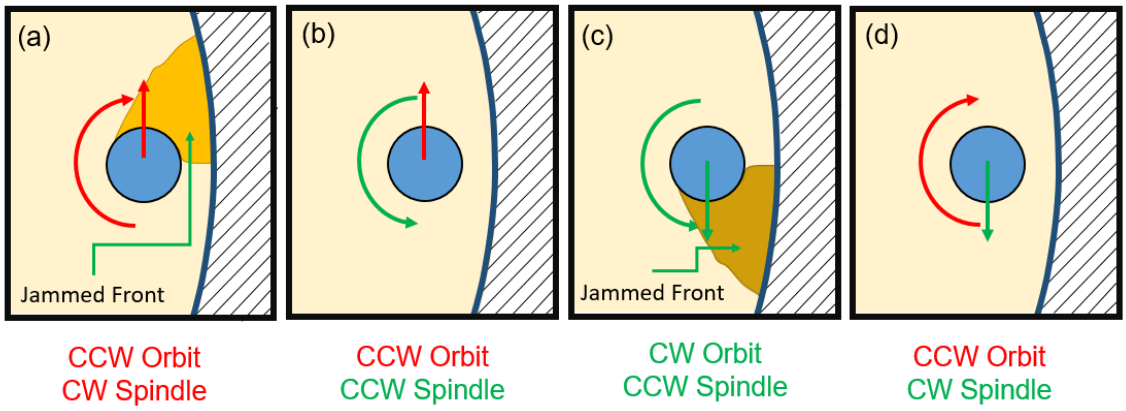

Figure 4.8: Spindle and Orbit Effect on Jamming

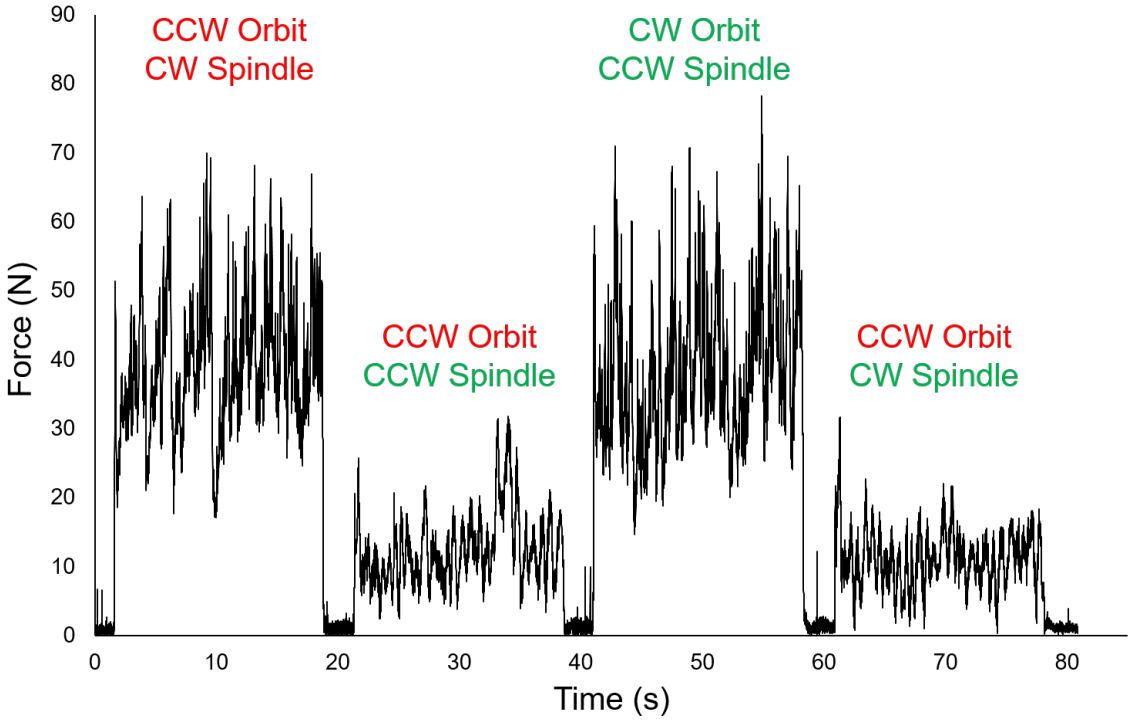

Figure 4.9: Force Signal For Spindle and Orbit Rotational Directions

One observation from studies where a rod impacts the surface of a cornstarch suspension showed that the texture of a jammed region changes from glossy and smooth to matte and rough [51],[60]. This was also observed in these tests. Figure 4.10 (a) shows the matte region which is directly in front of the rotating spindle while the rest of the fluid shows a glossy surface. This was also observed in Figure 4.10 (b) where the surface texture of the jammed region is clearly darker than the glossy unjammed area.

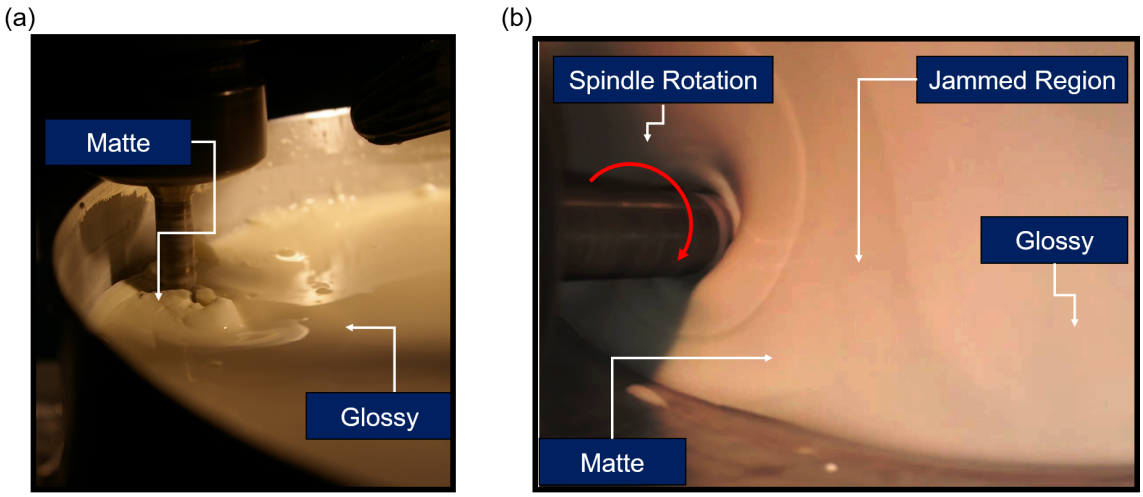

Figure 4.10: Observations of Dynamic Shear Jamming

The previous experiment only shows the trends present for a single boundary condition. If a double boundary condition exists, the jamming front can interact with either wall. A test was done to see if a double boundary configuration would change the force dependency on orientation. Figure 4.11 shows that the jammed state can happen on either the outward or the inner boundary. This also proves that the mechanism driving the increased normal force is jamming and not shear thickening. For an industrial application, this can be used to eliminate the normal

force dependency on spindle and orbit orientation if so desired.

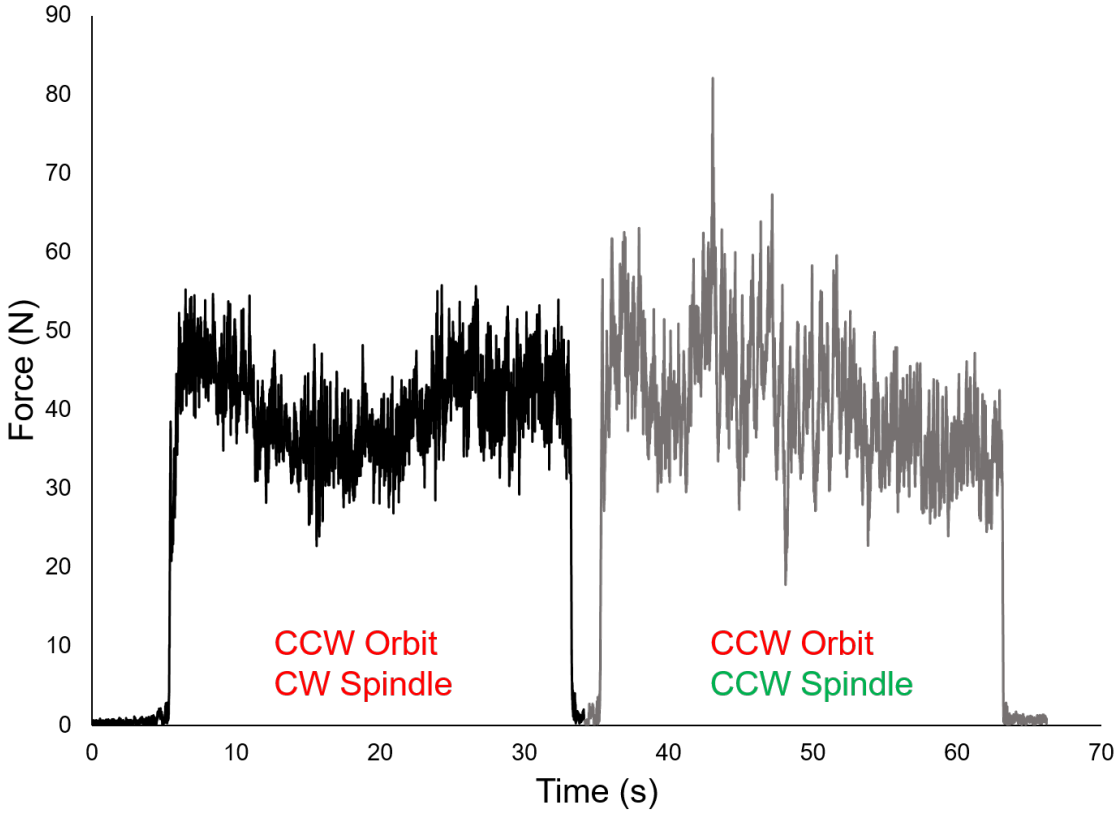

Figure 4.11: Force Signal For Jammed State In Double Boundary Condition

Because the mechanism appears to be shear jamming, the influence of cornstarch percentage was studied. The particle concentration has been heavily researched in terms of rheological studies. There seems to be a large change in viscosity as particle concentration increases past 50 percent by weight as seen in Figure 2.13. This has also been studied in terms of the jamming phenomenon. To achieve shear jamming, both adequate shear rate and mass fraction must be present [53].

An experiment was conducted to study the effect of the cornstarch percentage on RMS force for various orbital speeds. To perform this experiment, the orbital

speeds were varied in a random order while in a double boundary configuration. It was observed that the water content in the media would evaporate over long periods of time but yet required some time to achieve steady state. Figure 4.12 shows the force signal for 52.5 percent cornstarch varied over multiple orbit speeds and rotating at 1500 RPM. The fluid appeared to reach steady state within two minutes. To determine if evaporation was significant, and to study the repeatability of the process, the first orbital speed was repeated at the end of the experiment. After the two RMS normal forces were compared. It can be seen that the increase in force due to evaporation is within the variability of the signal for the 16 minute duration of this experiment.

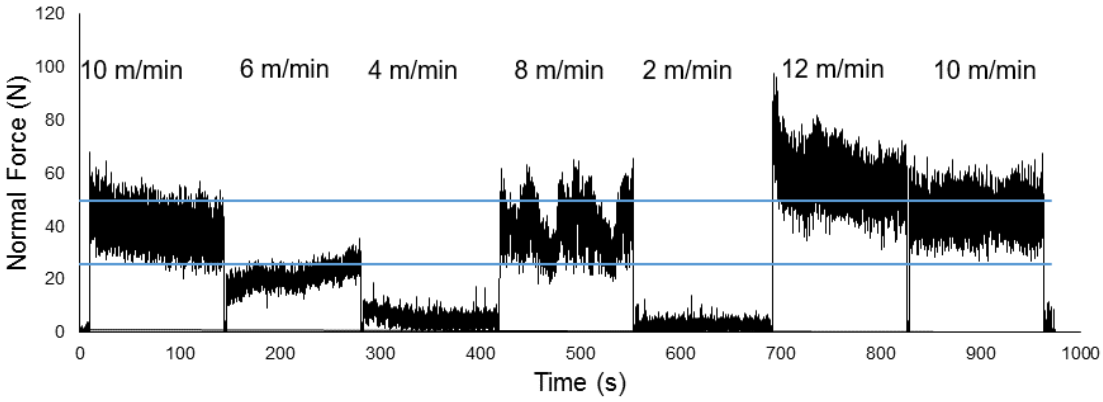

Figure 4.12: Normal Force Signal for Varying Orbit Speeds

Figure 4.13 shows that the normal force increases drastically as the cornstarch concentration is increased from 50 to 55 percent. This could be because adequate cornstarch particle concentration is critical to generating jamming fronts [53]. The increase in force does not seem to be discontinuous but rather fairly linear in regards to orbital speed. For this application, 52.5 percent cornstarch seems to have the

most favourable properties. The average standard deviation between the five RMS force measurements were 0.4 N for 50 percent, 1.9 N for 52.5 percent, and 4.0 for 55 percent. The average standard deviation underestimates the total variability in the force signal as the measurements have a 2 second window size. Figure 3.8 shows how window size reduces the variance in a signal.

Although the average standard deviation is an underestimation, the trend matches the raw force signal variability. Figure 4.12 shows that the variability in the force can be half the measured force. This is common to dense suspensions which is shown in Figure 2.16 [57]. It was also observed that orbital speeds over 8 m/min, at 55 percent cornstarch, would induce fluid spillover. The slurry in front of the coupon would jam and drive the fluid up the spindle and out of the container. When fluid is lost from the container, the weight percentage of cornstarch is unknown so 8 m/min was kept as the upper limit for this experiment.

The linear trend of 52.5 wt % and the relatively low variability in the force made this mixture ideal. For finishing applications adequate forces are required [26] and low variability is ideal. The force required is also shown in Figure 4.3. There the relationship between normal force and finishing performance yielded a linear trend. Due to these reasons a 52.5 percent mixture shows an ideal trend. The relationship between orbital speed and RMS normal force explains the results in the preliminary finishing experiments shown in Figure 4.2 (b). This correlates how an increase in orbital speed drove the normal force to increase which in turn is related to the total change in surface roughness over the 10 minute window shown in Figure 4.3 (a). This is in agreement with Preston's equation explained in Section 1.2.

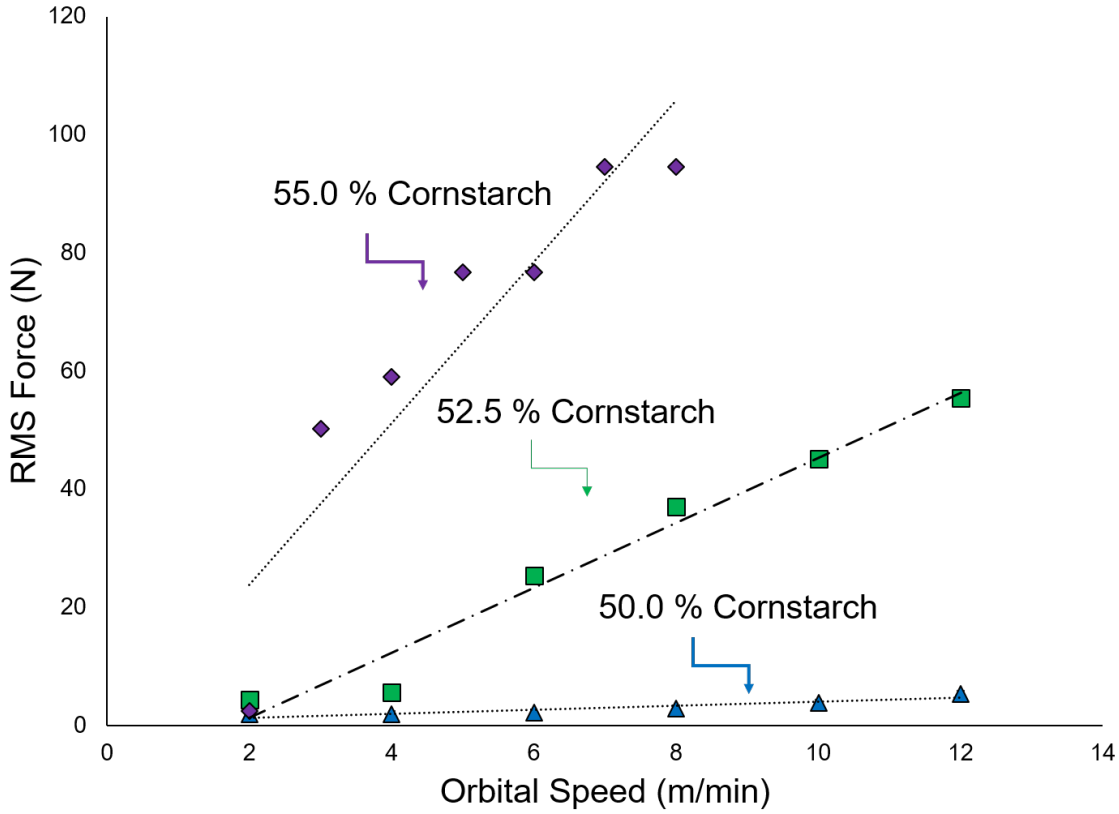

Figure 4.13: Effect of Cornstarch Percentage on RMS Force

The slurry has been shown to be sensitive to the boundary condition, orbit velocity, and direction. A test was performed to study the effect of various coupon paths. The coupon path changes how the fluid is either compressed or sheared. It has been shown that the force required to drive a sphere through a dense suspension increases 1000 times when a boundary is present [58]. It has also been observed that container size and fill height influence the spike in force when impacted [60]. From these studies two experiments were designed to study how boundaries affect the force response of the slurry. Figure 4.14 shows the two paths studied. Figure 4.14 (a) shows a coupon translating towards the outer boundary. This was to activate the

same mechanism shown while a sphere is driven towards a wall [58]. Figure 4.14 (b) shows a coupon translating through a blocked channel which both constrains the fluid between the coupon and boundary as well as the fluid's ability to translate perpendicular to the coupon's trajectory. These two set-ups are used to test the effect of multiple constraints in a jammed state.

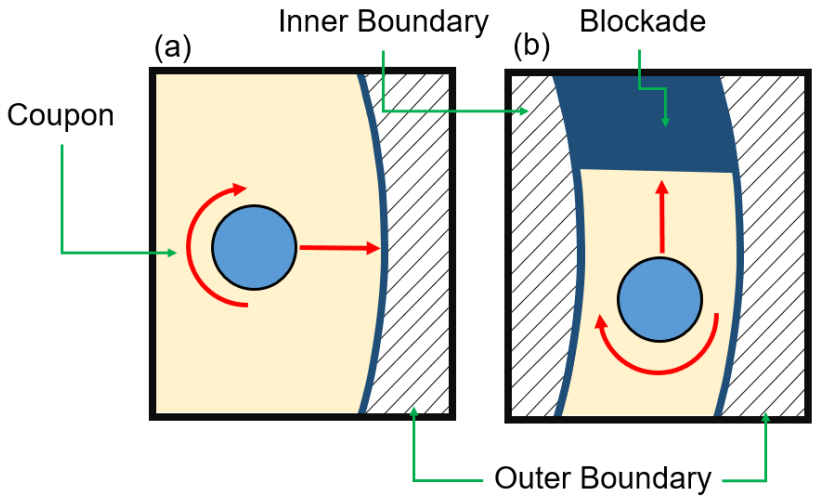

Figure 4.14: Constrained Boundary Vs. Channel Setup

Figure 4.15 shows the force signal when the coupon is translated towards a constrained plane with no perpendicular obstructions and stopped 1 mm before the wall. This was the same strategy as used in another study with spheres driven towards a boundary [58]. The spike in normal force occurred when the coupon approached the wall as expected. The resulting force spike is heavily dependent on translational velocity. When the coupon is translated faster than 2 m/min, the speed required for a jammed front to form is reached and a force spike is triggered. After 2 m/min the normal force spike seems to plateau. Something of interest are the fluctuations in force

before the jammed front is formed. They seem to only occur when the translational velocity exceeds 2 m/min. Fluctuations have been shown to occur when objects settle in dense suspensions [59]. It has also been shown that these oscillations are unique to cornstarch. The force fluctuations have also been observed when dense suspensions of cornstarch are impacted [60]. The fluctuations are expected to be caused by a solidification front reaching and interacting with a boundary [61]. The speed at which the solidification front translates through the suspension is a function of impact velocity [61]. This explains why in the 16 m/min result, many fluctuations are observed where the 8 m/min result shows less fluctuations. The solidification front generated at 2 m/min could be too slow to interact with the boundary and provide a force spike.

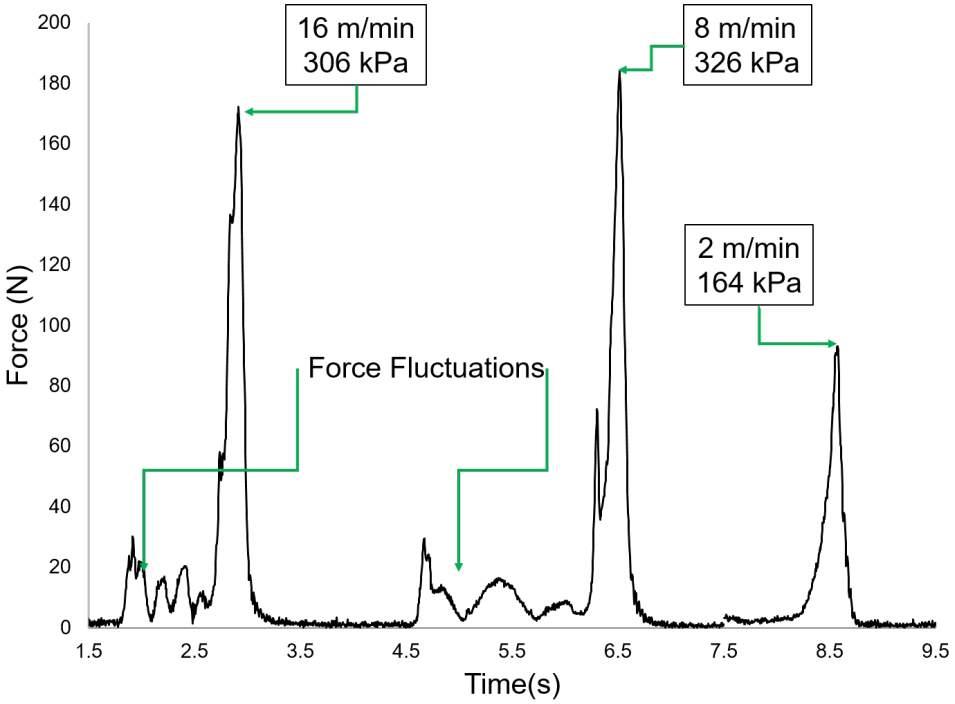

Figure 4.15: Effect of Constrained Plane on Force

The second experiment was performed with multiple geometric constraints as

depicted in Figure 4.14 (b). The force signals can be seen in Figure 4.16. The force had the same characteristic as seen in Figure 4.15 but the magnitude of the force is an order of magnitude larger. Again, the force was speed dependent with a dramatic increase in force after 2 m/min was exceeded. This experiment was performed at a finer resolution to show the increase in force around, and when, 2 m/min was surpassed. The fluctuations observed before were also present in this experiment. The primary difference between a single and a triple wall constraint was the magnitude of the force spike. In Figure 4.15, the maximum force observed was under 200 N. In Figure 4.16, the maximum force was over 1200 N.

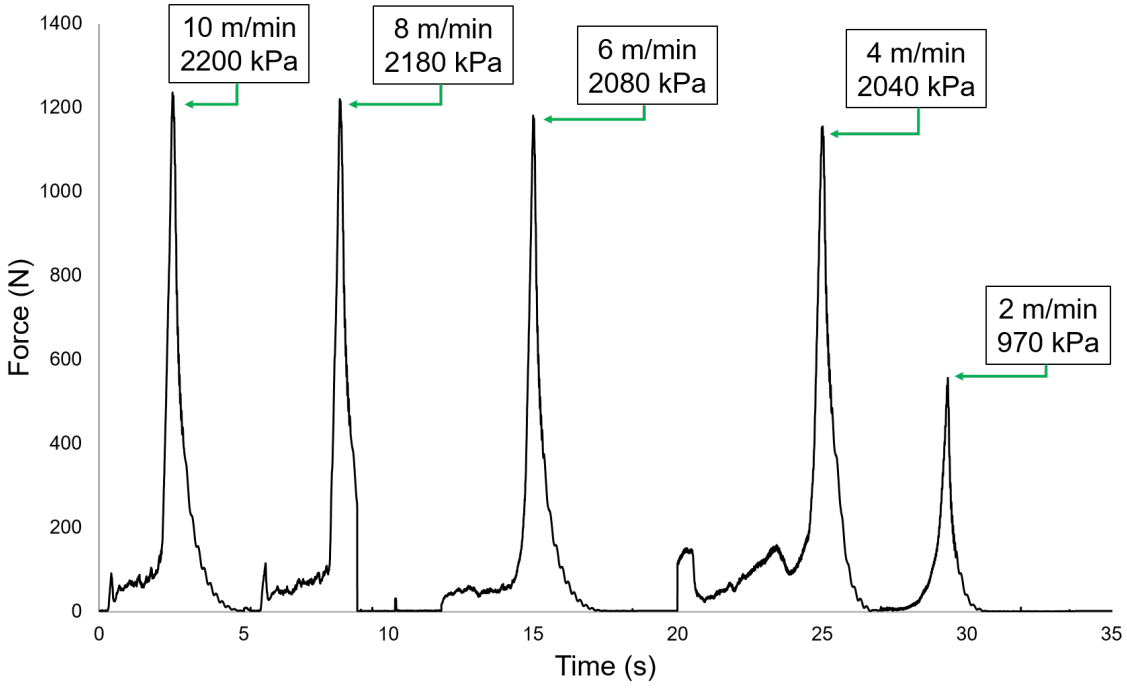

Figure 4.16: Effect of Constrained Channel on Force

From Figure 4.3 (a) finishing was linearly correlated to RMS normal force. To obtain and sustain a sufficient RMS force a path was created to repeatedly jam

the slurry between the coupon and the outer boundary. The path can be modelled from the following diagram. The path depends on how many scallops are performed per orbit. Here, in Figure 4.17 (a) a 8 scallop path is demonstrated. The circle radius is defined by the gap specified. For the sake of continuity between the linear experiments, a 1 mm gap was chosen. The arc radius is then calculated by the circle radius and the number of scallops specified.

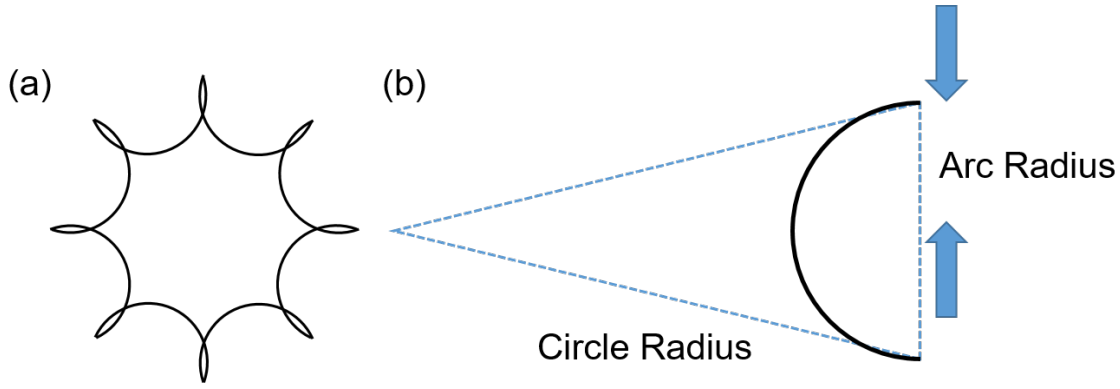

Figure 4.17: Scallop Path and Definitions

If a large number of scallops are performed, the maximum acceleration of the CNC milling machine becomes the upper limit of the feed rate. As the CNC milling machine had a digital readout of both the commanded feed rate and actual feed rate, the maximum speeds were determined experimentally. Figure 4.18 shows the effect of 30 scallops in a single pass. When performing 30 scallops in a single orbit, a maximum feed rate of 5 m/min could be achieved. Figure 4.18 shows the raw x and y channel force trends. The force trends are for a single orbit with 30 scallops. The force spikes correspond to each scallop performed while the sinusoidal trend shows the orbit motion. Their were 30 force spikes for a single oscillation.

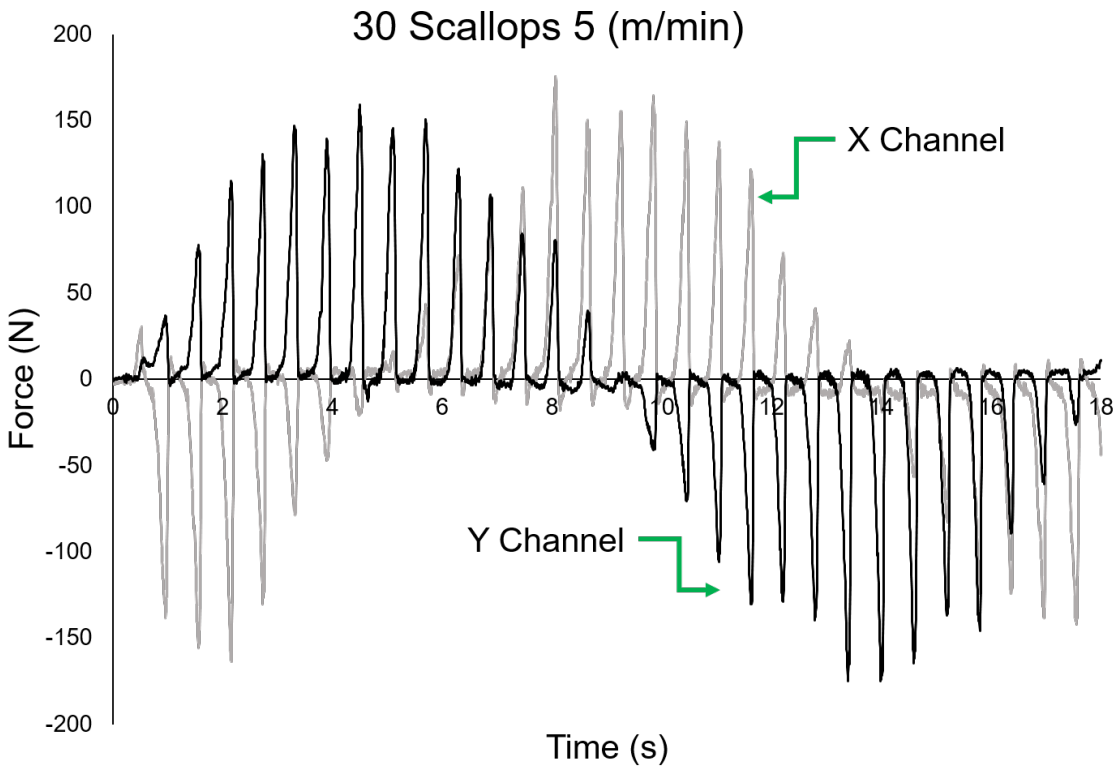

Figure 4.18: Effect of Multiple Passes on Constrained Plane

From Figure 4.19 the normal force was calculated and plotted in Figure 4.19. This shows multiple spikes ranging from 130 to 200 newtons. This range is similar to that found in Figure 4.15 indicating that the force spikes are readily repeatable. The primary constraint of this type of path is the maximum sustained RMS force. If a large number of scallops are performed, the maximum feed rate becomes the limitation. If a small number of scallops are performed, the time between force spikes limit the sustained RMS force.

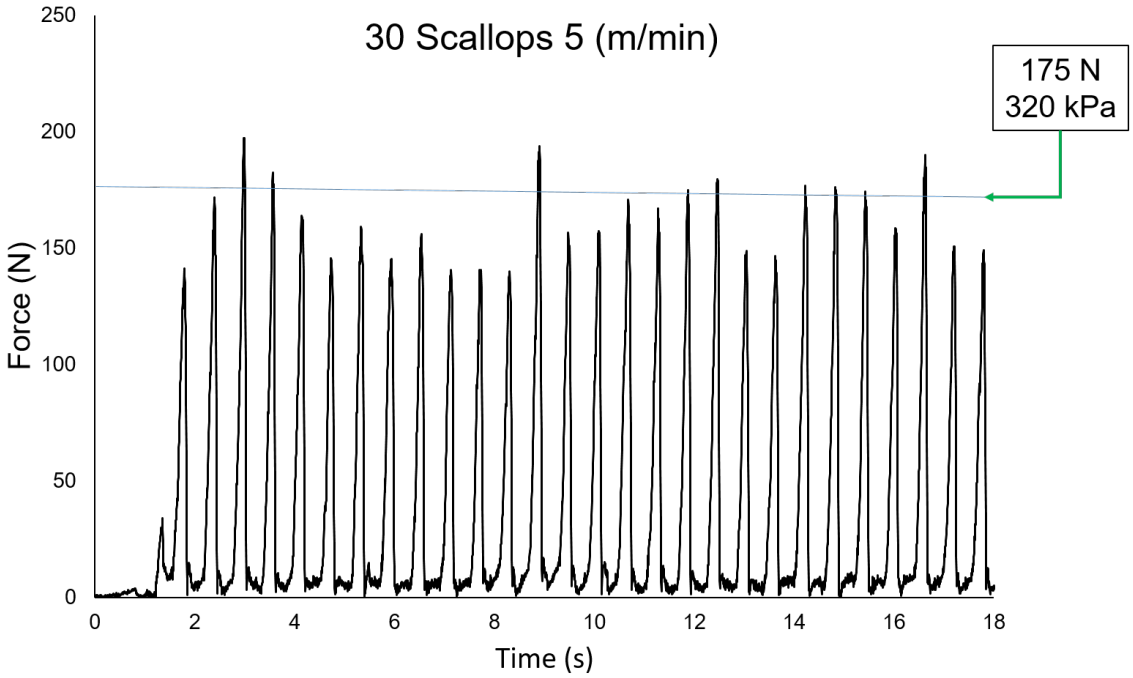

Figure 4.19: ABS Value of Multiple Passes on Constrained Plane

4.3 Abrasive Experiments

Since RMS force has an impact on the slurry's finishing capability, a study on the effect of adding abrasive to the cornstarch was performed. It has been observed in other studies that adding abrasives to shear thickening fluids changes the behaviour and response of the system [17]. It has been shown that adding silicon carbide abrasives to fumed silica dispersed in polyethylene glycol increases the initial viscosity of the suspension. It has also been shown that decreasing particle size can increase the viscosity [17]. It was observed in preliminary experiments that adding abrasives thickened the slurry. From Figure 4.13 it was found that a 52.5 percent mixture had

ideal properties for finishing. The cornstarch percentage was reduced to 50 percent to allow for some thickening to occur. Abrasives were added to this mixture and the RMS force was recorded for various orbital speeds while the spindle was rotating at 1500 RPM. The same methodology used in Figure 4.12 was used to perform this experiment. Figure 4.20 shows that the relationship between orbital speed and RMS force changes from a linear function to an exponential function. This could have multiple causes including a change in particle size distribution, increase of particle anisotropy, and change in friction coefficient between particles. The exact reason for this change in behaviour is currently not well understood. Adding abrasives to the 50 percent cornstarch water slurry clearly thickened the mixture. This is expected as the volume fraction ϕ_v increased. Although thickening is expected, the change from linear to exponential trends is noteworthy.

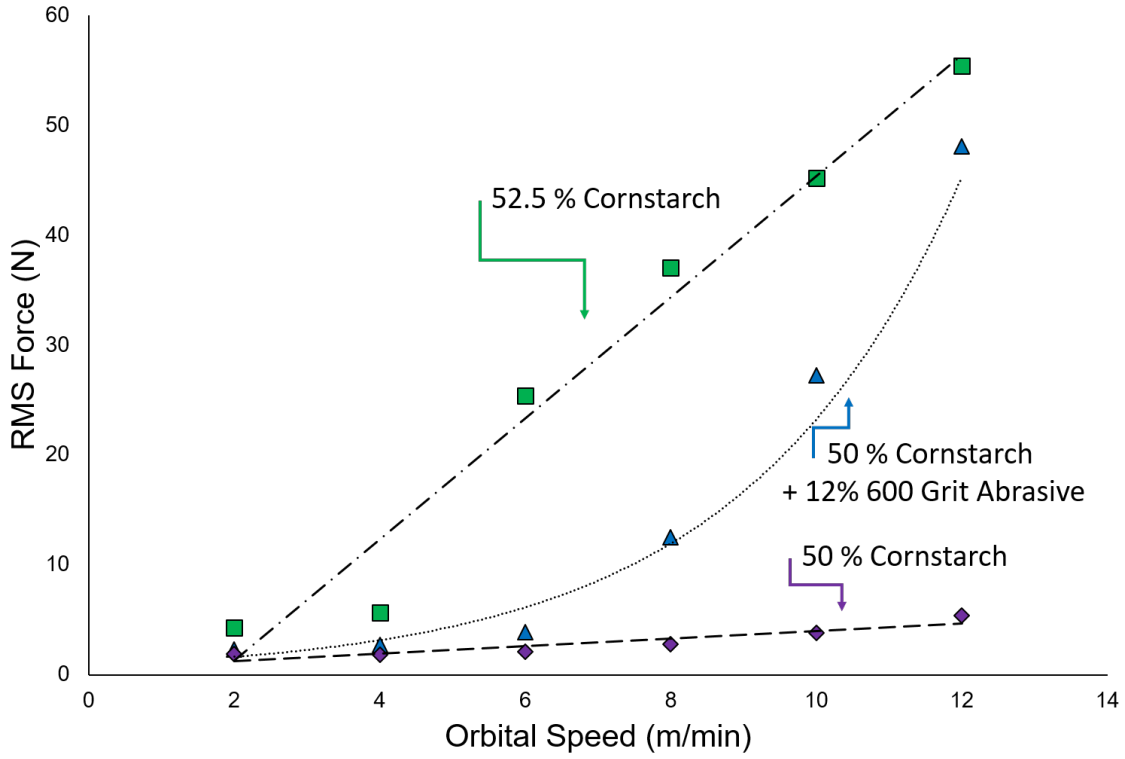

Figure 4.20: Effect of Adding Abrasives to Slurry on Force

To further study this phenomenon, the abrasive grit size was varied from 100 grit (128 μm) to 1200 (3.0 μm) grit and added to 50 percent cornstarch mixtures. The orbit speed was varied as per Figure 4.12 and the RMS normal force was measured. The results are shown in Figure 4.21. When the abrasive grit size was smaller than or equal to 400 grit (17.3 μm), the force increases exponentially with increasing orbit speed. The larger abrasive sizes, 220 grit (60 μm) and higher, show an initial increase in force but then plateau off after 10 m/min. This behaviour puts a constraint between the grit size and maximum force achievable. Slurries with 400, 600, and 1200 grit (17.3 μm, 9.3 μm, 3.0 μm)abrasives can deliver forces higher than 40 N at 12 m/min. This limits the range of starting surface conditions for a workpiece.

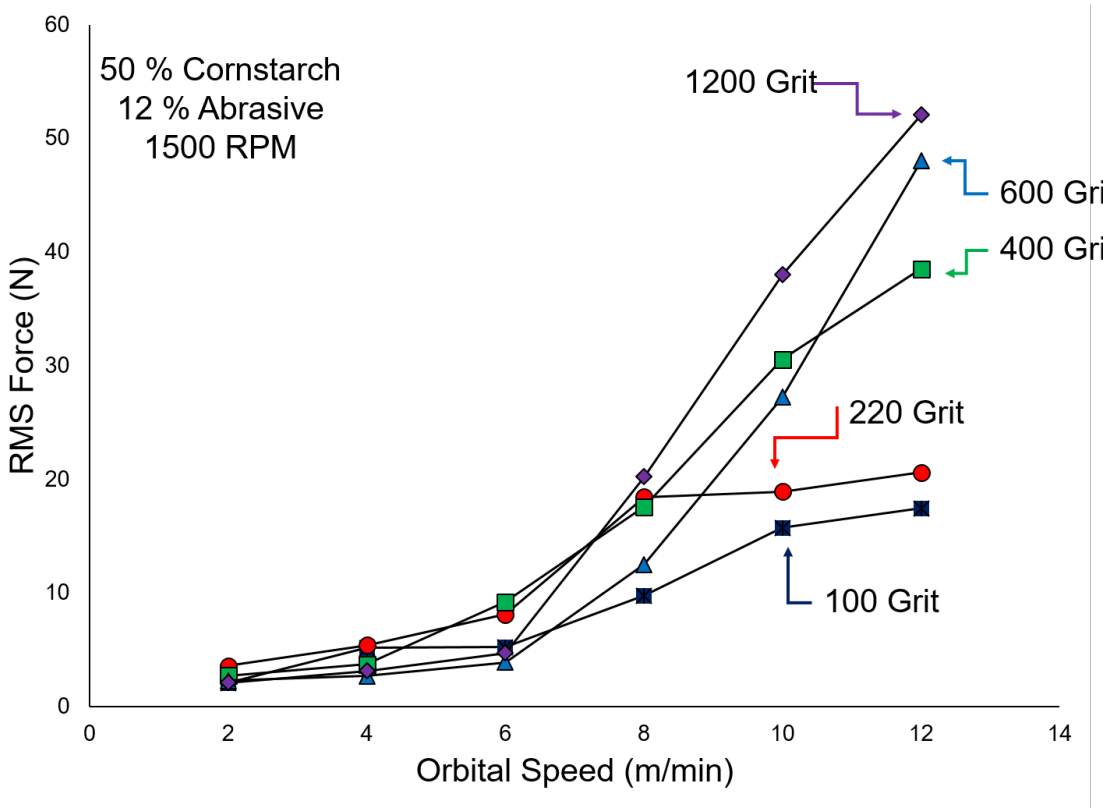

Figure 4.21: Effect of Grit Size on Force

Abrasive grit size was shown to be fairly influential on the RMS force for orbit speeds exceeding 8 m/min. To further study the effect of abrasive grit size a study on the abrasive percentage added was performed. The results are shown in Figure 4.22. The smaller grit sizes, 400 grit (17.3 μm) and smaller, show an exponential trend as abrasives are added to the system. The larger grit sizes, 220 grit (60 μm) and larger, show an initial increase in force then slightly decline after 16 percent is reached. This indicates that the average particle size and distribution have an influence on the slurry's jamming potential. This also confirms that the slurry's potential lies in the medium to fine finishing category.

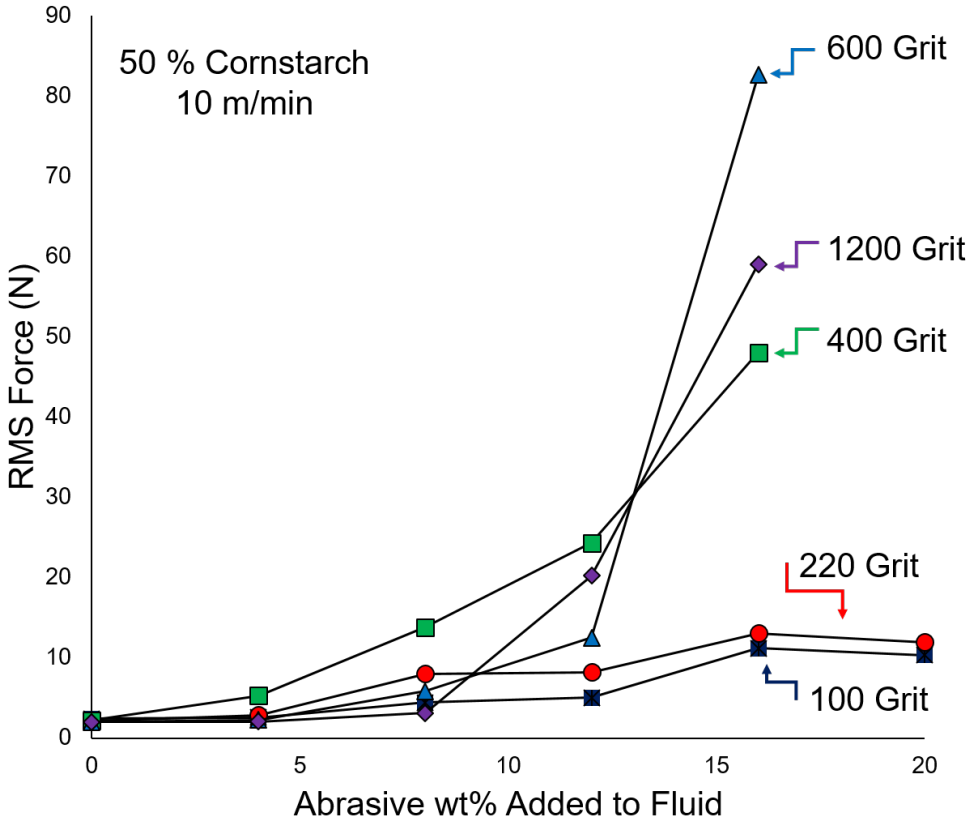

Figure 4.22: Effect of Abrasive Percentage on Force

To explain these two trends, the abrasive grit size and shape were analysed. Table 3.2 showed the abrasive grit size specified by the supplier. This data combined with a typical bulk cornstarch particle size is plotted in Figure 4.23 [16]. Here the 50 percent minimum and maximum particle size for the various abrasives used is represented by the high and low bars on the graph. We can see that the average particle size for bulk cornstarch falls between the average particle sizes of 400 grit and 600 grit abrasives. To ensure that the bulk cornstarch used was similar to that reported [16], 150 particles were measured using a Nikon AZ100 microscope. The average particle size was found to be 14.3 μm. This is within 10 percent of the average particle size recorded in the

literature. Other studies have published an average particle size of 15.8 $\pm 4.8 \mu$m [16].

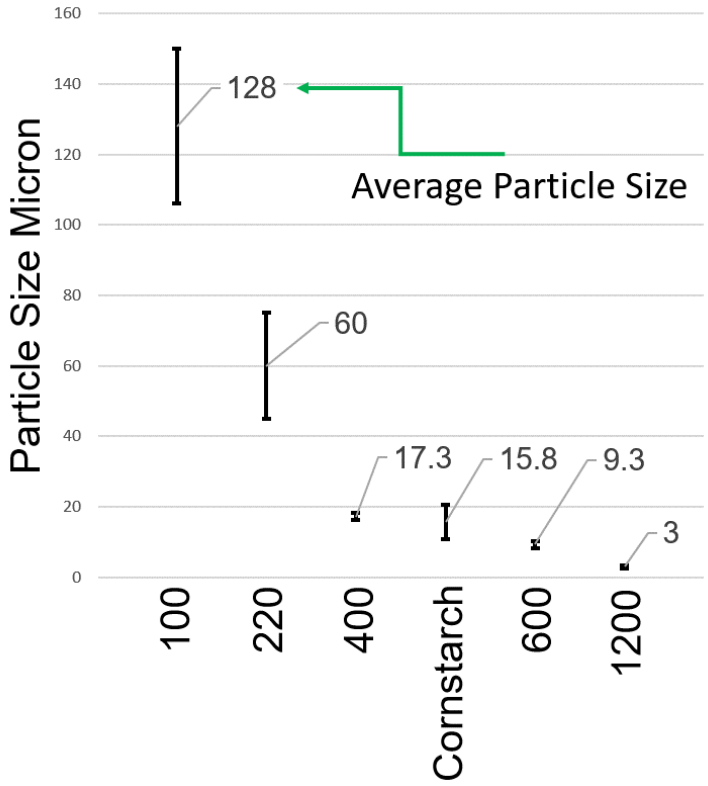

Figure 4.23: Particle Size Comparison for Various Grit Sizes and Cornstarch [16]

When these abrasives are added to cornstarch, it can be seen that 400 grit (17.3 μm) and higher would not significantly change overall particle size distribution of the slurry. However, 220 grit and lower abrasives are significantly larger grains which would widen the particle size distribution of the slurry. The particle size distribution has been shown to affect the dynamics of suspensions [47]. Typically a larger particle size distribution increases the critical volume packing fraction ϕ_j and decreases the severity of thickening. From Figure 4.21, it can be seen that when larger abrasive sizes are introduced the slurry shows less of a thickening effect than when the lower

grit sizes are added. Figure 4.22 shows that with increasing concentrations, the larger grit sizes can cause the slurry to start to reduce it's maximum force potential. These two trends indicate that the particle size distribution is a prominent factor to the force response and performance of the slurry.

The second factor which could affect thickening is the particle shape. It has been seen in other suspensions that the more anisotropic a suspension is, the more readily it tends to thicken [47]. To compare the particle size and shape, 400 grit (17.3 μm) abrasives and the bulk cornstarch were placed under a microscope. From Figure **??** (a) the sharp jagged shape of the aluminium oxide is shown. When compared with Figure **??** (b) it can be seen that aluminium oxide has a completely different shape than bulk cornstarch.

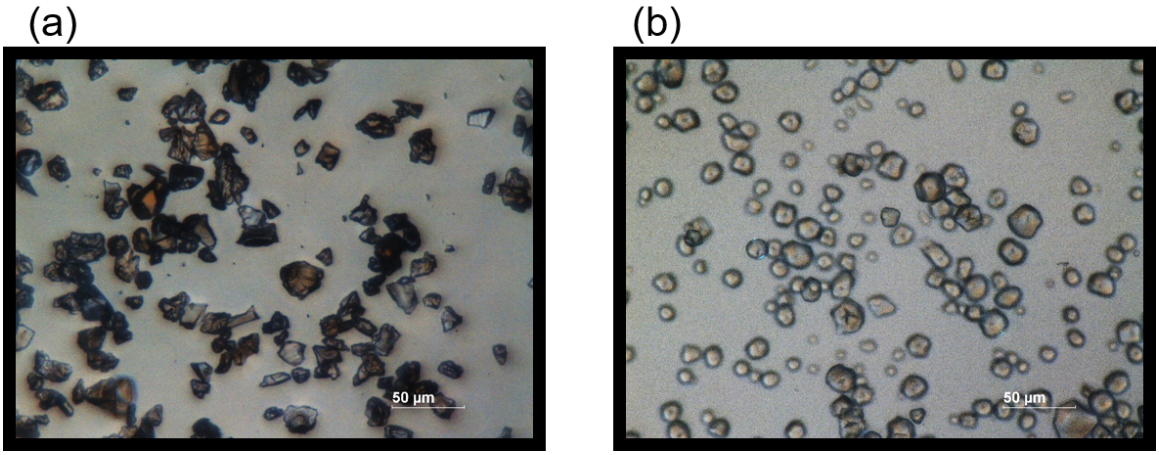

Figure 4.24: Particle Size and Shape Comparison Between 400 Grit Abrasives and Bulk Cornstarch

4.4 Finishing Experiments

With the results in Section 4.2 showing various trends in force dynamics when different abrasive grit sizes and concentrations are added, an adequate starting grit size to be used for finishing must be established. For this test fairly aggressive parameters were used. The container was set to a double boundary condition. The orbit was set to 10 m/min, spindle speed set to 2000 RPM, and 16 percent abrasives were added to a 50 percent cornstarch slurry. This was to discover a grit adequate for the initial rough finishing stage. Figure 4.22 shows that no further force is observed by adding above 16 percent abrasives.

Figure 4.25 shows various reductions in roughness, measured in Ra, for different grit sizes. When the abrasive grit is very fine, such as 600 and 400 grit, the rate of finishing is quite slow. The data for 600 Grit only shows a few nanometres reduction in Ra after a 30 minute time window. When the abrasive size is larger, such as 220 grit, a reduction from 500 nm to 93 nm was achieved. This surface is typical for processes such as stone super finishing, magnetic abrasive finishing, mass finishing, and lapping [2]. It is just beyond the upper limit of typical performance abrasive flow machining which produces typical surfaces between 100-250 nm Ra [2]. Typical surface finishes for these processes can be seen in table 4.1. No further benefit from increasing the abrasive size was found between 220 and 100 grit indicating that their exists some sort of optimum but classification of this optimum is beyond the scope of this work.

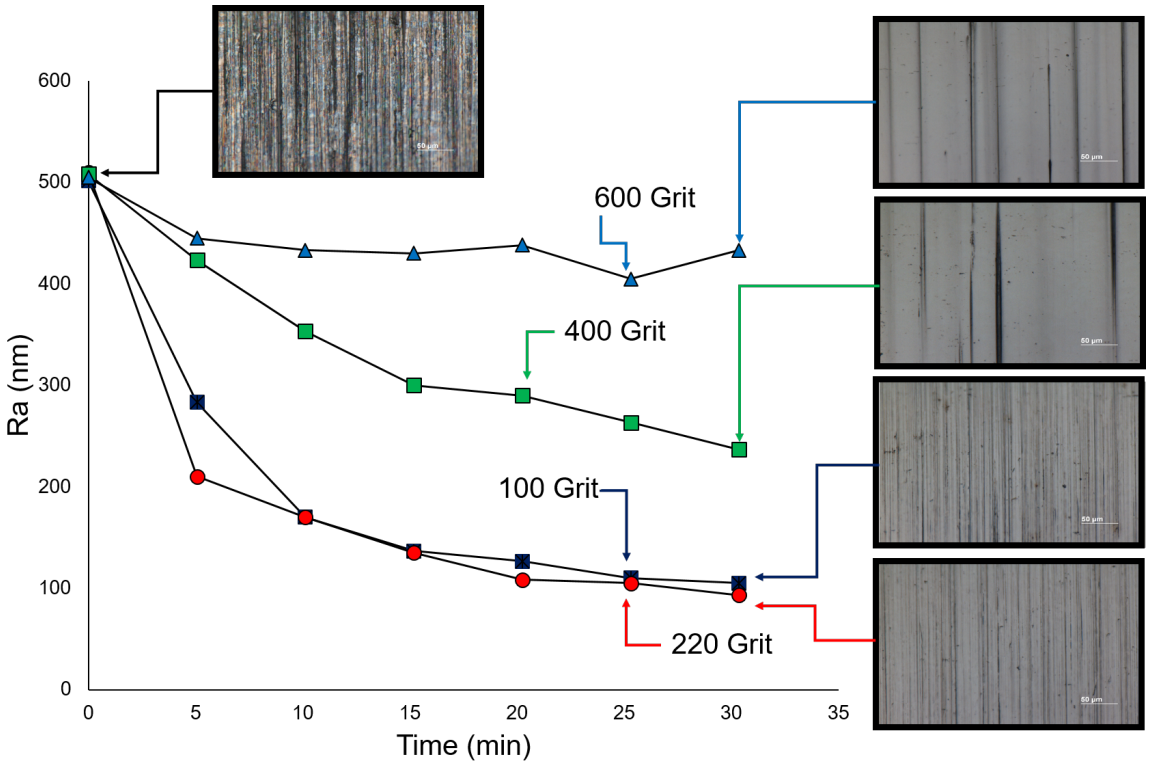

Figure 4.25: Effect of Grit Size on Finishing Performance

An interesting trend was in the reflectivity of the coupon. Figure 4.26 shows the surface of an unfinished coupon and the final surface of each coupon. Even though the surface roughness (Ra) did not change significantly for the 600 grit abrasive test, their is a clear difference between the surface in an unfinished state to that in a finished state. The 600 grit abrasive was effective at smoothing the surface but did not remove the deep scratches or groves in the surface. Figure 4.25 shows a microscope image of the surface. Deep scratches can be seen on the 600 and 400 grit abrasive final results. The scratches on the 100 and 220 grit final results are not as deep however they are more frequent.

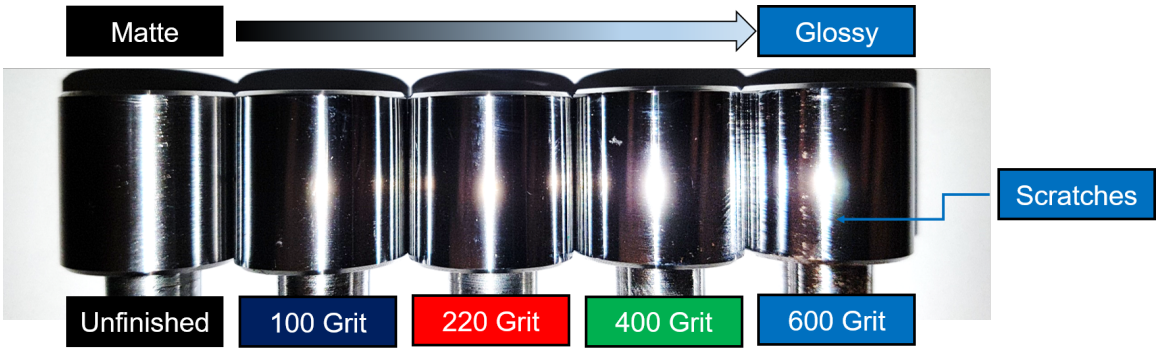

Figure 4.26: Coupon Surfaces After Finishing

Another interesting trend which exists is the linear trend the 400 grit slurry produced. The trends for 100 grit and 220 grit show a steep decrease in roughness in the first 10 minutes and then plateau out by the 30 minute mark. The trend for 400 does not show this plateau indicating that the finishing process has not stagnated but rather requires a longer cycle time for completion. This is similar to results found in MAF when the particle size decreases [3]. A similar trend is shown in Figure 2.2 where 50 μm abrasives are used.

The objective of this experiment was to establish which abrasive grit could deliver the strongest finishing performance at relatively aggressive parameters (10 m/min, 2000 RPM). 100 (128 μm) and 220 (60 μm) grit sizes seem to have the strongest performance out of the grit sizes chosen. 220 grit (60 μm) was used next to study which path, out of the paths described in Section 4.2, performed best. The rational for this was to study if two body abrasion could be achieved. From Figures 4.15 and 4.19, forces between 200-1200 N can be achieved. From the preliminary finishing experiments, a linear relationship between normal force and finishing was found. The goal of this experiment was to test the limits of the process by introducing the highest

Process		2D Surface finish					3D Surface finish		
		Ra µm	Rt µm	Rz µm	Rsk	Del-q °	Sa µm	Sz µm	Str µm
Base	Grinding	0.3~0.8	3~5	3~5	0~-1	12~18	0.2~0.4	2~4	0.01~0.05
	Hard turning	0.2~1.0	2~4	2~5	0.5~0	8~12	0.2~0.8	3~5	0~0.02
Abrasive fine-finishing	Stone superfinishing	0.05~0.15	1~2	1~2	-0.5~-1.5	5~12	0.2~0.3	2~5	0~0.05
	Tape superfinishing	0.05~0.2	1~2	1~2	-0.5~-1.5	5~12	0.1~0.2	2~5	0~0.05
	Honing	0.25~0.5	3~7	2.5~6	-2~-4	10~15	0.3~0.4	3~6	0.01~0.05
	Mass finishing	0.05~0.1	0.5~1	0.5~1	-0.5~-1.5	1~3	0.05~0.1	0.5~1	0.4~1
	Lapping	0.05~0.12	0.5~1	0.5~1	-0.2~-1.0	3~5	0.05~0.12	0.5~1	0.4~1
	Polishing	0.01~0.05	0.05~0.1	0.05~0.1	-0.5~-1.5	2~4	0.01~0.05	0.05~0.1	0.6~1
	Buffing	0.005~0.01	0.02~0.05	0.05~0.1	-0.5~-1.5	1~3	0.005~0.01	0.01~0.05	0.6~1
	Abrasive flow machining	0.1~0.25	1~2.5	1~2.5	-0.5~-1.5	1~3	0.1~0.25	1~2.5	0~0.1
	Magnetic abrasive finishing	0.003~0.07	0.03~0.7	0.03~0.7	0~-2	3~5	0.003~0.07	0.03~0.7	0~0.05

Table 4.1: Typical Surface Finish for Various Processes [2]

forces observed from the dynamic study.

The orbit speed was kept constant at 10 m/min. It was found that to maintain a feed rate of 10 m/min, 6 scallops per revolution could be performed. For the linear tests, the setup described in Section 3.5 was used to reduce spill over. The finishing performance for the double boundary condition, single boundary scallop path, and linear channel path are shown in Figure 4.27.

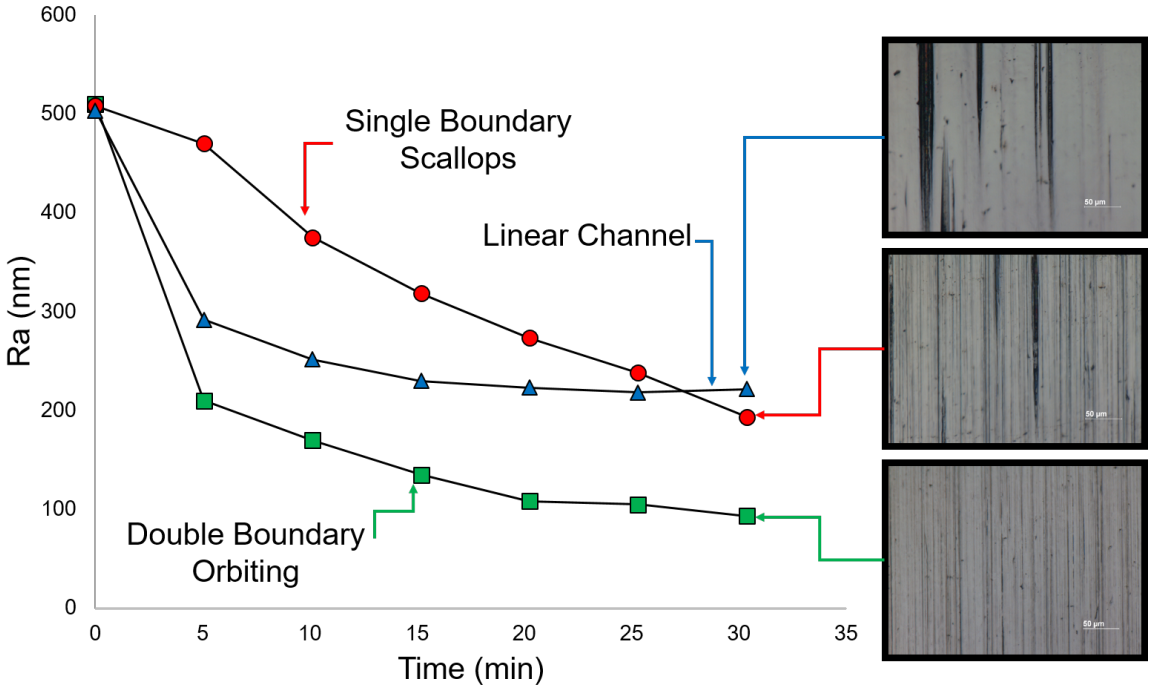

Figure 4.27: Effect of Various Translational Paths on Finishing Performance

Out of the paths chosen, the double boundary orbiting path still outperformed the scallops and linear paths. This could be due to the intermittent force spikes present in the linear and scallop patterns. Both the linear and scallop paths have high force spikes which are only triggered when a boundary is present. In the time travelling between respective boundaries there exists very little normal force. To analyse what happens to the overall RMS normal force, typical signals were plotted for each orbit path. These can be seen in Figure 4.28. From the forces measured, the linear channel had significantly higher RMS normal force than both the single boundary scallop orbit and the double boundary orbit. There was not much difference between the overall RMS normal force for the scallop orbit and the double boundary orbit but a slight difference between the average force. The primary difference between these three was

the large force variation in the scallop path which was not present in the orbiting path. From this, it can be seen that force variation has an effect on the finishing performance. One reason that the double boundary could have out performed the other two paths was the grit size chosen. The coarse 220 grit could have been too rough for the large force spikes in turn scratching the sample. The scratches produced can be seen in Figure 4.27. Further investigation with finer grits could show that the linear and scallop movements are beneficial for finishing.

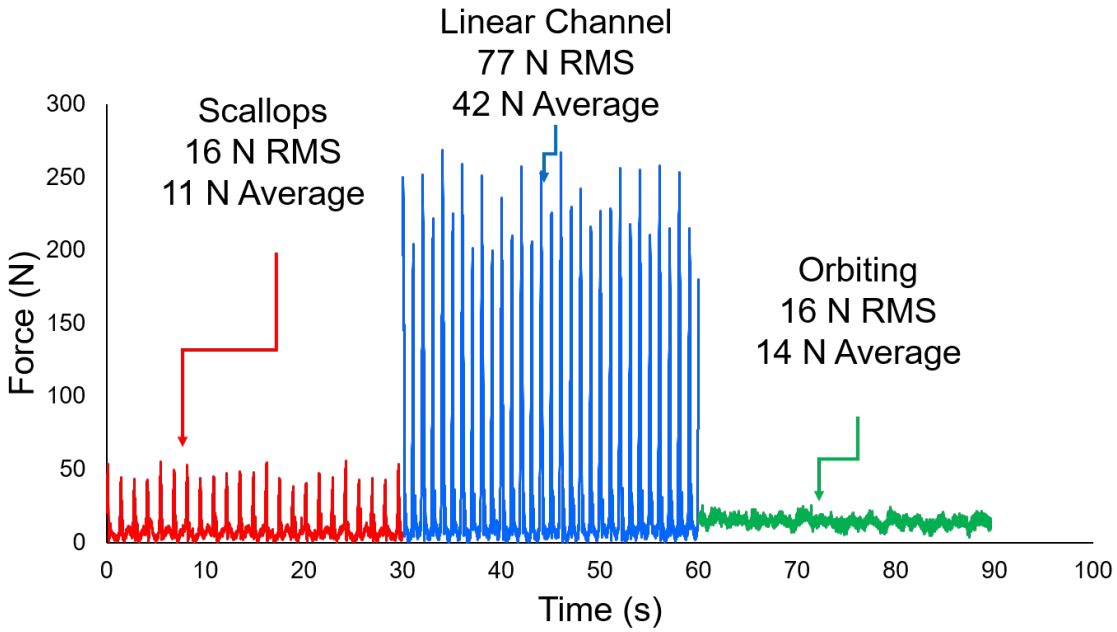

Figure 4.28: Effect of Various Translational Paths on Force

To try and utilize the relationship between force and orbital speed an experiment was run where the orbiting speed decreased half way through the finishing process. The goal of this is to aggressively finish the coupon in the first 15 minutes and then reduce that aggressiveness to achieve a low surface roughness. The results of this test are shown in Figure 4.29. When compared to a constant finishing process, shown in

Figure 4.25, the performance of the stepped study was slightly better than the single speed study leading to a 13 nm decrease in final surface roughens. As the stepped experiment already was out performing the single speed experiment before the speed was decreased at 15 minutes, this improvement can not be attributed to the process parameters but rather variability in the finishing performance. The step between 10 m/min and 5 m/min orbit might have not been a significant enough difference to showcase the change in finishing performance. Further investigation with larger changes in orbit velocity is necessary to prove this concept.

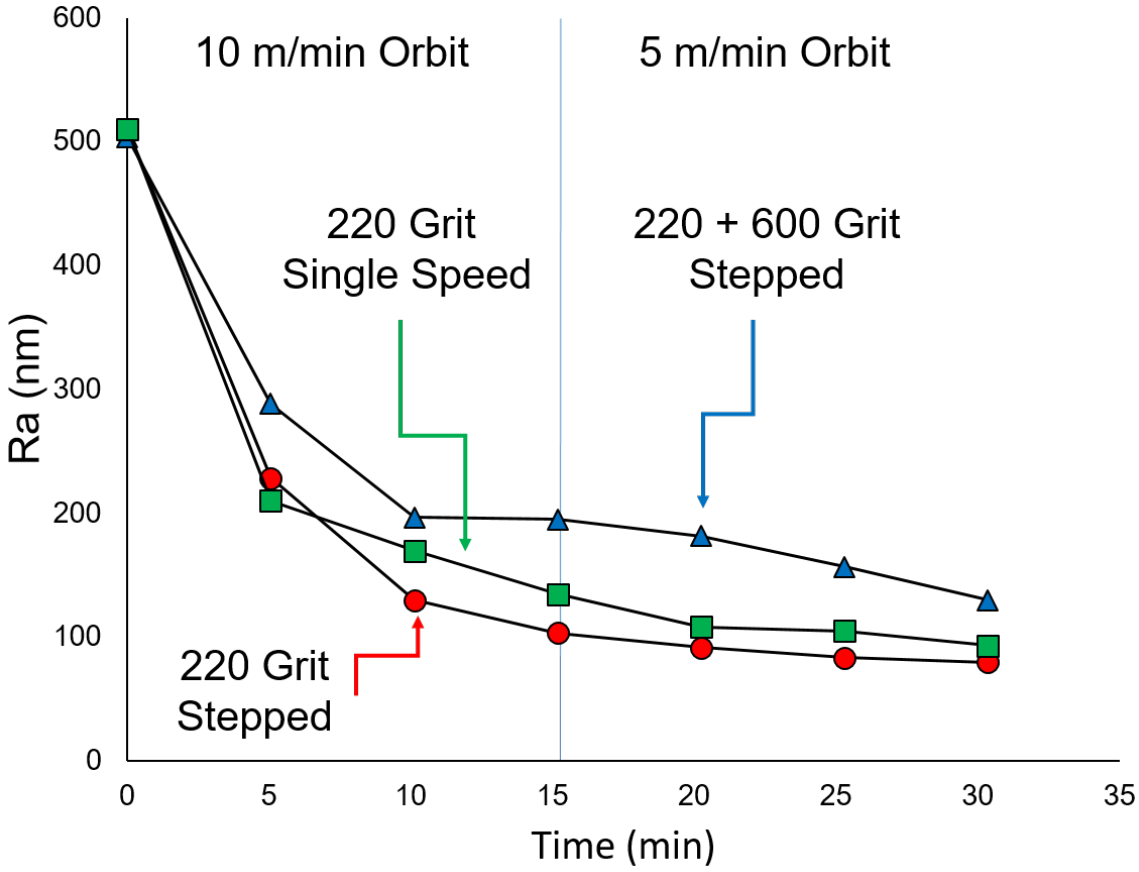

Figure 4.29: Effect of Slowing Orbit Mid Process on Roughness

Because, in Section 4.2, the overall rms force for a 220 grit slurry showed a decreasing force when additional abrasives were added a multi abrasive test was performed. Both 16 percent 220 and 4 percent 600 grit abrasives were added to the same slurry and a coupon was finished. The performance of this slurry, shown in Figure 4.29, did not show any immediate advantage over a standard single grit abrasive slurry. This could be because the amount of 600 grit abrasives added were not enough to thicken the fluid. The RMS force was measured for this experiment and was found to be 17 N. From Figure 4.22 it can be seen that with only 220 grit abrasives a 16 N RMS normal force is present. The mild decrease could be because of two oposing factors. The increase in volume fraction should thicken the fluid while the increased particle size distribution should reduce the thickening [47].

Chapter 5

Conclusions and Future Work

5.1 Conclusions

This research was motivated by the discovery of a novel media which shows promise as a finishing slurry. This media was tested in various capacities to study it's dynamic response to various input parameters. The media was also validated as a potential finishing compound. Several studies into the potential of this media were performed, the main results of these studies are summarized below.

1. Coupons were fabricated to test and prove the ability of the novel finishing slurry. The coupons were finished with both the presence and absence of an orbit motion while rotating about the coupon's center. It was shown that the orbit motion introduced a normal force which was linearly correlated to the finishing performance of the slurry. It was also shown that the coupon's RPM was correlated to the finishing performance but plateaued at a specific limit.

2. Experiments were carried out on the basic kinematic response of the slurry. The first test was performed with multiple boundary conditions to test the effect of

these constraints on the normal force produced. A double boundary setup induced a normal force significantly higher than a single boundary setup indicating that the boundary is a significant parameter. The effect of the gap size between boundary and coupon showed less of an influence as the presence of a second boundary but still had a weak negative correlation to the normal force. This was similar to the effect of orbit speed and RPM. The orbit speed was shown to have a significant effect on normal force where RPM had a slight negative correlation. The effect of orbit speed and cornstarch concentration was investigated. This showed a linear relationship between the orbit speed and normal force. This is beneficial as the orbit speed is easily varied during the process providing more control to the user.

3. The relative directions of both spindle and orbit rotation were studied to test their influence. It was discovered that in a single boundary test, the spindle rotational direction and orbit direction must be opposite for a significant normal force to exist. When the spindle and orbit are rotating in the same direction, the slurry is pulled away from the boundary resulting in low normal forces. When the slurry is jammed against the boundary, a significant normal force is produced. This effect highlights that the mechanism driving the normal force is shear jamming and not shear thickening. To further investigate, the double boundary setup was used. The second boundary added symmetry to the boundary conditions in turn removing the orientation dependency.

4. Various motions were studied to see which path produced the highest normal force. It was shown that a linear path towards a boundary produced a normal force spike roughly four times larger than a continuous orbit. A linear path towards a boundary with horizontal constraints produced a force spike roughly six times larger than without horizontal constraints. Repetitive motions towards an unconstrained

boundary showed that the force spikes were fairly consistent.

5. Abrasives were added in various grit sizes and concentrations and their effect on RMS force through various orbit speeds were studied. It was observed that abrasives thickened the slurry for all grit sizes chosen. Only the larger grit sizes showed any signs of an optimum concentration for thickening. The thickening effect was higher for abrasives close to the particle size of cornstarch. Because the abrasive size is limited, the initial surface to be finished must be smooth enough for these smaller abrasives to be effective.

6. Coupons were finished using aggressive parameters discovered in the kinematic study. A decrease in surface roughness from 500 nm to 93 nm was observed while using 220 grit abrasive. When reducing the orbit speed mid process, an additional 13 nm reduction was observed. This was concluded to be due to variability in the process and not an effect of process parameters. To prove this concept, further investigation is required.

These studies provided a proof of concept for shear jamming suspensions to be used in finishing applications. The kinematic response of the fluid for various input parameters was analysed. The influence of primary input parameters on the finishing performance were highlighted. It was shown that the input parameters provide the ability to fine tune and control the conditions required for finishing mid process. Although a significant portion of the fundamentals are understood, further work is needed to exploit the full potential of this novel finishing process.

5.2 Future Work

This section suggests and highlights some of the areas where additional research could prove to be beneficial. The goal of these suggestions is to outline areas which could be further studied to deepen understanding of this process.

1. The coupons fabricated were made from medium carbon steel ground shaft. Harder work steel coupons should be tested as typically harder steel will result in finer finished surfaces. Ground surfaces have lay direction which influences finishing performance. In this work the lay direction and the abrasive relative motion fall in the same direction as seen in Figure 5.1(a). Further performance can be achieved by arranging the lay direction and abrasive relative motion in different directions. This can be done through an inclination angle between the spindle and container as shown in Figure 5.1 (b).

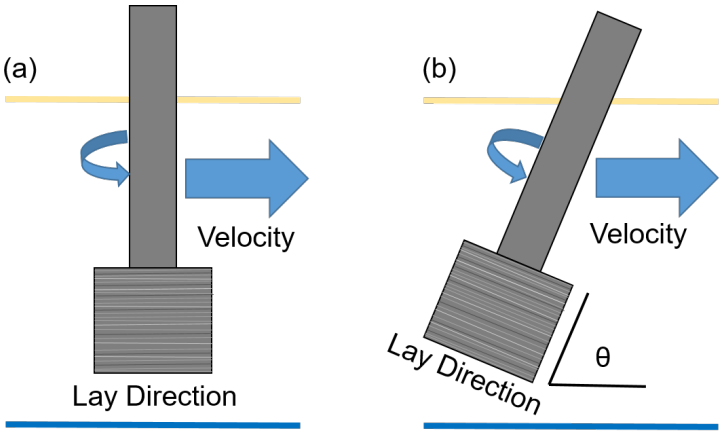

Figure 5.1: Lay Direction Vs. Translational Velocity

2. Texturing the outer surface of the boundary could limit slip between the slurry and wall. This could increase the normal force and increase finishing performance.

3. Separation and sedimentation between the abrasive, cornstarch, and water was observed. Density matching the cornstarch and water concentration by introducing CsCl can reduce the separation. Improving the agitation of the slurry could increase the contacts per unit area increasing finishing performance.

4. Studies have shown that vibration can increase finishing performance in magnetic abrasive finishing [20]. Vibration has also been shown to activate a thickening mechanism in cornstarch suspensions [16]. Adding vibration to assist in both relative motion between the slurry and workpiece and to activate other thickening mechanisms could have a significant effect on finishing potential.

References

[1] Larry Rhoades. Abrasive flow machining: a case study. *Journal of Materials Processing Tech.*, 28(1-2):107–116, 1991.

[2] Fukuo Hashimoto, Hitomi Yamaguchi, Peter Krajnik, Konrad Wegener, Rahul Chaudhari, Hans-Werner Hoffmeister, and Friedrich Kuster. Abrasive fine-finishing technology. *CIRP Annals - Manufacturing Technology*, 65(2):597–620, 2016.

[3] T. Shinmura, K. Takazawa, E. Hatano, M. Matsunaga, and T. Matsuo. Study on Magnetic Abrasive Finishing. *CIRP Annals - Manufacturing Technology*, 39(1):325–328, 1990.

[4] David a. Davidson. Mass finishing processes. *Metal Finishing*, 105(10):72–83, 2007.

[5] J. Domblesky, V. Cariapa, and R. Evans. Investigation of vibratory bowl finishing. *International Journal of Production Research*, 41(16):3943–3953, 2003.

[6] J. Domblesky, R. Evans, and V. Cariapa. Material removal model for vibratory finishing. *International Journal of Production Research*, 42(5):1029–1041, 2004.

[7] Vikram Cariapa, Hyunjae Park, Jongsoo Kim, Cunjiang Cheng, and Antonio Evaristo. Development of a metal removal model using spherical ceramic media in a centrifugal disk mass finishing machine. *International Journal of Advanced Manufacturing Technology*, 39(1-2):92–106, 2008.

[8] Paolo Claudio Priarone, Stefania Rizzuti, Luca Settineri, and Guido Vergnano. Effects of cutting angle, edge preparation, and nano-structured coating on milling performance of a gamma titanium aluminide. *Journal of Materials Processing Technology*, 212(12):2619–2628, 2012.

[9] J.D. Gates. Two-body and three-body abrasion: A critical discussion. *Wear*, 214(1):139–146, 1998.

[10] T. G. Bifano, T. a. Dow, and R. O. Scattergood. Ductile-Regime Grinding: A New Technology for Machining Brittle Materials. *Journal of Engineering for Industry*, 113(2):184, 1991.

[11] G.J. Gore and J.D. Gates. Effect of hardness on three very different forms of wear. *Wear*, 203-204(96):544–563, 1997.

[12] N. Belkhir, D. Bouzid, and V. Herold. Correlation between the surface quality and the abrasive grains wear in optical glass lapping. *Tribology International*, 40(3):498–502, 2007.

[13] N E Miller. Three-body Abrasive Wear with Small Size Diamond Abrasives. 58:249–259, 1980.

[14] T. Kuriyagawa, M. Saeki, and K. Syoji. Electrorheological fluid-assisted ultra-precision polishing for small three-dimensional parts. *Precision Engineering*, 26(4):370–380, 2002.

[15] Thomas D. Rossing. Chladni's law for vibrating plates. *American Journal of Physics*, 50(3):271, 1982.

[16] Nathan C. Crawford, Lauren B. Popp, Kathryn E. Johns, Lindsey M. Caire, Brittany N. Peterson, and Matthew W. Liberatore. Shear thickening of corn starch suspensions: Does concentration matter? *Journal of Colloid and Interface Science*, 396:83–89, 2013.

[17] Selim Gürgen, Weihua Li, and Melih Cemal Kuhan. The rheology of shear thickening fluids with various ceramic particle additives. *Materials and Design*, 104(May):312–319, 2016.

[18] S. C. Jayswal, V. K. Jain, and P. M. Dixit. Modeling and simulation of magnetic abrasive finishing process. *International Journal of Advanced Manufacturing Technology*, 26(5-6):477–490, 2005.

[19] Jae Seob Kwak. Enhanced magnetic abrasive polishing of non-ferrous metals utilizing a permanent magnet. *International Journal of Machine Tools and Manufacture*, 49(7-8):613–618, 2009.

[20] Shaohui Yin and Takeo Shinmura. Vertical vibration-assisted magnetic abrasive finishing and deburring for magnesium alloy. *International Journal of Machine Tools and Manufacture*, 44(12-13):1297–1303, 2004.

[21] B. Denkena, J. Köhler, and A. Schindler. Behavior of the magnetic abrasive tool for cutting edge preparation of cemented carbide end mills. *Production Engineering*, 8(5):627–633, 2014.

[22] Steven R Arrasmith, Irina a Kozhinova, Leslie L Gregg, Aril B Shorey, Henry J Romanofsky, Stephen D Jacobs, Donald Golini, William I Kordonski, Stephen J Hogan, and Paul Dumas. Details of the polishing spot in magnetorheological finishing (MRF). *SPIE's International Symposium on Optical Science, Engineering, and Instrumentation*, 3782(July):92–100, 1999.

[23] Ajay Sidpara and V. K. Jain. Rheological Properties and Their Correlation with Surface Finish Quality in MR Fluid-Based Finishing Process. *Machining Science and Technology*, 18(3):367–385, 2014.

[24] V. K. Jain. Magnetic field assisted abrasive based micro-/nano-finishing. *Journal of Materials Processing Technology*, 209(20):6022–6038, 2009.

[25] Ajay Sidpara and V. K. Jain. Experimental investigations into forces during magnetorheological fluid based finishing process. *International Journal of Machine Tools and Manufacture*, 51(4):358–362, 2011.

[26] Chunlin Miao, Shai N Shafrir, John C Lambropoulos, Joni Mici, and Stephen D Jacobs. Shear stress in magnetorheological finishing for glasses. *Applied optics*, 48(13):2585–2594, 2009.

[27] Y.Q. Wang, S.H. Yin, H. Huang, F.J. Chen, and G.J. Deng. Magnetorheological polishing using a permanent magnetic yoke with straight air gap for ultra-smooth surface planarization. *Precision Engineering*, 40:309–317, 2015.

[28] Lei Zhang, Tsunemoto Kuriyagawa, Tsuyoshi Kaku, and Ji Zhao. Investigation into electrorheological fluid-assisted polishing. *International Journal of Machine Tools and Manufacture*, 45(12-13):1461–1467, 2005.

[29] Binbin Chen, Haobo Cheng, Hon Yuen Tam, and Hui Li. Design of integrated-electrode tool for electrorheological finishing of optical glasses. *Frontiers of Optoelectronics in China*, 4(4):467–471, 2011.

[30] Y. Mori, K. Yamauchi, and K. Endo. Elastic emission machining. *Precision Engineering*, 9(3):123–128, 1987.

[31] Y Mori, K Yamauchi, and K Endo. Mechanism of atomic removal in elastic emission machining. 10(1):24–28, 1988.

[32] V. K. Jain and S. G. Adsul. Experimental investigations into abrasive flow machining (AFM). *International Journal of Machine Tools and Manufacture*, 40(7):1003–1021, 2000.

[33] B. H. Yan, Y. C. Lin, and F. Y. Huang. Development of magneto abrasive flow machining process. *International Journal of Machine Tools and Manufacture*, 42(8):953–959, 2002.

[34] T. R. Loveless, R. E. Williams, and K. P. Rajurkar. A study of the effects of abrasive-flow finishing on various machined surfaces. *Journal of Materials Processing Tech.*, 47(1-2):133–151, 1994.

[35] Oliver W. Fähnle, Hedser van Brug, and Hans J. Frankena. Fluid jet polishing of optical surfaces. *Applied Optics*, 37(28):6771, 1998.

[36] Anthony Beaucamp, Yoshiharu Namba, and Richard Freeman. Dynamic multi-phase modeling and optimization of fluid jet polishing process. *CIRP Annals - Manufacturing Technology*, 61(1):315–318, 2012.

[37] M. Tricard, W. I. Kordonski, and A. B. Shorey. Magnetorheological jet finishing of conformal, freeform and steep concave optics. *CIRP Annals - Manufacturing Technology*, 55(1):309–312, 2006.

[38] Min Li, Binghai Lyu, Julong Yuan, Chenchen Dong, and Weitao Dai. Shear-thickening polishing method. *International Journal of Machine Tools and Manufacture*, 94:88–99, 2015.

[39] Min Li, Binghai Lyu, Julong Yuan, Weifeng Yao, Fenfen Zhou, and Meipeng Zhong. Evolution and equivalent control law of surface roughness in shear-thickening polishing. *International Journal of Machine Tools and Manufacture*, 108:113–126, 2016.

[40] J A Seckold. Optical polishing with titanium dioxide. *Appl. Opt.*, 15(7):1693–1693, 1976.

[41] Andreja Zupani-it, Roman Lapasinb, and Miha Turnera. IN ORGANIC Rheological characterisation of shear thickening Ti02 suspensions in low molecular polymer solution. 30, 1997.

[42] F. Irgens. *Rheology and non-newtonian fluids*. Springer US, 2014.

[43] Malcolm M. Cross. Rheology of non-Newtonian fluids: A new flow equation for pseudoplastic systems. *Journal of Colloid Science*, 20(5):417–437, 1965.

[44] A B Metzner and J C Reed. Flow of Non-Newtonian Fluids-Correlation of the Laminar , Transition , and Turbulent-flow Regions. *AlChE Journal*, 1(4):434–440, 1955.

[45] Howard A. Barnes. Thixotropy - A review. *Journal of Non-Newtonian Fluid Mechanics*, 70(97):1–33, 1997.

[46] Howard A. Barnes. A review of the slip (wall depletion) of polymer solutions, emulsions and particle suspensions in viscometers: its cause, character, and cure. *Journal of Non-Newtonian Fluid Mechanics*, 56(3):221–251, 1995.

[47] H. a. Barnes. Shear-Thickening (Dilatancy) in Suspensions of Nonaggregating Solid Particles Dispersed in Newtonian Liquids. *Journal of Rheology*, 33(2):329, 1999.

[48] Endao Han, Ivo R. Peters, and Heinrich M. Jaeger. High-speed ultrasound imaging in dense suspensions reveals impact-activated solidification due to dynamic shear jamming. *Nature Communications*, 7:1–9, 2016.

[49] Charles E Chaffey and Ian Wagstaff. Shear thinning and thickening rheology. *Journal of Colloid and Interface Science*, 59(1):63–75, 1977.

[50] P. Rangnes and O. Palmgren. Particle size of poly (vinyl chloride) latices and rheology of poly (vinyl chloride) pastes. *Journal of Polymer Science Part C: Polymer Symposia*, 33(1):181–192, mar 2007.

[51] Eric Brown and Heinrich M Jaeger. Shear thickening in concentrated suspensions: phenomenology, mechanisms and relations to jamming. *Reports on progress in physics.*, 77(4):046602, 2014.

[52] Scott R. Waitukaitis. *Impact-Activated Solidification of Cornstarch and Water Suspensions [Ph.D. Thesis].* The University of Chicago, Chicago, 2013.

[53] A. Fall, F. Bertrand, D. Hautemayou, C. Mezière, P. Moucheront, A. Lemaître, and G. Ovarlez. Macroscopic discontinuous shear thickening versus local shear jamming in cornstarch. *Physical Review Letters*, 114(9):1–5, 2015.

[54] R.P. Chhabra J.F. Richardson. *Non-Newtonian Flow and Applied Rheology: Engineering Applications*. Butterworth-Heinemann, Oxford, 2 edition, 2008.

[55] Erica E Bischoff White, Manoj Chellamuthu, and Jonathan P. Rothstein. Extensional rheology of a shear-thickening cornstarch and water suspension. *Rheologica Acta*, 49(2):119–129, 2010.

[56] Yannick Dziechciarek, Jeroen J G van Soest, and Albert P. Philipse. Preparation and properties of starch-based colloidal microgels. *Journal of Colloid and iIterface Science*, 246:48–59, 2002.

[57] Didier Lootens, Henri Van Damme, Yacine Hémar, and Pascal Hébraud. Dilatant flow of concentrated suspensions of rough particles. *Physical Review Letters*, 95(26):1–4, 2005.

[58] Bin Liu, Michael Shelley, and Jun Zhang. Focused force transmission through an aqueous suspension of granules. *Physical Review Letters*, 105(18):1–4, 2010.

[59] Stefan Von Kann, Jacco H. Snoeijer, and Devaraj Van Der Meer. Velocity oscillations and stop-go cycles: The trajectory of an object settling in a cornstarch suspension. *Physical Review E - Statistical, Nonlinear, and Soft Matter Physics*, 87(4):1–14, 2013.

[60] Scott R. Waitukaitis and Heinrich M. Jaeger. Impact-activated solidification of dense suspensions via dynamic jamming fronts. *Nature*, 487(7406):205–209, 2012.

[61] S R Waitukaitis, L K Roth, V Vitelli, and H M Jaeger. Dynamic jamming fronts. *Europhysics Letters*, 102(4):44001, 2013.

[62] Sayantan Majumdar, Ivo R Peters, Endao Han, and Heinrich M Jaeger. Dynamic shear jamming under extension in dense granular suspensions. *ArXiv e-prints*, pages 1–5, 2016.

[63] Ivo R. Peters, Sayantan Majumdar, and Heinrich M. Jaeger. Direct observation of dynamic shear jamming in dense suspensions. *Nature*, 532(7598):214–217, 2016.

[64] David J Whitehouse. *Surfaces and their Measurement*. Elsevier, 2004.

[65] Ving-lang Wang. Re-Examination of Pressure and Speed Dependencies of Removal Rate during Chemical-Mechanical Polishing Processes. 144(2):111–113, 1997.